HIGH MASS RESOLUTION, HIGH ANGULAR ACCEPTANCE TIME-OF-FLIGHT MASS SPECTROSCOPY FOR PLANETARY MISSIONS

Under the

Planetary Instrument Definition and Development Program (PIDDP)

Final Report

Period Covered: January 1, 1988 - February 28, 1991

Submitted to:

Dr. William Brunk, Code EL
Discipline Scientist, PIDDP
Solar System Exploration Division
NASA Headquarters
Washington, DC 20546

Prepared by:

Dr. David T. Young, Principal Investigator
Southwest Research Institute
P.O. Drawer 28510
San Antonio, TX 78228-0510

NASA Grant NAGW-1286 and Supplement 2 to SwRI
NASA Contract W-7405-ENG-36 to LANL
SwRI Project 15-2351

HIGH MASS RESOLUTION, HIGH ANGULAR ACCEPTANCE TIME-OF-FLIGHT MASS SPECTROSCOPY FOR PLANETARY MISSIONS

Under the

Planetary Instrument Definition and Development Program (PIDDP)

Final Report

Period Covered: January 1, 1988 - February 28, 1991

Submitted to:

Dr. William Brunk, Code EL
Discipline Scientist, PIDDP
Solar System Exploration Division
NASA Headquarters
Washington, DC 20546

Prepared by:

Dr. David T. Young, Principal Investigator
Southwest Research Institute
P.O. Drawer 28510
San Antonio, TX 78228-0510

NASA Grant NAGW-1286 and Supplement 2 to SwRI
NASA Contract W-7405-ENG-36 to LANL
SwRI Project 15-2351

TABLE OF CONTENTS

I. INTRODUCTION

This final report covers three years and several phases of work in which we have successfully developed instrumentation for the Planetary Instrument Definition and Development Program (PIDDP). The end result of this effort is that the Principal Investigator and members of the original PIDDP proposal group from SwRI and LANL have been selected to provide a subset of this instrumentation for both the Cassini Orbiter and the Comet Rendezvous Asteroid Flyby (CRAF) missions. In order to reach this level of success we have built, tested, and in some cases rejected, a number of promising instrument designs. In the earliest phases our original proposal was titled "Instruments to Measure 3-Dimensional Distributions and Mass-Resolved Ions on 3-Axis Stabilized Spacecraft Without the Use of Scan Platforms". In subsequent work this evolved to the title of our second proposal "High Mass Resolution, High Angular Acceptance Time-of-Flight Mass Spectroscopy for Planetary Missions". Both were funded as NAGW-1286 to SwRI with the former only being funded as NASA Contract W-7405-ENG-36 to Los Alamos National Laboratory (LANL). This final report combines results from both grants and contracts and covers the entire period of performance.

There were two main thrusts to the research described here: (1) Develop and test methods for electrostatically scanning detector field-of-views, and (2) improve the mass resolution of plasma mass spectrometers to $M/\Delta M \sim 25$; improve their field-of-view (FOV) to 360°; and improve their E-range to cover $\sim$ 1 eV to 50 keV.

We originally made the case that because the 3-axis stabilized spacecraft is the vehicle of choice for planetary exploration (primarily due to antenna-pointing, imaging, and other remote sensing requirements) and because plasma particle detectors preferentially wish to view $\sim 4\pi$ sr of the sky with a high duty cycle ($\sim$ 1/min. or faster) there is a basic incompatibility between planetary mission design and plasma particle measurement goals. This is amply demonstrated on the CRAF mission where the dust, neutral gas, and imaging instruments must view the comet nucleus exclusively, whereas the plasma particle instruments must simultaneously view <u>all</u> particle arrival directions, i.e. ideally, 4π sr. Our solution was to develop scanned field-of-view instruments based on particle deflection in electrostatic fields. Out of this work grew the "Beacon" instruments (Bame et al., 1989) and several improvements to the scanned FOV Fast Ion Mass Spectrometer (FIMS) originally planned for the CRAF Suprathermal Plasma in Cometary Environments (SPICE). As it turned out, although both of these methods do allow a swept FOV, it is in fact necessary in the end to place the instrument on a mechanically scanned platform. However, the electrostatically scanned FOV concept may still prove useful on missions where the energy range of interest is relatively low ($\lesssim$ 20 keV) and where the poles of the unit sphere either do not need to be covered, or can be covered in some other way. Prototypes of two different approaches to electrostatic scanning were built and tested successfully as part of our PIDDP effort.

Our second primary objective was to develop time-of-flight plasma mass spectroscopy to the point where its energy range capabilities were $\sim$ 1 eV to $\gtrsim$ 50 keV and its FOV covered a full $\sim$ 10° x 360° fan, thus providing some overlap with both thermal ion (e.g., RPA) and energetic particle techniques and the capability for 4π sr coverage. At the same time, mass resolution should be brought up to the level of $M/\Delta M \gtrsim 25$ over this full energy range, something that magnetic mass spectroscopy cannot do within typical size and weight limitations

of planetary spacecraft while maintaining a large geometric factor ($\sim 10^{-2}$ cm^2 sr eV/eV for total FOV coverage). In this area we examined primarily two devices, the Isochronous TOF (or ISOTOF), using PIDDP, and some SwRI internal funds), and the Linear Electric Field 3-Dimensional (LEF3D) TOF (using LANL internal and some SwRI PIDDP funds). We mention the LANL TOF device here because our work in the area of high resolution TOF lead us into the investigation of LEF3D in the first place and, ultimately, to the optical design for the Ion Mass Spectrometer (IMS) sensor included in our Cassini and CRAF plasma investigations. The ISOTOF has been described in the literature (Young and Marshall, 1990) but proved to be something of a dead end for space flight instrumentation when it was found that, in fact, the ion optics of a polar toroid are peculiarly sensitive to electrode misalignments. This is, in itself, a heretofore unknown fact in ion optics and thus is a valuable result (albeit in a losing cause.)

This final report also mentions several developments that were proposed in the original August 1987 PIDDP submission, but eventually had to be deleted from the Statement of Work (SOW) due to lack of funding. Included in this category is the development of digital TOF electronics and, to a great extent, the LEF3D. Both topics were pursued primarily with internal SwRI and LANL/DOE funding respectively. We mention them here for completeness so that this report may serve a useful purpose. The technical chapters of our successful Cassini proposal are also included to document trade-off studies, etc., that do not appear elsewhere but are nonetheless directly attributable to our PIDDP efforts.

II. SUMMARY OF STATEMENT OF WORK (SOW) AND ACCOMPLISHMENTS

Based on SOW's submitted August 1987 (SwRI/LANL proposal PIDDP-87-36; revised November 1987 and January 1989) and January 1989 (SwRI proposal PIDDP-90-33, revised August 1989).

1. Science determination of instrument parameters (Completed, See Appendix B for relevant findings included in Cassini Proposal).

2. Design and ray trace optics for energy analyzers and time-of-flight sensors; design TOF electronics:

   a. Beacon electrostatic analyzer (EA) (completed).

   b. Gridded Hemisphere (GH) and Gridded-Truncated-Hemispherical (GTH) electrostatic analyzers (completed).

   c. Isochronous TOF analyzer (completed).

   d. Linear electric field (LEF3D) TOF analyzer (not originally proposed but studied with SwRI PIDDP funds and LANL internal funds; completed).

   e. Combinations of electrostatic and TOF analyzers. (Completed for GTH with magnetic analyzer, Beacon with non-isochronous TOF, isochronous TOF with toroidal electrostatic analyzer, and LEF3D with toroidal electrostatic analyzer.)

f. Digital TOF electronics (deleted from original SOW due to costs, design carried out under internal SwRI funds).

3. Mechanical design and fabrication of laboratory prototypes:

   a. Beacon EA (completed at LANL).

   b. GH and GTH EA's (completed at SwRI).

   c. ISOTOF (completed at SwRI with internal funds).

   d. LEF3D (one model each at LANL and SwRI built under internal funding).

   e. Various combinations of individual analyzers were tried (see below).

   f. Digital TOF electronics (completed at SwRI with internal funds).

4. Laboratory testing in ion beams:

   a. Beacon EA (completed successfully at SwRI).

   b. GH and GTH EA's (completed successfully at SwRI).

   c. ISOTOF (partially successful testing at SwRI).

   d. LEF3D (completed successfully at LANL under internal funding; Model 2 tested without success at SwRI under PIDDP).

   e. Combinations (Prototype ISOTOF and final ISOTOF tested with toroidal top-hat analyzers, GTH tested with non-isochronous TOF, other combinations not tested due to decreased PIDDP funding.)

   f. Digital TOF electronics with ISOTOF (Completed successfully at SwRI under internal funding).

5. Reports and publications:

   a. Beacon EA (Grant Rept. 12/31/88; Bame et al., AGU Monograph Series, Vol. 54, 441, 1989).

   b. GH and GTH EA's (Grant Rept. 12/31/89; Bame et al., ibid.).

   c. ISOTOF (Grant Repts. 12/31/89, 6/30/89, 12/31/89; Young and Marshall, Nuclear Instrum. Meth. in Phys. Res., Vol. A298, 227, 1990).

d. LEF3D (Grant Rept. 12/31/89, SwRI Proposal 15-9376 for Cassini PLS; McComas and Nordholt, Rev. Sci. Instrum., 61, 3095, 1990; data analysis carried out under LANL internal funding.)

e. Combinations (Grant Rept. 12/31/88; SwRI Proposal 15-9376; Young and Marshall, ibid.; SwRI Proposal 15-9376 for Cassini PLS).

f. Digital TOF electronics (SwRI Proposal 15-9376 for Cassini PLS; Lockhart et al., IEEE Trans. Nucl. Sci., 36, 1396, 1989; carried out under SwRI internal funding.)

III. DISCUSSION OF RESULTS

Section IV of this report contains four publications and portions of our Cassini proposal that detail the results of our instrument development program under PIDDP. Here we present an overall discussion of the entire program, including some details not found in Section IV.

Our original PIDDP proposal was based on a comprehensive program of instrument design and development aimed at investigation of plasma distribution functions and ion composition in various planetary environments. Because modern planetary spacecraft are exclusively 3-axis stabilized, we concentrated on methods of scanning instrument look directions over $\sim 4\pi$ sr in order to obtain complete distribution functions. Going hand-in-hand with this effort was our second objective of improving the overall field-of-view (FOV) of mass analyzing instruments as well as their mass resolution and the energy range over which this resolution can be maintained. Our particular target missions were Cassini and CRAF, the latter plasma instrument, Suprathermal Plasma Investigation in Cometary Environments (SPICE), having already been selected with J. L. Burch as PI. Thus much of the early work was aimed at improving the scanning and FOV capabilities of the SPICE instrument particularly the Fast Ion Mass Spectrometer (FIMS), with later work concentrating on design of a high resolution, wide FOV time-of-flight sensor for the Cassini Orbiter PLS instrument.

As might be expected in a program covering 3 years, we developed some ideas and rejected others, gained and lost funding from PIDDP and other (internal) sponsors, all the while pursuing the ultimate goal of designing an instrument that would eventually win selection for Cassini. In this regard we have been successful, and, in addition, we have now agreed among our original PIDDP and CRAF teams and with the CRAF/Cassini Project, that the Cassini design developed with PIDDP funds will be flown in place of the original SPICE design on CRAF as well. One small irony is that in the end we decided it will be easier to mechanically scan the CRAF sensor over 360° of rotation than to combine electrical and mechanical scanning as was originally proposed for SPICE on CRAF.

A. Beacon Electrostatic Analyzer

Figure 1a shows the Beacon D analyzer in cross section with computed ion trajectories. The Beacon C analyzer is similar in deflection optics, but has a reversed toroid (Fig. 1b). Prototype Beacon C and D analyzers were built and tested and do indeed produce the desired selectivity in elevation angle as a function of deflector voltage (Figure 2).

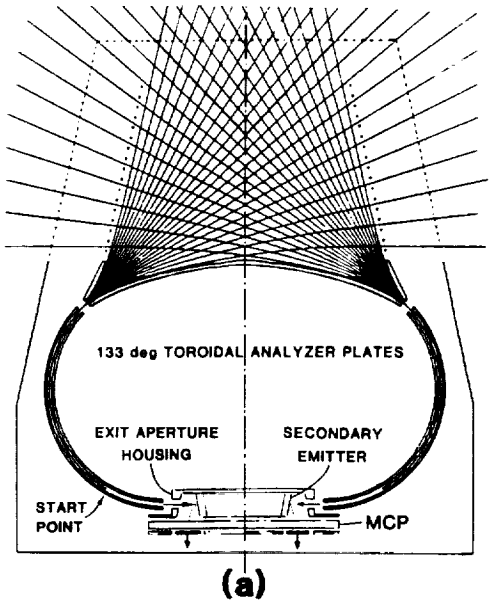

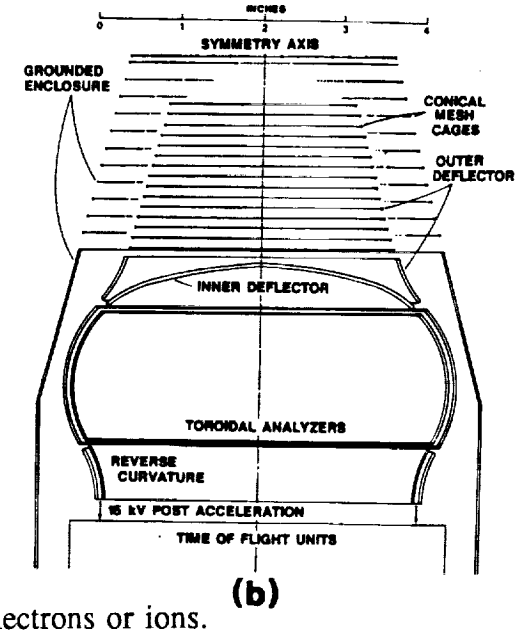

Figure 1(a). Beacon-D Elevation Analyzer for electrons or ions.
Figure 1(b). Beacon-C Elevation Analyzer for ion composition.

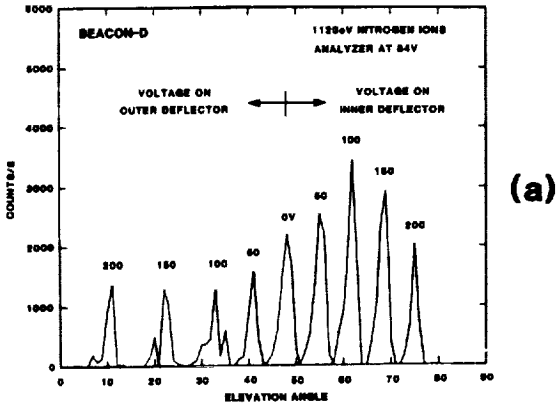

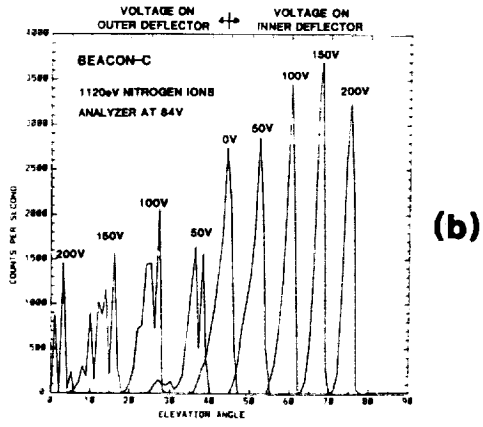

Figure 2(a). Beacon-D elevation angle response with deflection voltage.
Figure 2(b). Beacon-C elevation angle response with deflection voltage.

The Beacon-C FWHM resolution is ~ 25% at 40° to 80° and ~ 50% at $\lesssim$ 40°, whereas Beacon-D produces resolutions ~ 12% at all angles. The difference is that Beacon-C is designed with a re-curved toroidal section (Fig. 1b) in order to straighten out ion trajectories for entry into TOF analyzers. This appears to result in lower angular resolution than Beacon-D, possibly because of fringe electric fields at the interface of the two toroidal analyzers. Beacon analyzers are able to cover 78% of 2π sr, so that a second analyzer and/or mechanical scans are required.

B. Gridded Elevation Analyzers

Figure 3a and b shows the cross section and ray tracing through GH and GTH analyzers (respectively) developed for the SPICE/FIMS instrument on CRAF. Elevation angle analysis is produced by varying the voltage on the inner hemispherical surface while the outer (gridded) surface shield at ground. In the case of the GH the inner hemisphere is composed of

a set of 8 discrete rings to which a given voltage is applied. Response of both devices is similar without any significant gain in angular resolution or sensitivity.

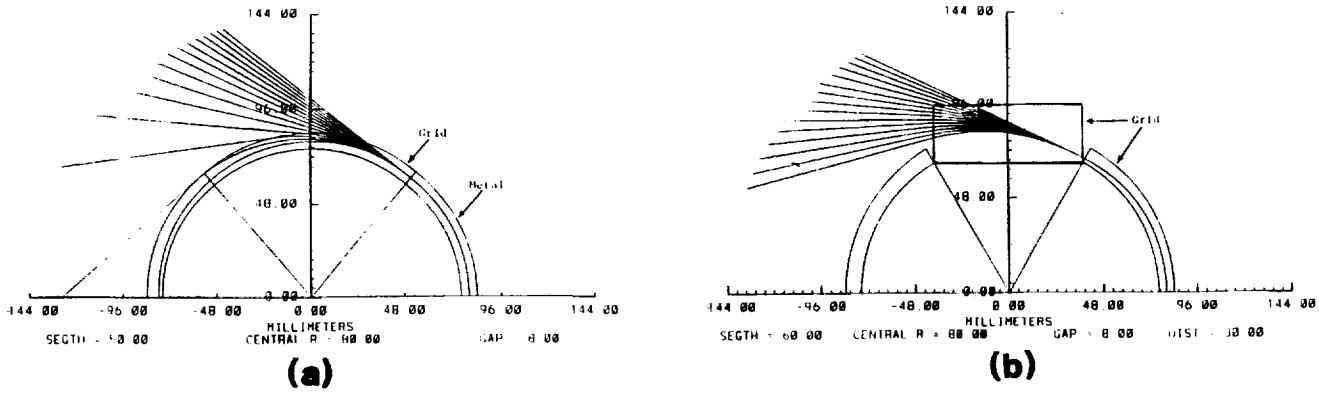

Figure 3(a). GH Elevation Analyzer cross section with rays.
Figure 3(b). GTH Elevation Analyzer cross section with rays.

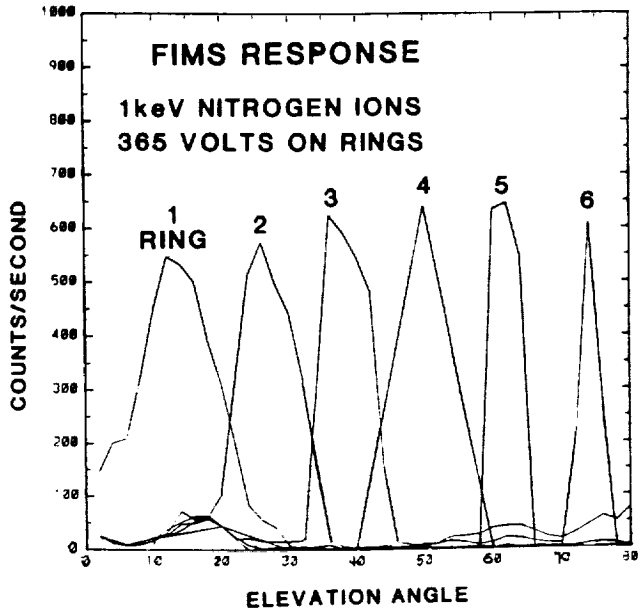

Figure 4. Response of the SPICE/FIMS GH Elevation Analyzer to 1 kV N^+ ions.

The final elevation analyzer development for the CRAF/SPICE/FIMS spectrometer is shown in Fig. 5. In the end it was necessary to find a solution in which deflection occurred within $\pm 45°$ of the central optical plane of the instrument FOV (Fig. 5) rather than the 0° to ~ 80° coverage offered by the Beacon, GH, and GTH designs. This is termed the "LIPS" design (not an acronym!).

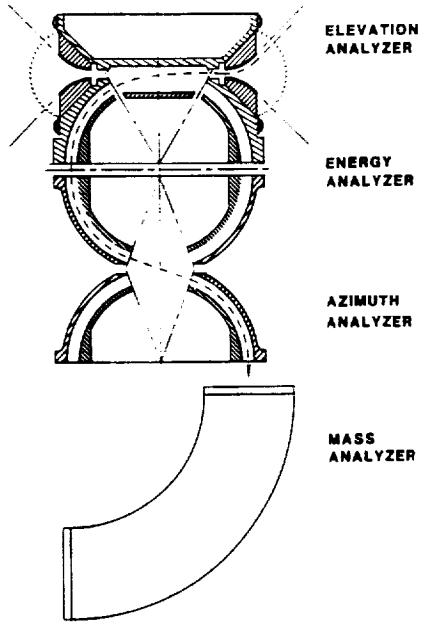

Figure 5. Cross section of final SPICE design showing the "LIPS" Elevation Analyzer.

The "LIPS" deflection system was chosen for the FIMS sensor onCRAF. It produces $\pm 45°$ deflection about the central optical plane and operates in tandem with toroidal electrostatic analyzers and a motor-driven magnetic sector for mass analysis. This final FIMS design still left two conical "holes" in the FIMS FOV (located at $90° \pm 45°$ in elevation) and thus required motion of the CRAF spacecraft itself and/or the Low Precision Pointing Platform to fill in the gaps in the FIMS FOV.

C. Isochronous Time-of-Flight (ISOTOF) Analyzer

The TOF analyzer design that was the basis for the original PIDDP proposal (Fig. 6a) was not truly isochronous and produced only moderate mass resolution. It served nonetheless as the starting point for our ISOTOF design studies. The point of departure for the ISOTOF (Fig. 6b) was a double focusing (in energy and angle) design of two tandem toroids. These reduce TOF peak widths by rejecting ions outside the analyzer energy-angle transmission range, but did not actually focus ions in a temporal sense. One critical item in our design was the use of poloidal ion rather than azimuthal trajectories in order to take advantage of the fact that a toroidal analyzer used in this way is capable of viewing 360° (cf. Ghielmetti and Shelley, 1990). One drawback of this design, as we found out, is that the analytical particle optics theory is not developed, and one faces an enormous amount of ray tracing in order to develop focusing solutions (Young and Marshall, 1990).

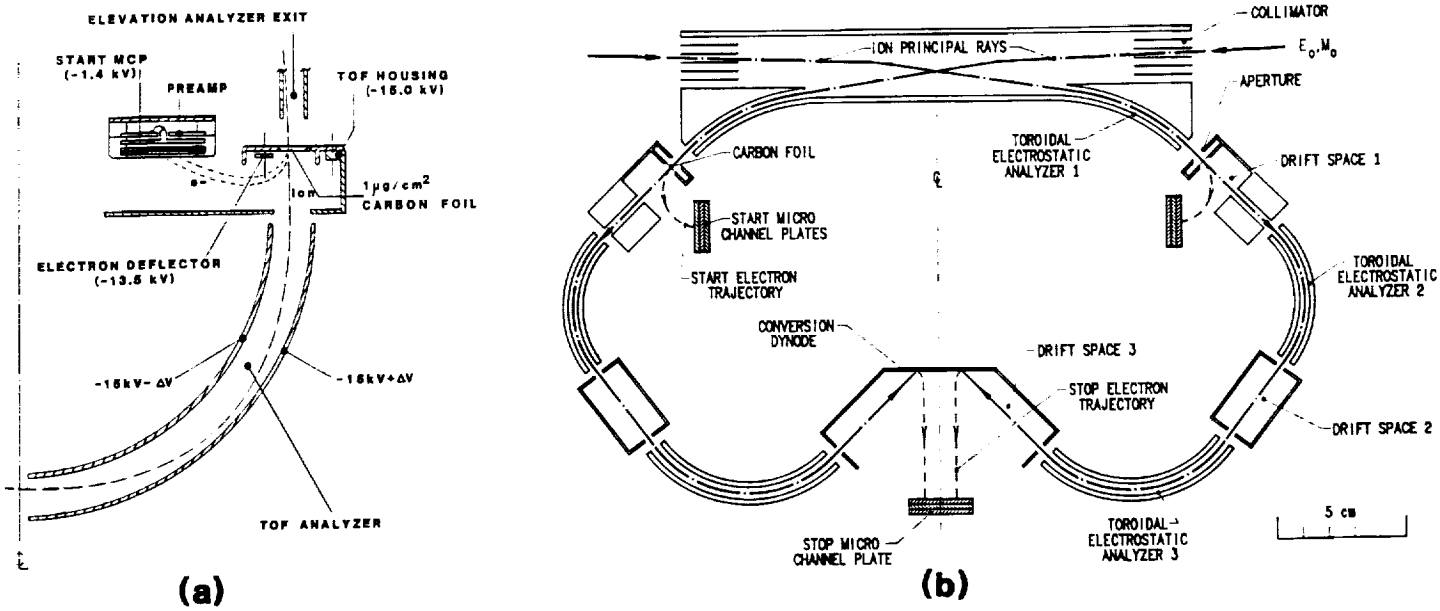

Figure 6(a). Energy-angle filtered TOF system.
Figure 6(b). ISOTOF design in cross section.

Using the concepts found in laboratory TOF designs (Poschenrieder, 1971, 1972) we varied the length of the toroid drift regions to adjust ion flight times and compensate for the tendency of more energetic ions at the upper end of the ΔE/E range to take trajectories that travelled near the outer analyzer plates, thereby arriving too "late" at the detector. In other words, the faster ions wee actually overcompensated in our initial double focusing design; adjustment of the drift regions removed this over compensation. Fig. 7 shows a plot of relative time dispersion (ΔTOF) as a function of normalized values of energy (ΔE) and angle ($\Delta\theta$) dispersion.

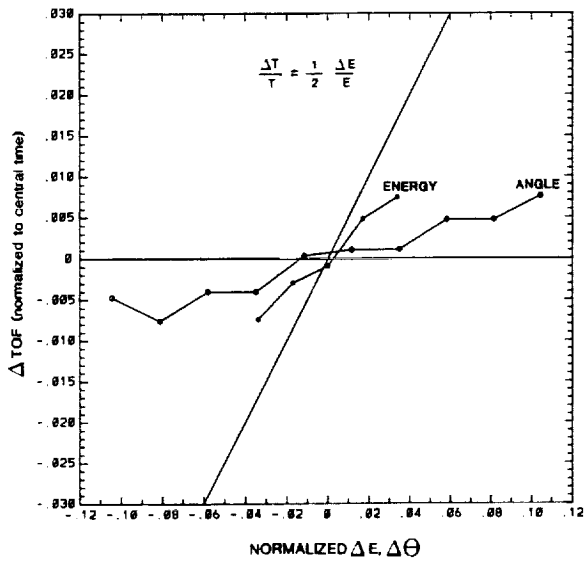

Figure 7. Relative time dispersion in ISOTOF.

The straight diagonal line represents the free space time resolution that results from pure energy dispersion, namely $\Delta T/T = \Delta E/2E$. the fact that the energy and angle dispersion curves lie at smaller slopes for the ISOTOF indicates that the device indeed produces true temporal focusing. Fig. 7 also shows that angular-temporal focusing is achieved much more readily than energy-temporal focusing.

The ray tracing gave a reasonably isochronous solution in which $\Delta T/T = 0.02$ due to all sources of dispersion ($\Delta E/E = \pm 3\%$, $\Delta\alpha = \pm 6\%$, $\Delta X = 2.0$ mm). A laboratory instrument was then designed and fabricated to specifications that produced a full size prototype suitable for the Cassini proposal (Fig. 8).

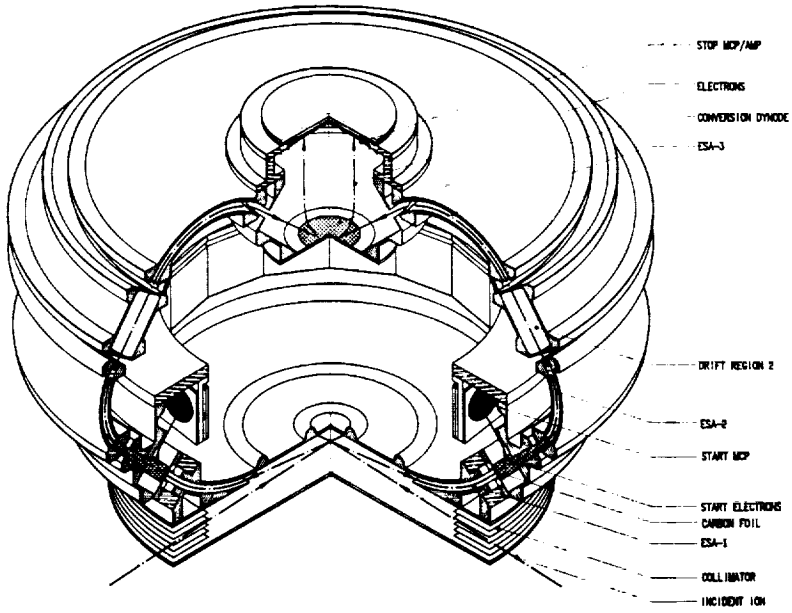

Figure 8. Orthographic drawing of ISOTOF laboratory prototype.

Unfortunately, preliminary transmission tests established that the toroidal ESA's did not have the correct analyzer constants. Machined values were $R/\Delta R = 5.32$ for ESA 3 and 5.56 for ESA 2, compared to the ray tracing requirement for equal values of 5.22. Deformations were caused by relaxation of the aluminum toroids following machining. We eventually corrected the $R/\Delta R$ problem, but were still faced with poor matching of the central ray position of the prototype toroids with the central ray position required by raytracing. This is a critical problem for poloidal toroidal optics due to the fact that incorrect positioning of the rays exiting ESA 2 as they enter ESA 3 produces a much larger positional error (aberration) than it does in non-toroidal optics. The reason is that the electric field is a function of particle phase angle in its orbit in poloidal toroidal optics (cf. Young and Marshall, 1990; Ghielmetti and Shelley, 1990) whereas this is not the case in spherical, cylindrical, and azimuthal toroidal optics.

Particle transmission through the combination of ESA 1, 2, and 3 of the ISOTOF was found to be very low due to mechanical misalignments (on the order of 0.5 mm) discussed above. After correcting these misalignments transmission increased, but we were never able to obtain a satisfactory TOF spectrum. In order to reduce spectral noise to is lowest level we have

ordered a commercial TOF electronics system out of SwRI funds and are currently awaiting delivery. If ISOTOF spectra can be obtained with new equipment then a supplement to the present report will be filed later detailing our results.

D. Linear Electric Field 3-Dimensional (LEF3D)

Strictly speaking most of the development of LEF3D has taken place at LANL under LANL internal funding. The decision to pursue LEF3D was undertaken, however, as an outgrowth of PIDDP studies of the ISOTOF. Furthermore, a lab prototype of LEF3D was built at SwRI for testing prior to submission of the Cassini proposal. Fig. 9 shows a cross section of the LEF3D while Fig. 10 shows mass spectra obtained in beam tests together with ray tracing simulation. The LEF3D was chosen by our PIDDP/PLS team as the candidate Ion Mass Spectrometer design for our successful Cassini proposal.

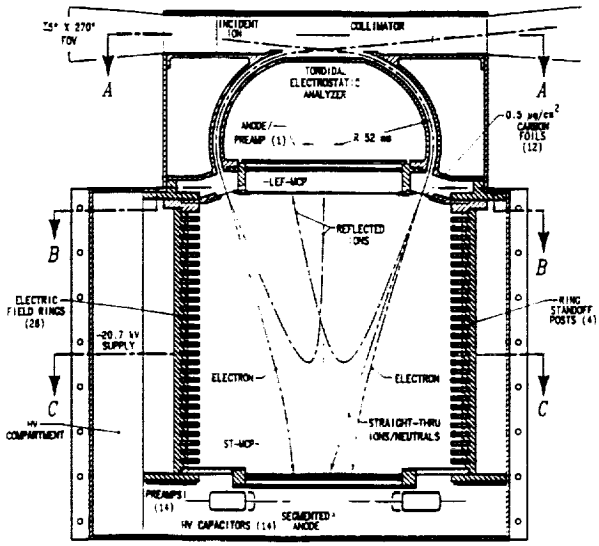

Figure 9. Cross section of LEF3D design chosen for the Cassini CAPS instrument.

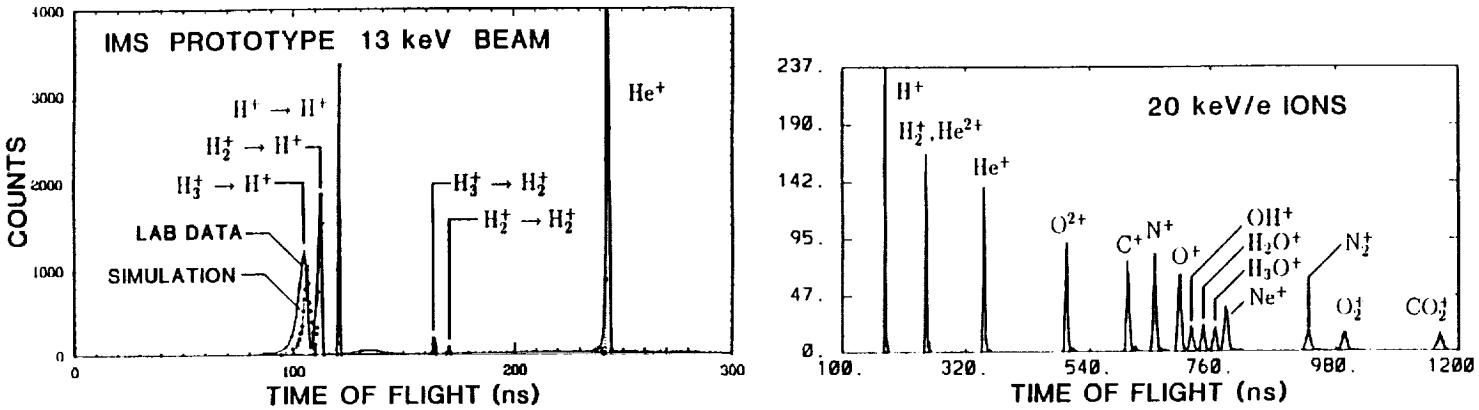

Figure 10. Simulated spectra for LEF3D.

E. Combinations

Figure 5 shows the LIPS elevation analyzer and magnetic sector developed for SPICE/CRAF. The long ion trajectory path through the tandem toroidal analyzers in FIMS tends to decouple the front-end elevation analyzer optics from the mass spectrometers. At the same time it was found that this solution reduces ion throughput to the mass spectrometer to a large degree. Whereas this is acceptable on the CRAF mission where spacecraft velocities are very low and cometary feature development is relatively slow, it was judged to lack sensitivity and time resolution for the Cassini/PLS proposal. Figure 11 shows an ion TOF spectrum obtained through the SPICE system in Figure 5.

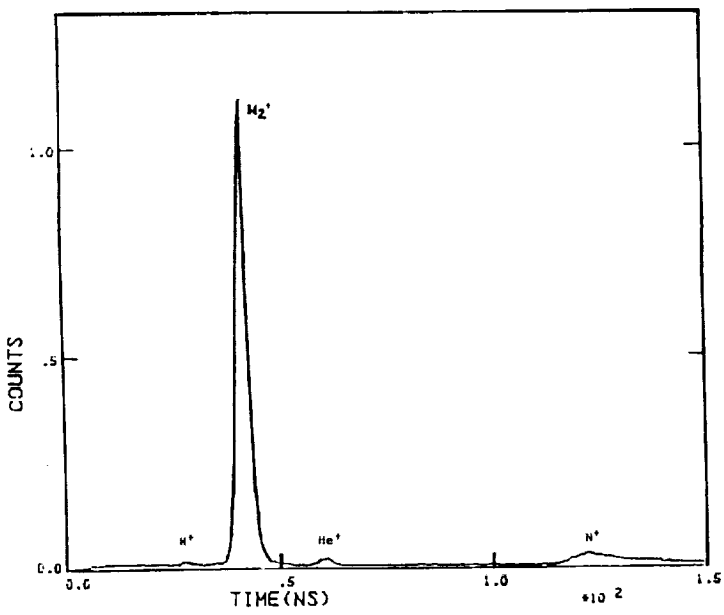

Figure 11. TOF spectrum obtained with SPICE/FIMS Elevation Analyzer system.

F. Digital TOF

Figure 12a shows a block diagram of the digital TOF (DTOF) measurement system developed at SwRI. The DTOF uses a gated 125 MHz oscillator to provide a low resolution measurement (to 8.25 ns) in combination with a 16 delay line vernier system that latches the clock waveform upon receiving a "stop" signal. the vernier thus provides ~ 0.5 ns timing resolution. Figure 12b is a sample DTOF spectrum.

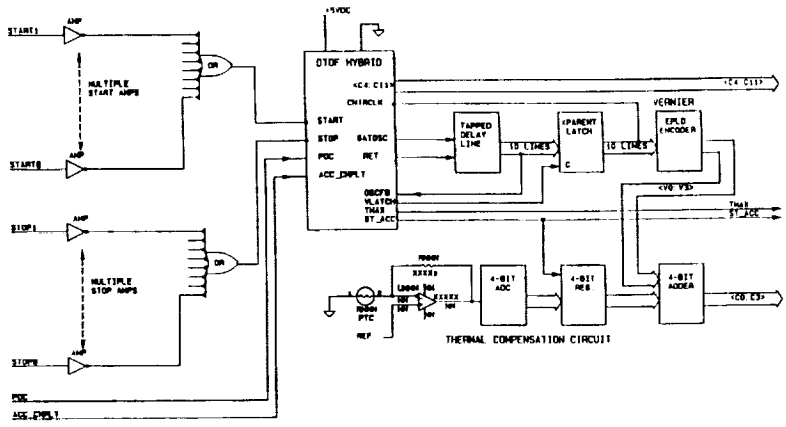

(a)

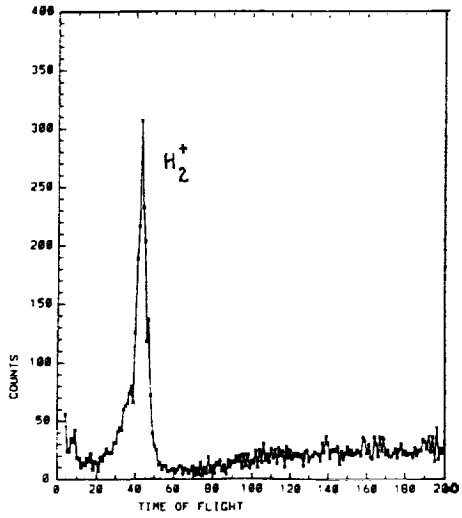

(b)

Figure 12(a). DTOF block diagram.
Figure 12(b). DTOF mass (time) spectrum.

One problem with our DTOF system was unevenness in the delay line vernier pickoffs (which are actually matched inductances rather than actual delay lines) that lead to bunching in the DTOF spectrum. A second problem was distortion of the initial clock waveform when the gated oscillator was turned on at the start of a measurement. Nonetheless we believe the principle is sound and are studying a similar, slightly more complex, DTOF for CRAF and Cassini. At the same time we are acquiring a newly developed commercial DTOF chip from LeCroy electronics which promises to provide the needed accuracy and stability at the power consumption required for our own DTOF design. This chip has become available only recently in response to the Superconducting Super Collider (SSC) and will not be available until mid 1991--hence it was not considered in our PIDDP or Cassini proposals.

IV. APPENDICES

A. Annual and Semi-Annual Reports on SwRI Grants NAGW 1286, NAGW 1286 Supplement 2, and LANL Contract W-7405-ENG-36.

B. Chapter C (Investigation Approach), Chapter D (Instrumentation), and Investigation Summary Sheet from SwRI Proposal 15-9376, "Plasma Science (PLS) Investigation for the Cassini Orbiter Spacecraft", by D. T. Young et al., Feb., 1990. This proposal was successfully completed for the PLS instrument (now renamed Cassini Plasma Spectrometer (CAPS)) on the Cassini Orbiter.

C. Publications based on PIDDP funding and related internal SwRI and LANL/DOE funding:

i. "Three-Dimensional Plasma Measurements from Three-Axis Stabilized Spacecraft", S. J. Bame, R. H. Martin, D. J. McComas, J. L. Burch, J. A. Marshall, and D. T. Young, Geophys. Monograph Ser., Vol. 54, 441, 1989.

ii. "A High-Speed Low-Power Spectrum Accumulator Using Dual-Port RAM and State Machine Control", W. L. Lockhart, J. H. Greene, and D. T. Young, IEEE Trans. Nuclear Sci., NS-36, 1396, 1989.

iii. "New Approach to 3-D, High Sensitivity, High Resolution Space Plasma Composition Measurements", D. J. McComas and J. E. Nordholt, Rev. Sci. Instrum., 61, 3095, 1990.

iv. "An Isochronous Poloidal Geometry Time-of-Flight Ion Mass Spectrometer for Energetic Space Plasmas", D. T. Young and J. A. Marshall, Nucl. Instrum. Methods Phys. Res., A298, 227, 1990.

V. REFERENCES

Bame, S. J., R. H. Martin, D. J. McComas, J. L. Burch, J. A. Marshall, and D. T. Young, Three-Dimensional Plasma Measurements from Three-Axis Stabilized Spacecraft, Geophys. Monograph Ser., Vol. 54, 441, 1989.

Ghielmetti, A. G., and E. G. Shelley, Angle, Energy, and Time-of-Flight Focusing With Poloidal Toroid Electrostatic Analyzers, Nucl. Instrum. Meth. Phys. Res., A298, 181, 1990.

Lockhart, W. L., J. H. Greene, and D. T. Young, A High-Speed Low-Power Spectrum Accumulator Using Dual-Port RAM and State Machine Control, IEEE Trans. Nuclear Sci., NS-36, 1396, 1989.

McComas, D. J. and J. E. Nordholt, New Approach to 3-D, High Sensitivity, High Resolution Space Plasma Composition Measurements, Rev. Sci. Instrum., 61, 3095, 1990.

Poschenrieder, W. P., Multiple-Focusing Time of Flight Mass Spectrometers Part I. TOFMS With Equal Momentum Acceleration, Int. J. Mass Spectrom. Ion Phys., 6, 413, 1971.

Poschenrieder, W. P., Multiple-Focusing Time of Flight Mass Spectrometers Part II. TOFMS With Equal Energy Acceleration, Int. J. Mass Spectrom. Ion Phys., 9, 357, 1972.

Young, D. T. and J. A. Marshall, An Isochronous Poloidal Geometry Time-of-Flight Ion Mass Spectrometer for Energetic Space Plasmas, Nucl. Instrum. Methods Phys. Res., A298, 227, 1990.

APPENDIX A

INSTRUMENTS TO MEASURE 3-DIMENSIONAL DISTRIBUTIONS OF ELECTRONS AND MASS-RESOLVED IONS ON 3-AXIS STABILIZED SPACECRAFT WITHOUT THE USE OF SCAN PLATFORMS

under the

PLANETARY INSTRUMENT DEFINITION AND DEVELOPMENT PROGRAM

Annual Report for the period 1/1/88 through 12/31/88

Submitted to:

Dr. Paul Mahaffy, Code EL
Discipline Scientist
Planetary Instrument Definition and Development Program
Solar System Exploration Division
NASA Headquarters
Washington, DC 20546

Prepared by:

Dr. David T. Young, Principal Investigator
Space Sciences Department
Southwest Research Institute
P.O. Drawer 28510
San Antonio, TX 78284

NASA Grant NAGW-1286 to SwRI
NASA Contract W-7405-ENG-36 to LANL

1. Introduction

Our results in instrument development during the period of performance have been reasonably successful and have followed closely on preliminary work that formed the basis for our original proposal. The goals of the proposed effort are 1) to develop plasma analyzers with electrostatically scanned fields-of-view (FOV), 2) to study time-of-flight (TOF) as a means of providing mass per charge analysis, and 3) to seek ways of combining the two.

Laboratory studies of one type of electrostatically scanned analyzer (the "Beacon" designs) show that this method of scanning is definitely workable, whereas a second type of scanning device (the "Gridded Truncated-Hemisphere") is less so. Details of these results are discussed below, as is a third type of scanning design which has given promising results in initial laboratory tests. On the second aspect of our proposal, time-of-flight (TOF) development, we have produced improved laboratory results using our low resolution TOF unit, and have carried out theoretical studies of a higher resolution, isochronous TOF design.

2. Summary of Progress

(In order to be brief, our original proposal is assumed as the point of departure for the remaining two sections of this report.)

2.1 Beacon Elevation Analyzers

Following extensive ray-tracing, a Beacon-C analyzer was fabricated at LANL and later tested in the ion calibration facility at SwRI. A sample of data from these tests is shown in Figure 1 to demonstrate that the Beacon elevation analysis concept works to deflect ions over a FOV cone of 15° - 90° thereby covering 1.93 π ster, or 96% of the half-sphere FOV. The structure seen in the left-hand peaks of the ion transmission profile are likely due to coarse (.020") grid wires used in the Beacon's grounded enclosure (cf. Figures 1, 3 of proposal). Deflection voltages given in Figure 1 agree well with those predicted from ray-tracing.

2.2 Gridded-Truncated-Hemisphere (GTH) Elevation Analyzer

A GTH prototype was constructed by forming a woven mesh grid over a mandrel and then securing (with epoxy) the base of the GTH thus formed. Unfortunately, tests of the GTH showed that, although it allows scanning of the analyzer FOV, transmission losses occur at several elevation angles where trajectories enter tangentially through more than one layer of mesh material. It was felt that the resulting strong variation in effective geometric factor with elevation angle would not be acceptable. Further design effort at SwRI has therefore gone into a deflection system that would scan $\pm$ 45° in elevation (vs. 0° $\rightarrow$ 90° for the GTH). This elevation analyzer concept (Figure 2) would also match with the requirements for the SPICE/FIMS instrument on CRAF. As with our original Beacon and GTH concepts, two such analyzers would be required to cover a full 4π ster. The elevation analyzer, shown in the upper portion of

Figure 2, has been ray traced and constructed as a lab prototype. It has demonstrated the required ±45° of deflection. The deflection sensitivity of this device varies with deflection angle, decreasing to $E_o/\Delta V \simeq 3.0$ at maximum deflection. Thus, for typical maximum analyzer plate voltages of +7.0 kV, maximum ion energies of 20 keV could be accommodated over the full ±45° of elevation. The lower part of Figure 2 shows the energy and low resolution TOF analyzers which have been tested separately as reported below. The actual combination shown in Figure 2 has not been ray traced or tested, and will be one subject of study in the second year of our program.

2.3 Time-of-Flight (TOF)

Recent tests of the low-resolution TOF system (Figure 2, this unit already existed before this PIDDP effort began) and upgrades made to our existing TOF electronics unit show that a resolution M/ΔM of 4 to 5 is all that be realistically expected of the non-focusing system (Figure 7a of proposal). We have experimented with "thinner" foils made of Formvar 15/95E (polyvinyl formal, Monsanto) in order to reduce straggling and improve M/ΔM, however it appears to us that Formvar foils are not uniform enough and, on average, possibly not even thin enough, to compete with the 1.0 $\mu g/cm^2$ carbon foils that we presently use.

As a result of the low resolution TOF tests, subsequent efforts have been put into finding an improved isochronous TOF (ITOF) design that can satisfy the rigorous requirements of the Cassini strawman payload, namely M/ΔM = 20. In our original PIDDP proposal we suggested that a resolution of 10 (measured at 1% of peak height) would be sufficient for Cassini, however it now appears that we will have to push our design to meet the newer and more difficult goal of 20. To accomplish this and still meet requirements for a 360° FOV that can be coupled to the elevation analyzers discussed above, we have investigated tandem toroidal analyzers that depart rather widely from our original concept (Fig. 7b of proposal) but that offer double focusing (i.e., focusing in angle-energy) and are a first step forward a triple focusing (angle-energy-time) system. Figure 3 shows raytracing through one such design. The most difficult issue to date is the problem of making the analyzer isochronous with respect to an energy dispersed beam. Ray tracing of this class of design has up to now produced mass resolutions of M/ΔM = 16 for incident beams of ±5° in angle, ±3.5% in ΔE/E and foil widths of 2.0 mm (in the plane of Figure 3). 3-D ray tracing shows that non-meridional rays degrade this resolution very little, thus a 360° FOV with the required mass resolution seems feasible.

3. Planned Activity for 1/1/89 through 10/31/89

3.1 Beacon Elevation Analyzers

A) Problems with the Beacon-C transmission will be corrected by mounting a much finer mesh (.001" wires vs. .020", although this is a technical challenge). The unit will be retested.

B) Further ray tracing will be used to map out the Beacon energy-angle passband for comparison with lab results.

C) The Beacon-D configuration will be tested.

3.2 GTH Elevation Analyzers

A) The new ±45° scanning design will be lab tested for full transmission properties as a function of azimuthal angle and energy. This has direct applicability to the SPICE design for CRAF.

B) Ray tracing will be run and used to confirm the properties of exit rays and to verify results of laboratory tests.

3.3 Time-of-Flight

A) Ray tracing of an isochronous design will be completed.

B) A mechanical design will be made based on 3.3(A) and taking into account the known constraints placed on such an instrument by the Cassini strawman payload for the PLS instrument (viz. 12.5 kg for electrons and ion composition).

C) Fabrication of a low cost lab prototype. Analyzer plates and insulating structures will be massive in order to cut machining costs. Microchannel plate detectors already in house for other programs, as well as existing TOF electronics, will be used.

D) Lab tests of lab PT and comparison of results with ray tracing.

3.4 Combining Elevation Analysis and TOF

We will attempt to carry out this final objective of our original proposal. However the loss of about $70 K from our original funding request (representing a reduction of 20%) makes it uncertain whether this can be accomplished. It is likely that additional PIDDP funds will be sought to complete this task.

FIGURE CAPTIONS

Figure 1. Nitrogen ion passbands for the Beacon-C laboratory prototype model measured in the SwRI calibration system. The analyzer voltage was held constant while the various deflection voltages shown above the individual peaks were applied one at a time. It is believed that the structure in the passbands below 45° elevation angle is caused by the .020 inch wires in the outer deflector cage through which the particles must pass at those angles. A revised deflector using fine mesh is being prepared for a test of this hypothesis.

Figure 2. Conceptual design of a low resolution TOF analyzer fitted with an elevation analyzer capable of ±45° elevation deflection up to energies of 20 keV. A similar elevation analyzer design is under study for the CRAF/SPICE instrument. Although the elevation and TOF elements have been ray traced and laboratory tested separately, they have not been studied in the configuration shown in Figure 2.

Figure 3. Ray tracing of an isochronous TOF design illustrating energy focusing of the transmitted ion beam. The axis of rotational symmetry is at the bottom of the page. Data in the figure give initial ion position (XO, YO) energy (EO), angle (THETA) and charge and mass (Q, M). Final energy (E) and elapsed trajectory time (T) are also given.

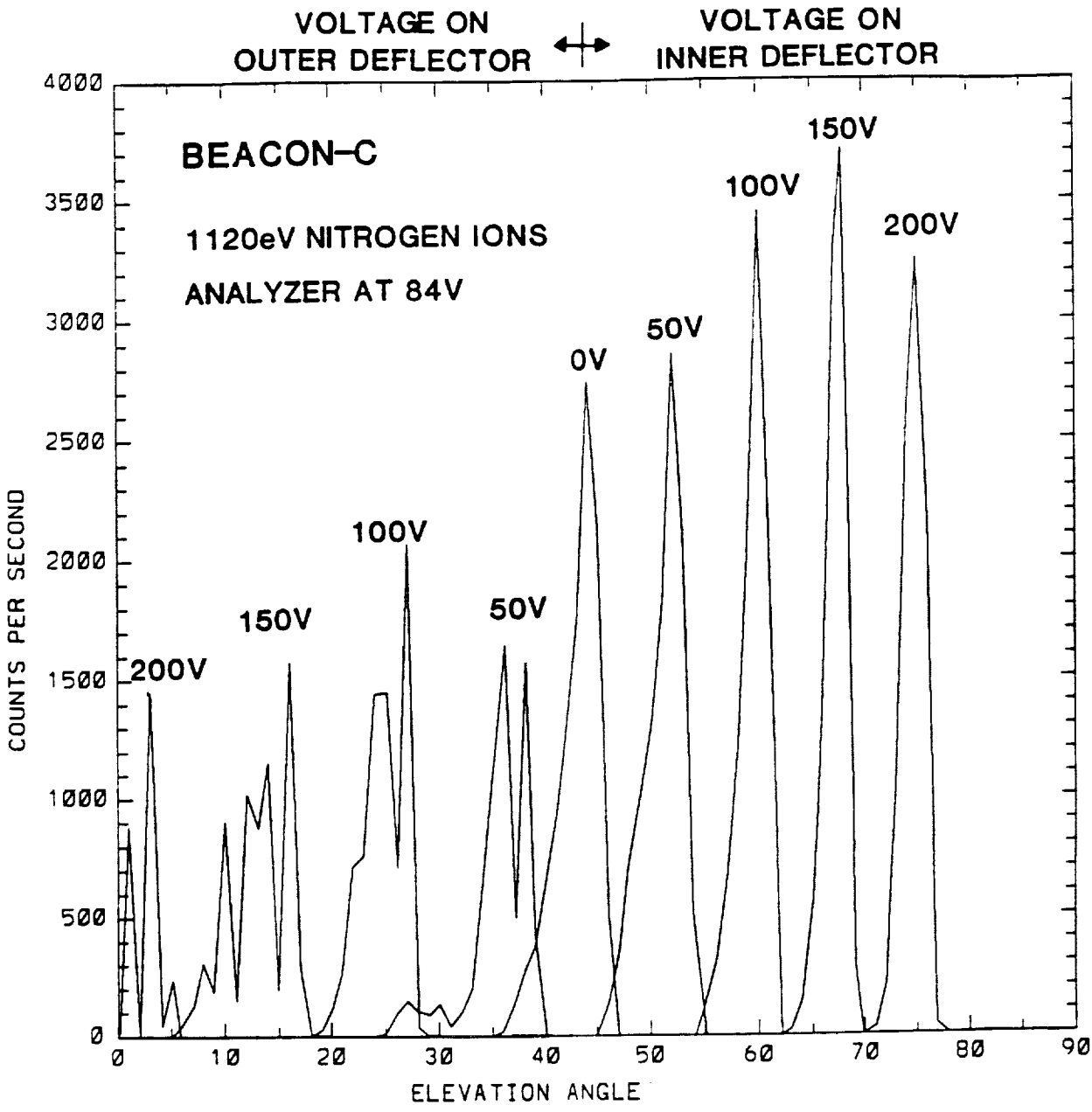
VOLTAGE ON
OUTER DEFLECTOR
VOLTAGE ON
INNER DEFLECTOR
BEACON-C
1120eV NITROGEN IONS
ANALYZER AT 84V
200V
150V
100V
50V
0V
50V
100V
150V
200V
COUNTS PER SECOND
ELEVATION ANGLE
0
500
1000
1500
2000
2500
3000
3500
4000
0
10
20
30
40
50
60
70
80
90

Figure 1

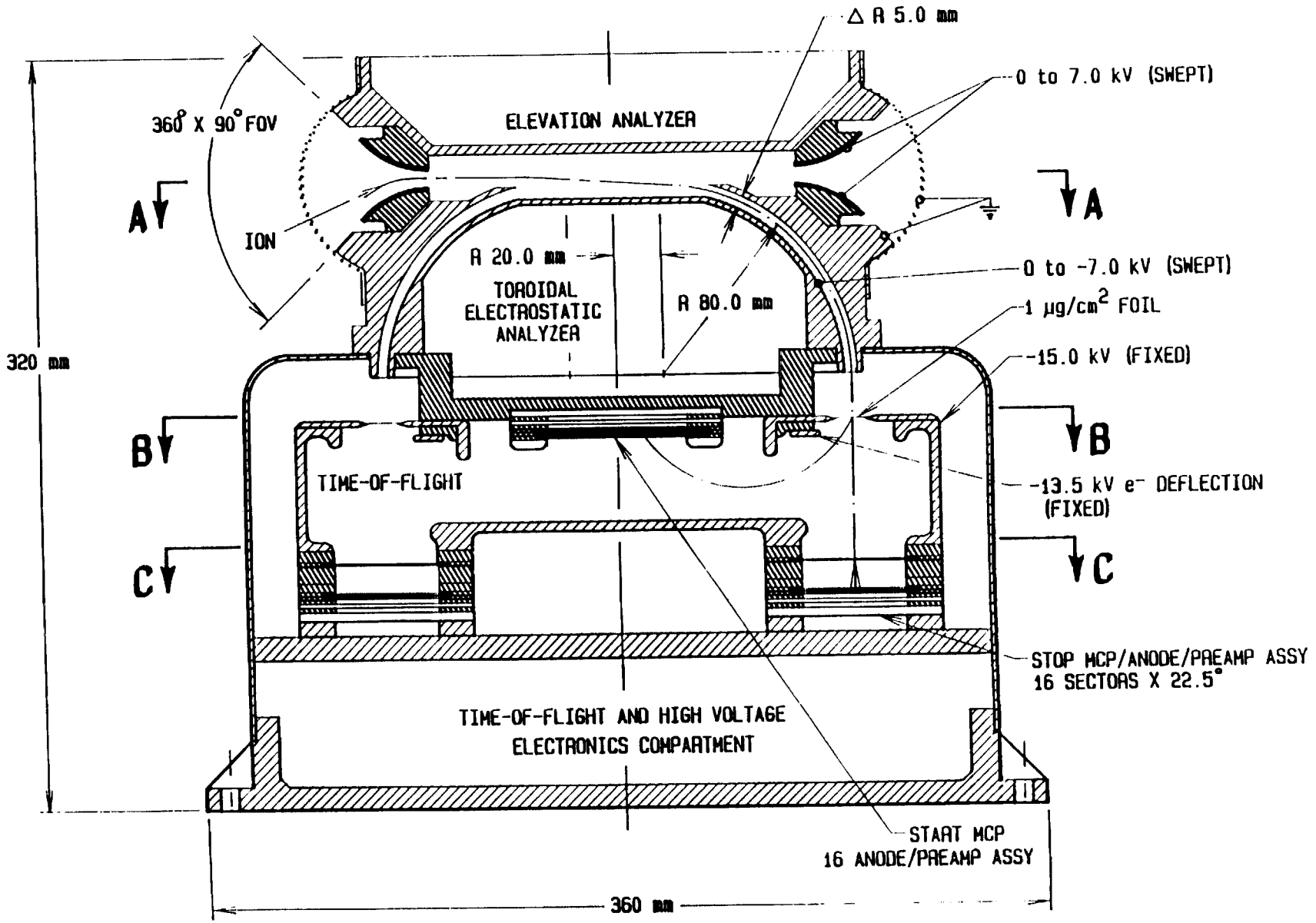

HOT PLASMA COMPOSITION ANALYZER

Figure 2

ISO-TOF Double Focus; +/-900. from -30kv; 4mm stops; on CONVEX

K	X0	Y0	E0	THETA	Q	M	B	E	T
1	1.041E+01	1.041E+01	2.350E+04	42.500	1.	1.00	0.000E+00	3.022E+04	2.613E-08
2	1.041E+01	1.041E+01	2.400E+04	42.500	1.	1.00	0.000E+00	2.612E+04	2.695E-08
3	1.041E+01	1.041E+01	2.450E+04	42.500	1.	1.00	0.000E+00	3.019E+04	2.873E-08
4	1.041E+01	1.041E+01	2.500E+04	42.500	1.	1.00	0.000E+00	3.080E+04	3.051E-08
5	1.041E+01	1.041E+01	2.550E+04	42.500	1.	1.00	0.000E+00	2.533E+04	3.304E-08
6	1.041E+01	1.041E+01	2.600E+04	42.500	1.	1.00	0.000E+00	2.637E+04	3.284E-08
7	1.041E+01	1.041E+01	2.650E+04	42.500	1.	1.00	0.000E+00	2.613E+04	3.301E-08
8	1.041E+01	1.041E+01	2.700E+04	42.500	1.	1.00	0.000E+00	2.697E+04	3.282E-08
9	1.041E+01	1.041E+01	2.750E+04	42.500	1.	1.00	0.000E+00	2.762E+04	3.963E-08
10	1.041E+01	1.041E+01	2.800E+04	42.500	1.	1.00	0.000E+00	2.949E+04	8.131E-08
11	1.041E+01	1.041E+01	2.850E+04	42.500	1.	1.00	0.000E+00	2.995E+04	8.203E-08
12	1.041E+01	1.041E+01	2.900E+04	42.500	1.	1.00	0.000E+00	3.040E+04	8.276E-08
13	1.041E+01	1.041E+01	2.950E+04	42.500	1.	1.00	0.000E+00	3.098E+04	8.383E-08
14	1.041E+01	1.041E+01	3.000E+04	42.500	1.	1.00	0.000E+00	3.143E+04	8.459E-08
15	1.041E+01	1.041E+01	3.050E+04	42.500	1.	1.00	0.000E+00	3.202E+04	8.568E-08
16	1.041E+01	1.041E+01	3.100E+04	42.500	1.	1.00	0.000E+00	3.108E+04	3.868E-08

3-Nov-88
16:52:18

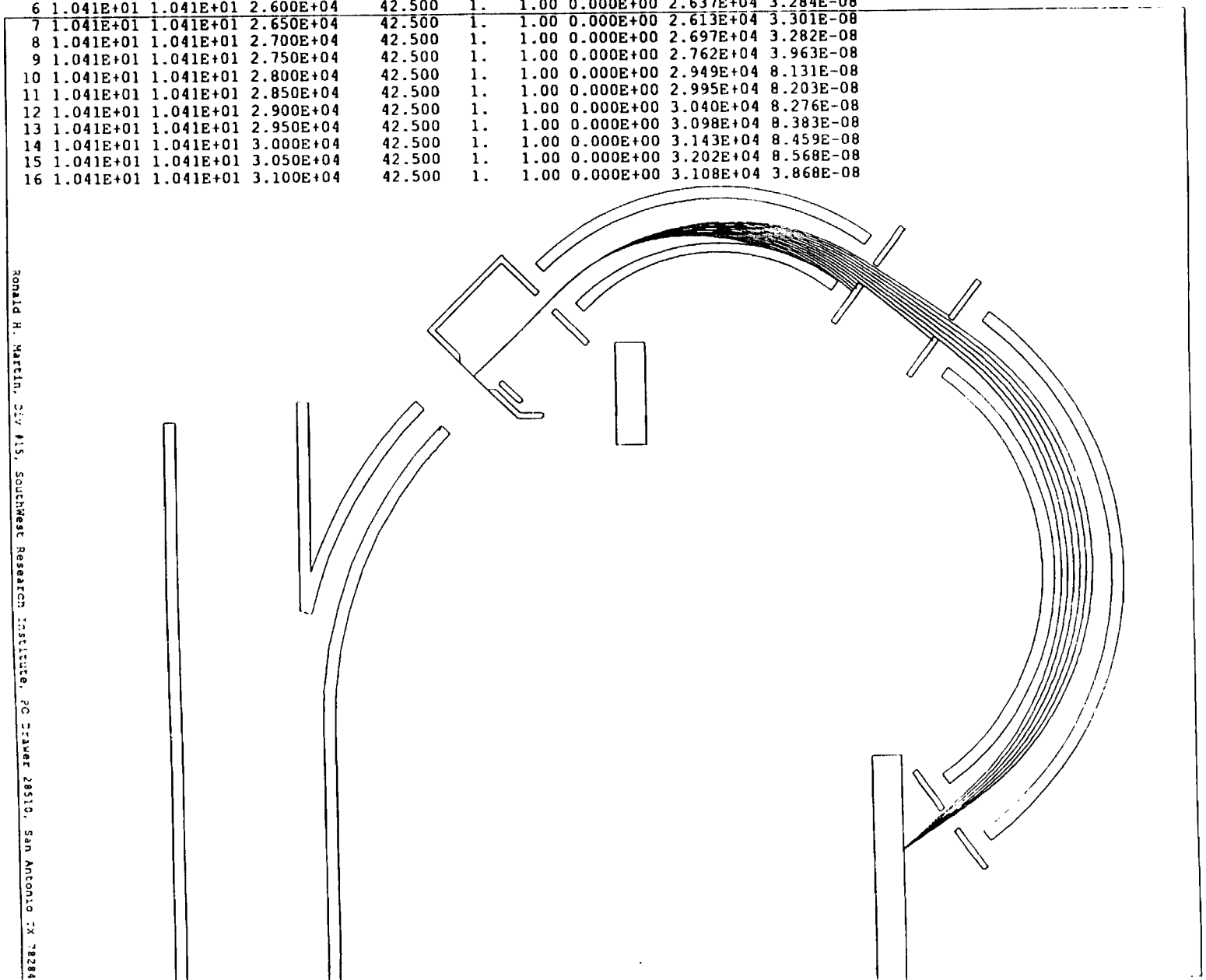

Ronald H. Martin, Div #15, SouthWest Research Institute, PO Drawer 28510, San Antonio TX 78284

Figure 3

INSTRUMENTS TO MEASURE 3-DIMENSIONAL DISTRIBUTIONS OF ELECTRONS AND MASS-RESOLVED IONS ON 3-AXIS STABILIZED SPACECRAFT WITHOUT THE USE OF SCAN PLATFORMS

under the

PLANETARY INSTRUMENT DEFINITION AND DEVELOPMENT PROGRAM

Semi-Annual Report for the period 1/1/89 through 6/30/89

Submitted to:

Dr. Paul Mahaffy, Code EL
Discipline Scientist
Planetary Instrument Definition and Development Program
Solar System Exploration Division
NASA Headquarters
Washington, DC 20546

Prepared by:

Dr. David T. Young, Principal Investigator
Space Sciences Department
Southwest Research Institute
P.O. Drawer 28510
San Antonio, TX 78284

NASA Grant NAGW-1286 to SwRI
NASA Contract W-7405-ENG-36 to LANL

1. Introduction

Following completion last year (see Annual Report for 1988) of the bulk of our research with swept field-of-view electrostatic analyzers, we have concentrated on development of the time-of-flight (TOF) method of ion mass analysis. In particular the isochronous TOF (ITOF) concept has been pursued vigorously at both SwRI and LANL. The system at SwRI is presently more advanced and will be discussed in more detail. Efforts at LANL center on a harmonic oscillator linear electric field concept which has been thoroughly ray traced, but not yet prototyped. The ITOF design at SwRI is presently being fabricated.

2. Isochronous-Time-of-Flight

The initial stage of ray tracing of a toroidal analyzer system that accomplishes ITOF measurements has been completed at SwRI. This system has been further developed into a workable mechanical design and sent out for fabrication. One rather surprising result of ray tracing studies is that we have found it may be feasible to incorporate a third dimension of focusing into the ITOF design.

By judiciously applying our 2 1/2-D ray tracing code we have found that the electrons leaving the start-TOF foil in our Cassini design can be forced to focus onto a small MCP by the intervention of a number of narrow electrodes placed in a regular pattern along the field boundaries of the (formerly) axisymmetric design. In this way the analyzer is no longer axisymmetric, but the advantage is that start electrons are focused in a 3-D sense as they travel from the start foil to the MCP. This has the practical advantages that start MCPs can be made smaller (with smaller, cheaper, simpler and lighter weight housings) and of conventional design (hence MCPs will be cheaper and more reliable as well).

Because no fully 3-D particle codes are available we will have to await fabrication of the Cassini ITOF laboratory prototype to test 3-D focusing. However, the 2 1/2-D simulations of pseudo 3-D focusing were promising enough that we are fabricating the necessary parts for lab tests.

3. Future Work

The remainder of the year will be devoted to completing ITOF fabrication and initiating testing on all aspects of 3-D ITOF. It is expected that LANL will complete a prototype of the linear electric field TOF and perform at least preliminary tests. Some work remains to be done on the scanned FOV electrostatic analyzers as originally proposed. This will be carried out, however in the time since our original PIDDP proposals were written it has become increasingly apparent that NASA will use a turntable to alleviate the scanning problem on the Cassini MMII spacecraft. Scanned FOVs do remain a viable option for SPICE instruments on CRAF and will continue to be investigated.

HIGH MASS RESOLUTION, HIGH ANGULAR ACCEPTANCE TIME-OF-FLIGHT MASS SPECTROSCOPY FOR PLANETARY MISSIONS

under the

PLANETARY INSTRUMENT DEFINITION AND DEVELOPMENT PROGRAM

Semi-Annual Report for the period 7/1/89 through 12/31/89

Submitted to:

Dr. Paul Mahaffy, Code EL
Discipline Scientist
Planetary Instrument Definition and Development Program
Solar System Exploration Division
NASA Headquarters
Washington, DC 20546

Prepared by:

Dr. David T. Young, Principal Investigator
Space Sciences Department
Southwest Research Institute
P.O. Drawer 28510
San Antonio, TX 78284

NASA Grant NAGW-1286
SwRI Project 15-2351

Note: Although Supplement 2 to NAGW-1286 has been approved, no funds have been received at SwRI. The following is an interim report.

REPORT

Due to some loss of funding from our original PIDDP proposal, and to the absence of supplemental funds, we have continued studies primarily in the area of time-of-flight (TOF) instruments suitable for the Cassini Orbiter spacecraft. We have completed ray-tracing studies of a TOF analyzer and have constructed a laboratory prototype of the isochronous TOF (ISOTOF) design. Initial testing of the first (E/Q) analyzer has been completed in the ion beam at SwRI. Following these tests, the Cassini instrument consortium of which SwRI is the leader, decided to investigate a second, more promising, TOF design, the linear-electric-field (LEF) time-of-flight (LEFTOF). IN collaboration with Los Alamos National Laboratory (LANL) we have built a prototype of the LEFTOF design for testing at SwRI during January 1990. (The LEFTOF has been constructed using a small amount of funding from our NRA program, and internal research funds.) We expect to use some of the PIDDP supplemental funds to complete testing of both ISOTOF and LEFTOF designs in the next half year and prepare publications comparing the designs. One design or the other will be chosen for our Cassini proposal and will be fully described therein.

HIGH MASS RESOLUTION, HIGH ANGULAR ACCEPTANCE TIME-OF-FLIGHT MASS SPECTROSCOPY FOR PLANETARY MISSIONS

under the

PLANETARY INSTRUMENT DEFINITION AND DEVELOPMENT PROGRAM

Annual Report for the period 7/1/89 through 6/30/90

Submitted to:

Dr. William Brunk, Code EL
Discipline Scientist
Planetary Instrument Definition and Development Program
Solar System Exploration Division
NASA Headquarters
Washington, DC 20546

Prepared by:

Dr. David T. Young, Principal Investigator
Space Sciences Department
Southwest Research Institute
P.O. Drawer 28510
San Antonio, TX 78284

NASA Grant NAGW-1286
SwRI Project 15-2351
Supplement 2

1. Introduction

The Isochronous Time-of-Flight (ITOF) is a mass spectrograph of novel design that consists of a set of three toroidal electrostatic analyzers arranged in tandem (Fig. 1). The purpose of this device is to simultaneously provide high mass resolution ($M/\Delta M \sim 25$) and very broad angular coverage (up to 360°) over the full range of ion energies found in the plasmas of the outer planets (~ 1 eV to 50 keV). The ITOF incorporates a novel ion optical design in which ions travel through the toroidal analyzers in the poloidal direction as shown in Fig. 1. Poloidal trajectories have the peculiar property that the electric field vector changes continuously along a particle trajectory. This makes the ITOF optics fundamentally different from other optical systems described in the literature, allowing a longer flight path and higher resolution than would otherwise be available. It also makes their design more problematic.

During the past year we have completed fabrication, assembly and initial testing of an ITOF system capable of meeting our requirements. Following an initial design period, the subsequent delays in the funding of the PIDDP (we received FY 90 funding only in April 1990) have slowed the pace of laboratory work and, as a result, testing of the ITOF is not complete.

We have used the intervening time to write the attached paper giving a detailed description of work on ITOF to date. This paper has been accepted for publication in Nuclear Instruments and Methods and is attached in preprint form to give more detail on the ITOF work. Highlights of work during the past year are given below.

2. The Isochronous Time-of-Flight System

During laboratory testing of the ITOF it was found that mechanical alignment of the toroidal analyzer plates and matching of the voltages applied to them had to be more precise than previously thought. The reason is the property of poloidal trajectories in toroidal electric fields referred to above. Thus we have obtained ion transmission through the complete set of analyzers (see Fig. 6 of the attached paper) with the center analyzer potential at ground, but are unable to do so at elevated potentials due to stray electric fields and toroid misalignments. This hypothesis is currently under analysis with ray tracing and will be tested in the laboratory.

3. Future Work

In the remainder of this calendar year we will re-test the ITOF prototype with improved mounting accuracy for the mechanical parts and, in some cases, with different fringe-field corrections in place. Once we have corrected alignment and stray field problems, ITOF mass spectra will be obtained and the instrument performance will be documented for a range of incident energies and angles. Mass resolution will be measured for a range of ion species including molecular ions.

4. Appendix (See Attached)

"An Isochronous Poloidal Geometry Time-of-Flight Ion Mass Spectrometer for Energetic Space Plasmas," D. T. Young and J. A. Marshall, Nucl. Instrum. Methods, accepted for publication, June 1990.

ISOCHRONOUS TIME-OF-FLIGHT MASS SPECTROGRAPH (SCHEMATIC)

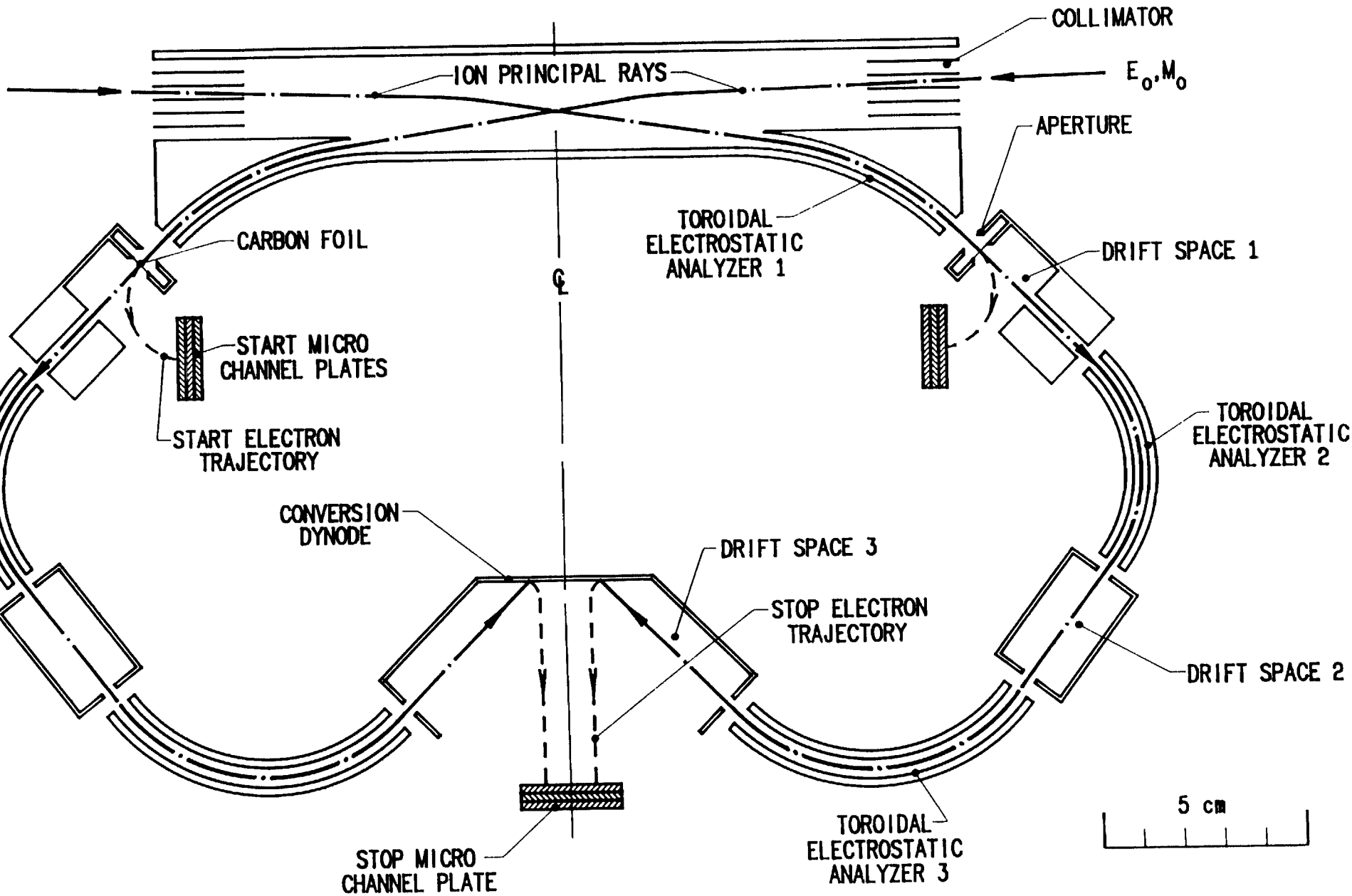

Figure 1

APPENDIX B

CASSINI PLASMA SCIENCE INVESTIGATION SUMMARY

SUBSYSTEM	IMS Ion Mass Spectrograph	IBS Ion Beam Spectrometer	ELS Electron Spectrometer
Principle of analysis	Toroidal electrostatic, isochronous time-of-flight with linear electric field	Hemispherical electrostatic with crossed fans	Spherical section electrostatic
Heritage	CRRES, Polar, PIDDP	Ulysses, ISEE-1, IMP	Cluster, AMPTE-UKS
Analysis parameters(1)	E/Q, M/Q, Q, AZ, EL	E/Q, AZ, EL	E/Q, AZ, EL
E/Q range	1 to 50,000 eV/e	1 to 50,000 eV/e	0.8 to ~~20,000~~ 30,000 eV/e
E/Q resolution (ΔE/E)	0.17	0.013	~~0.12~~ 18.5%
FOV(2) (AZxEL)	11° x 270°	1.4° x 160° (3 fans)	5° x 270°
Angular resolution	11° x 22.5°	1.4° x 1.4°	5° x 22.5°
M/Q range	1 to > 50 amu/e	----	----
M/Q resolution (M/ΔM at 10%)	>30(1<E/Q<24,000 eV/e) ≥8(24,000<E/Q<50,000 eV/e)	----	----
Geometric factor x efficiency (cm^2 sr eV/eV) a) full FOV b) per pixel	 1.3×10^{-2} 1.1×10^{-3} (M/ΔM>8) 1.0×10^{-4} (M/ΔM>30)	 6.0×10^{-5} 1.0×10^{-6}	 1.3×10^{-2} 1.1×10^{-3}
Dynamic range	$<10^{-2}$ to 5×10^{5} cts/s	1 to 10^{7} cts/s	1 to 10^{7} cts/s
Time resolution(3) Single sample 2-D snapshot 3-D snapshot	 52.1 ms 1.67 s 30 s	 52.1 ms 1.67 s 60 s	 52.1 ms 1.67 s 30 s
Data Processing Unit: two SA3300 microprocessors; 896 kbytes RAM; heritage = CRAF, GGS/Polar			
Mass: total including 6% margin = 12.5 kg **Volume:** 24.1 liters total (irregular shape 44.2 cm x 40.4 cm x 30.0 cm) **Power:** maximum consumption including 13% margin = 14.5 W (includes 0.75 W BIU power) **Telemetry:** minimum required 20 b/s (cruise phase), 1600 b/s (encounter); maximum = 16,000 b/s **Temperature Range:** -10°C to +50°C operating, -20°C to +60°C storage **Location:** Orbiter turntable **EMI Suffered:** minimization of S/C charging is desired **EMI Caused:** elecrically shielded to pass MIL-STD-461A, no static magnetic field sources			

Notes:
(1) E/Q = energy/charge, M/Q = mass/charge, AZ = azimuthal angle, EL = elevation angle
(2) Field-of-view (FOV), IMS and ELS are capable of 360°; limited to ~270° by spacecraft obscuration
(3) Assuming 1 rpm nominal turntable rate, but compatible with 0.1 rpm and 3.0 rpm rates

C. INVESTIGATION APPROACH

C.1. Introduction

The scientific objectives described above encompass an unprecedented variety of plasma processes and parameters, not only within the Saturn system but also during the cruise and Jupiter-flyby phases of the mission. At the same time, the Cassini mission is tightly constrained with respect to all spacecraft resources, including cost, mass, volume, power, and telemetry. We propose to meet this challenge by providing a complement of three plasma sensors based on proven technology: the Ion Mass Spectrograph (IMS), the Ion Beam Spectrometer (IBS), and the Electron Spectrometer (ELS), all under the control of a single Data Processing Unit (DPU) that is based on dual SA3300 microprocessors. This sensor triad will ensure measurements of complete mass-resolved plasma distribution functions over a sufficient parameter range and with sufficient resolution to attack the problems raised by PLS science objectives.

The sensor energy ranges extend high enough to overlap the anticipated MIMI and energetic particle investigations that are part of the strawman payload. Although obscuration by the spacecraft itself limits the IMS and ELS fields-of-view to 85% of the full 4π sr field-of-view ideally desired, it is anticipated that modeling of particle distribution functions in combination with spacecraft maneuvers planned for other purposes will prevent any compromise of significant data. Time resolution for fully 3D measurements will be 30 s, driven primarily by the nominal turntable spin period of 1 minute. This is fully adequate for nearly all science objectives except for the steepest spatial/temporal gradients, for which 2D snapshots will be available at 1.67 s resolution. The selection of dual SA3300 microprocessors for instrument control and data processing is based on the need for significant in-flight data management and computation and on our experience with this system on the Polar and CRAF missions. Dual processors are needed to handle the large computational load; however, the system is cross-strapped to provide a limited level of redundancy.

All three sensors have been developed through extensive analytical particle optics and computer simulations to arrive at estimates of basic design parameters and expected performance. Sensors have been built and tested either as prototypes (IMS, ELS) or as flight hardware (IBS). Figure 2 shows the PLS sensor configuration on the turntable and photographs of sensor prototypes. Similarly, the DPU microprocessor and related circuits have been built as a single-board computer for the GGS/Polar and CRAF programs and tested with simulated mass spectrometer data in order to establish critical timing information for on-board reduction and compression algorithms. Thus the following approaches to sensor design have all been thoroughly developed and tested in the laboratory. It is expected that minimal effort will be required to reach a final design for production of flight hardware. This is a necessary condition given the time and cost constraints of the MMII/Cassini Program.

C.2. Ion Mass Spectrograph (IMS)

The need to resolve multiple sources of hot magnetospheric plasmas requires high mass resolution up to 50 keV/e, a demand that is unique to the Cassini mission. For

CASSINI PLASMA SCIENCE INVESTIGATION

PLS

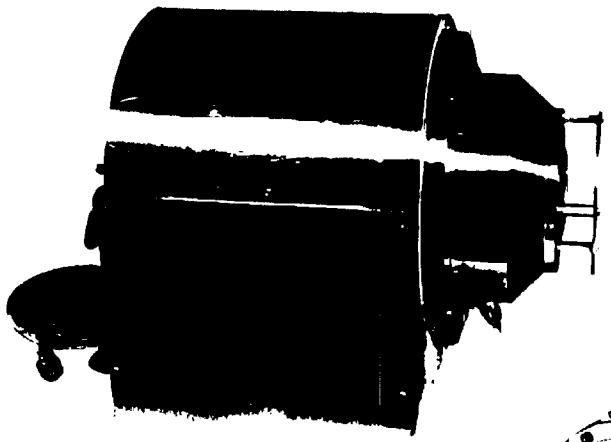

IMS

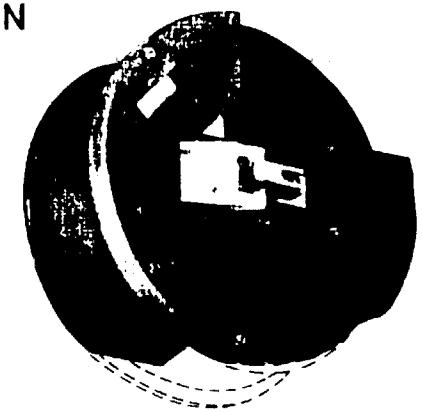

IBS

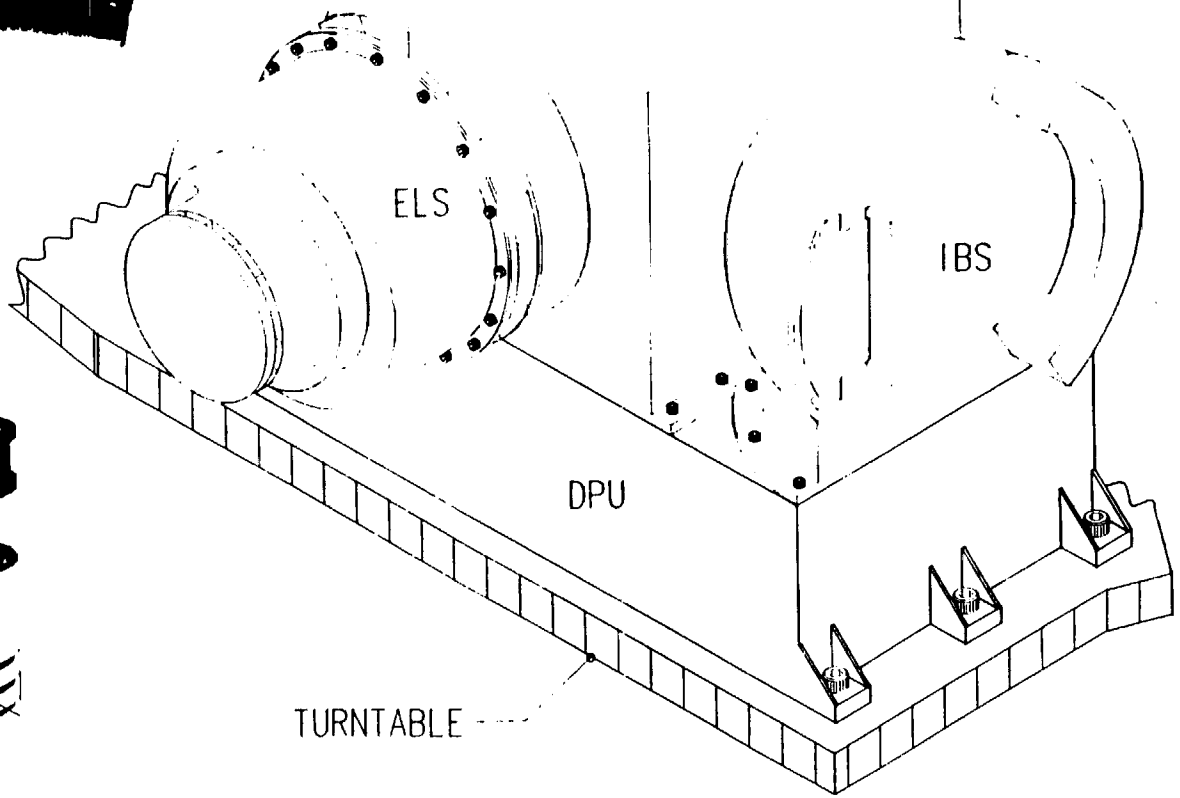

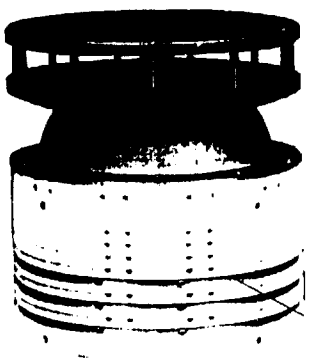

ELS

Figure 2. An isometric drawing of the Cassini **PLS** sensor units (shown in the 3 photographs) integrated in flight configuration with the **Data Processing Unit**. The **Ion Mass Spectrograph (IMS)** prototype shown is one of two constructed and tested as development models. The toroidal electrostatic analyzer appears to the right in this photo. Based on the ISEE-1 crossed-fan electrostatic analyzer (photo in upper right-hand corner), the **Ion Beam Spectrometer (IBS)** optics and technology are sufficiently well known that a prototype is not required. The version of the **Electron Spectrometer (ELS)** shown in the lower left-hand corner was flown on the Polar ARCS sounding rocket. It serves as a prototype for spectrometers on both Cluster and Cassini. The fully integrated **PLS** occupies 44.2 cm x 40.4 cm x 30.0 cm in height and weighs 12.5 kg including a 6% margin.

example, we have shown in Section A.2.a. that it is important to separate N^+ from O^+, for which $M/\Delta M > 7$ is required, and also to separate the water group of molecules near M/Q = 18 for which $M/\Delta M > 18$ is required. It is also evident that there are potential ambiguities in the identification of many other ion species, given the existence of atomic and molecular species that are identical or nearly identical in mass such as O^+ and CH_4^+. Still heavier hydrocarbon compounds are expected to be represented by a multiplicity of molecular species for which $M/\Delta M$ as high as 30 is desirable.

Considerations of the need for high mass resolution at relatively high ion energies, for the separation of molecular vs. atomic species, for high sensitivity, and for a very wide acceptance geometry of 270° or more have led our design effort away from magnetic mass spectroscopy. The amount of magnetic material required for resolution of energetic ions near the upper limit of the PLS energy range (~50 keV) rapidly increases instrument weight for a given geometric factor and mass resolution. The same is true of any attempt to increase spectrometer sensitivity. Furthermore, magnetic spectroscopy cannot cope with the problem of resolving the identity of molecular versus atomic species or of H_2^+ from He^{2+}.

Time-of-flight (TOF) methods, on the other hand, generally benefit from high particle energies because of decreased straggling in the carbon foils that are used to generate timing signals. However, because of the lack of focusing in many TOF systems, straggling also severely limits their mass resolving capabilities. Straggling introduces energy and angle dispersion in addition to that caused by finite E/Q analyzer passbands, which translates into temporal dispersion that limits mass resolution compared to that of a focusing device unless very high (~50 kV) accelerating potentials and very narrow E/Q analyzer passbands are used. In addition, although the carbon foils used in TOF can have areas one order of magnitude larger than the corresponding aperture of a magnetic system (e.g., ~1 cm^2 vs. 0.1 cm^2), this gain in aperture is offset by a loss in detection sensitivity if the TOF device cannot respond to the largely neutral flux of charge-exchanged particles exiting the foil. Thus the ideal TOF system would incorporate both temporal focusing to guarantee high mass resolution, and neutral particle detection to maintain high sensitivity. Our IMS approach meets both of these requirements with an isochronous (i.e., temporal focusing) design that focuses ions yet allows neutrals to be detected as well. We have taken further advantage of the isochronous feature to choose IMS energy ($\Delta E/E = 0.17$) and angular (11°) acceptances that are relatively wide in order to meet the need for "fast" (i.e., high sensitivity) plasma composition measurements. Our team has designed and built low-resolution TOF plasma analyzers for the CRRES and Polar missions, as well as a prototype for Cluster (Young *et al.*, 1989). Experience with these systems led us to use PIDDP support to investigate several isochronous TOF devices, which has resulted in the approach described here.

Finally, the TOF approach lends itself easily to spectrographic as opposed to spectrometric capabilities. The TOF system detects any ion species at any time, at a rate of up to 500,000 events/s. Since all species are seen "simultaneously" (within the electronic dead time) there is no need for mass scans that reduce measurement duty cycle. Still another advantage of the TOF technique is its inherent background rejection; because it requires coincidence (within $\leq 1\mu s$) between start, stop, and anode position pulses, the majority of the background due to radiation and thermal noise is rejected.

C.3. Ion Beam Spectrometer (IBS)

As described above, the IMS sensor is specialized for hot, diffuse, very low density plasmas. It cannot, without significant functional compromises, measure the very narrow and locally intense ion beams associated with high-Mach-number flows in the solar wind (M ~40), in auroral ion beam outflows, or in Titan ram distributions. Nor can it cope with narrow features of pitch angle distributions expected for ion loss and source cones in the auroral ionosphere. The IBS perfectly complements the IMS by meeting these requirements and providing, once per spin, a detailed map of features as narrow as 1° in the ion distribution corresponding approximately to $2\Delta E/E \sim \Delta\theta \sim 1/M$. The design of the IBS is fully developed, being based on that of a "crossed-fan" solar wind ion spectrometer successfully flown on ISEE-1 (Bame *et al.*, 1978). The IBS is composed of a single hemispherical electrostatic analyzer with three fan-shaped fields-of-view. The analyzer design makes it easy to meet the 50 keV/e energy requirement. This FOV arrangement is scanned by orbiter turntable motion to give a 3D ion velocity measurement that yields all ion distribution parameters including ion heat flux.

C.4. Electron Spectrometer (ELS)

The electron sensor must be capable of measuring relatively broad as well as narrow angular distributions over a wide range of density and energy. In addition, sufficiently high sensitivity is required in order to meet time resolution constraints. As in the case of the IBS, our approach in designing the electron sensor has been to meet these measurement goals while taking into account the need to fly well-developed and tested instrumentation. This is best achieved by using a spherical top-hat analyzer based on the design chosen for the electron sensor on the Cluster mission. The energy range from 0.8 to 20,000 eV covers the solar wind as well as the Saturn environment.

C.5. Data Processing Unit (DPU)

Each of the three sensors, but particularly the IMS, produces a large array of measurements during one spin period. Given the nominal PLS telemetry allocation of 1600 b/s, on-board data reduction and compression by a factor ~25:1 must take place in order to transmit the full 3D distributions to Earth. We are confident that this reduction/compression goal can be met by using the same approach to DPU design as that taken on the TIDE/Polar (where the corresponding factor is ~80:1 without loss of pertinent information) and SPICE/CRAF programs, namely a DPU built around the SA3300 processor and associated chip set. Since the SA3300-based system is entirely adequate for PLS requirements, the Polar program leads Cassini development by 3 years, and the same dual-SA3300 processor design is being used by our group for SPICE and CRIMS on CRAF, we are confident that the SA3300 represents a conservative yet high-performance approach to the PLS DPU requirements.

D. INSTRUMENTATION

D.1. Sensor Design Requirements

The purpose of this section is to justify performance features of the PLS sensors summarized in the table on page iii. This provides the link between science objectives and the actual instrument designs described in Sections D.2 to D.4. Design features common to all three sensors, including high-voltages, sensor covers, and radiation tolerance, are described in Section D.5. Figure 3 gives details of sensor mechanical accomodation on the Orbiter turntable, fields-of-view, and overall package dimensions.

D.1.a. Field-of-view (FOV). Three-dimensional plasma measurements are an essential science requirement. However, full 3D is impractical for turntable (TT) mounted sensors on the Orbiter because of FOV obscuration caused by the spacecraft body, which subtends a cone of roughly 45° half angle centered on the TT boom. Thus the ELS and IMS fields-of-view have been limited intentionally to 270° of elevation (85.4% coverage of the unit sphere). The remaining occluded 90° of the sensor cylinder is used to house mechanical structure, signal wires to the ELS and IMS sensors, and aperture opening mechanisms (Fig. 4a, c). The IBS suffers no FOV obscuration.

D.1.b. Energy Range and Resolution, Angular Resolution. Voyager data indicate that the bulk of ion distributions will be found below 50 keV and electrons well below 20 keV. Moreover the IMS and IBS energy ranges ensure good overlap with the anticipated ranges of the HPD and MIMI instruments included in the Cassini strawman payload. Energy resolution is consistent with throughput requirements and is set to match science requirements. The IBS has very high energy resolution (1.3%) requiring 600 log-spaced energy steps, which suggests that its energy stepping be guided by the on-board identification of ion peaks in either its own or IMS data. IBS resolution meets requirements for observations of high-Mach-number (M ~ 40) solar wind and for angular resolution (1.4°) that is adequate for loss cone observations at high latitudes. All PLS sensors have lower energy limits ~1 eV. Actual limits to measurement are determined by the spacecraft floating potential over which there is no control since it is set by secondary emission properties of spacecraft surfaces and by ambient plasma conditions. (Differential spacecraft charging is to be limited to 10 V maximum as a MMII project requirement.) However, PLS sensors are capable of measuring the Orbiter floating potential, thereby allowing corrections for this effect to be made to the plasma data. Angular resolution is fixed at 22.5° elevation x 11° azimuth for IMS and 22.5° x 5° for ELS. As the TT turns at 1 rpm, a selected portion of the E/Q range of all 3 sensors is scanned 36 times over 32 E/Q steps. The exact stepping sequences are programmable so that energy steps may be interleaved on alternate scans and the energy range covered may be changed.

D.1.c. Sensitivity and Dynamic Range. Strawman requirements for sensitivity of the ELS and IBS can be met rather easily. The toroidal top-hat geometry used in the IMS (the only sensor for which sensitivity is a critical factor) is the most efficient possible E/Q analyzer geometry (Young, 1989). The IMS design is capable of measuring ion densities as low as ~10^{-2} cm^{-3} at plasma mean energies ~1 eV. Comparable

FIELDS-OF-VIEW		
ELS	A	±2.5° x 270°
IMS	B	±5.0° x 270°
IBS	C1	±0.7° x 160°
	C2	±0.7° x 160°
	C3	±0.7° x 160°

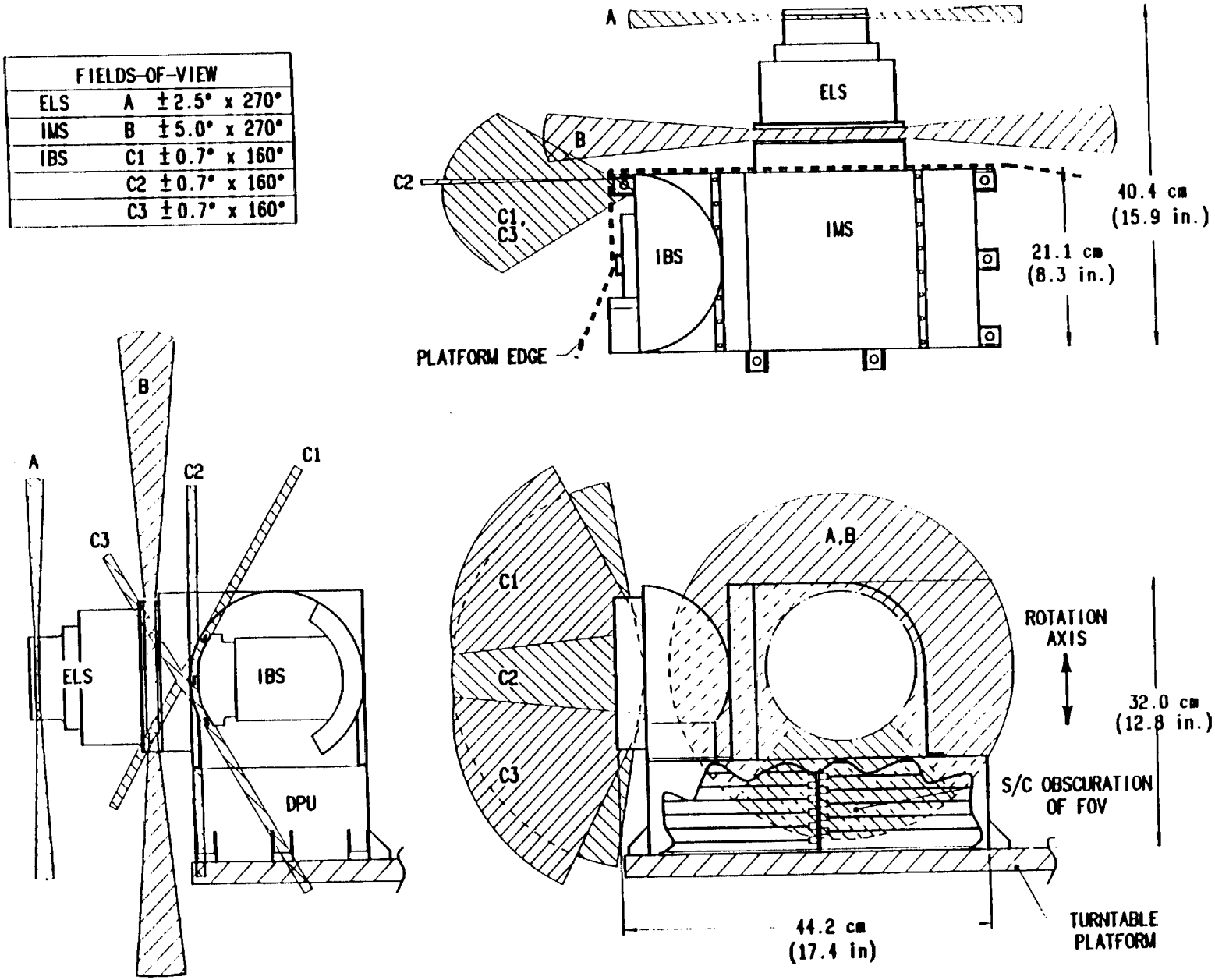

Figure 3. Three-view projections of the PLS instrument mounted on the Orbiter Turntable. Fields-of-view (FOV) of IMS and ELS are obstructed over ~90° by the presence of the Orbiter spacecraft body. Sensor FOVs are therefore limited by baffles to 270° acceptance fans in order to reduce detection of particles scattered mechanically or electrically by the spacecraft body. (In principle both IMS and ELS can be built with 360° FOV.) The turntable rotation axis is indicated on the far right. Spacecraft connector locations are not shown, but can be placed most easily on the DPU sidewall below the IBS apertures, or on the opposite sidewall.

numbers for ELS and IBS are ~10^{-3} and ~1 cm^{-3}. Moreover, the TOF technique has inherent anti-coincidence properties so that rates of <10^{-2} counts/s are significant. Upper limits to sensor dynamic range correspond to counting rates of 5 x 10^5 s^{-1} (IMS) and 10^7 s^{-1} (IBS, ELS).

D.1.d. Time Resolution. The nominal Orbiter TT rate of 1.0 rpm (± 10%) dictates basic sensor time resolution for a single 3D measurement. In order to obtain sufficient angular resolution consistent with this rate, a single spin is divided into 36 measurement sectors of 10° each. Within each sector we then require an energy scan of 32 steps so that one energy step has a duration of 52.1 ms. This, in turn, determines sensor geometric factor requirements for adequate statistical sampling for the major ion species. Of course, the faster data are sampled, the greater the demands on telemetry resources and on DPU processing. We have determined that a 52.1 ms sample period is optimum from this point of view as well.

D.2. Ion Mass Spectrograph (IMS)

D.2.a. Introduction. The Ion Mass Spectrograph (IMS) will provide reliable, high sensitivity, mass-resolved measurements of Saturnian plasmas from 1 eV/e up to 50 keV/e. The design combines a toroidal top-hat electrostatic analyzer with a newly developed time-of-flight (TOF) sensor (Fig. 4a) that incorporates a Linear Electric Field (LEF) to give exceptionally high mass resolution for so simple and compact an instrument ($M/\Delta M$ > 30 up to 24 keV/e). The concept of an LEF sensor in one dimension has appeared in the instrument literature [Hovestadt *et al.*, 1989]; however, to our knowledge it has not been developed into a two-dimensional field configuration, nor into a 3D plasma sensor as presented here. For reasons to be discussed below, the LEF detects on the average about 10% of the ions incident on the sensor with a mass resolution > 30. The remainder of the incident flux is detected with higher efficiency (90%) but lower mass resolution ($M/\Delta M$ > 8 up to 50 keV/e). These lower resolution data endow the IMS with a very large energy-geometric factor that rivals that of purely E/Q analyzers, while at the same time the LEF provides very high mass resolution measurements for a smaller fraction of the data. Other features of the IMS design are its low resource requirements (< 4.0 kg for sensor and high voltage supplies), its robust optical design that does not require highly precise component alignments, the use of static high voltage supplies for all but the toroidal ESA, and its heritage of ESA and TOF concepts developed for the CRRES, GGS/Polar, and PIDDP programs.

D.2.b. Overall Description. The IMS consists of two optical sections: a toroidal top-hat electrostatic analyzer (ESA) that selects ion energy per charge and arrival direction, and a Linear Electric Field (LEF) section that measures TOF. The two sections are co-axial and cylindrically symmetric as shown in Fig. 4a.

Ions enter the IMS through a collimator at ground potential. Inside the collimator, ions are deflected into a toroidal top-hat ESA developed previously (Young *et al.*, 1988). The ESA transmits ions within a range of energies ($\Delta E/E$ = 0.17) and azimuthal angles (11°) while accepting a wide range in elevation (270°). Transmitted ions are then accelerated through a -20 kV potential onto thin (0.5 $\mu g/cm^2$) carbon foils placed at the entrance to the LEF region. (The carbon foils are identical to those used in our CRRES and Polar TOF instruments and have been proven by flight-level tests to

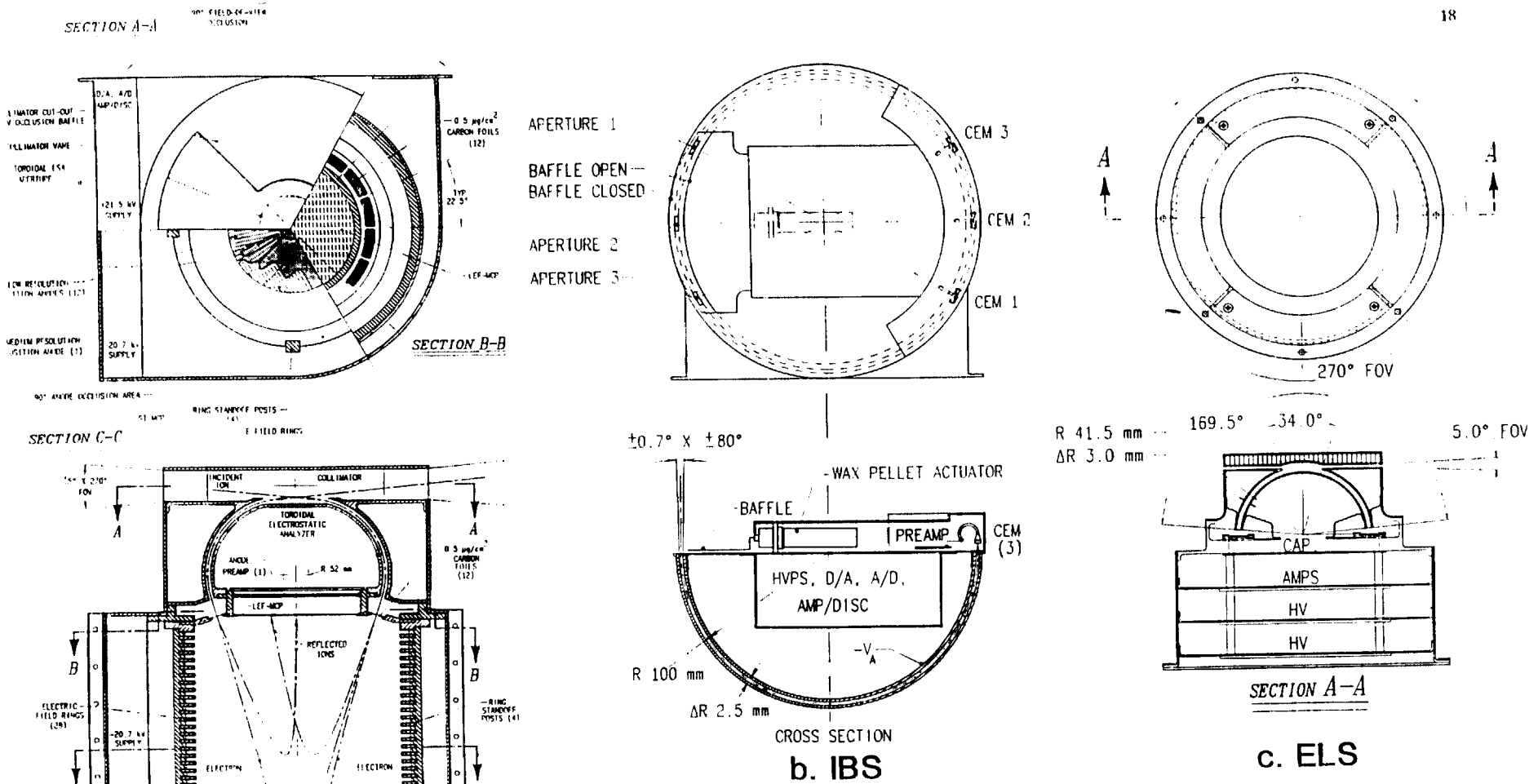

Figure 4. Cutaway drawings of the three PLS sensors showing plan view above and elevation view below. All three sensors are cylindrically symmetric as shown, except for deliberate baffling of the IMS and ELS to restrict FOVs to 270°. (a) Ion Mass Spectrograph (IMS), (b) Ion Beam Spectrometer (IBS) and (c) Electron Spectrometer (ELS) are shown. For details of instruments see text.

be robust despite their thinness.) The -20 kV potential provides sufficient acceleration that even at the lowest energies incident on the IMS (~1 eV), ions easily penetrate the foils. As they exit, ions eject electrons from the back of the foils. These electrons are collected on a microchannel plate (MCP) detector to provide timing signals as described below. During passage through the foils molecular species are usually broken up into constituent atoms or into smaller molecular fragments. All atoms and fragments exit the foil as either neutrals or ions, both of which are detectable by the IMS. In fact the bulk of the particles (roughly 90%) exiting the foils do so as neutral atoms rather than as singly charged ions. The exact ratio of charged to neutral constituents depends on ion species and energy. An important feature of the LEF design is its ability to measure both the neutral and charged species with high efficiency (≥80%).

All particles exit the foils into the LEF region where they encounter an electric field whose strength increases linearly with distance Z parallel to the axis of symmetry of the LEF (Fig. 5). The field is created by a stack of 28 equally-spaced

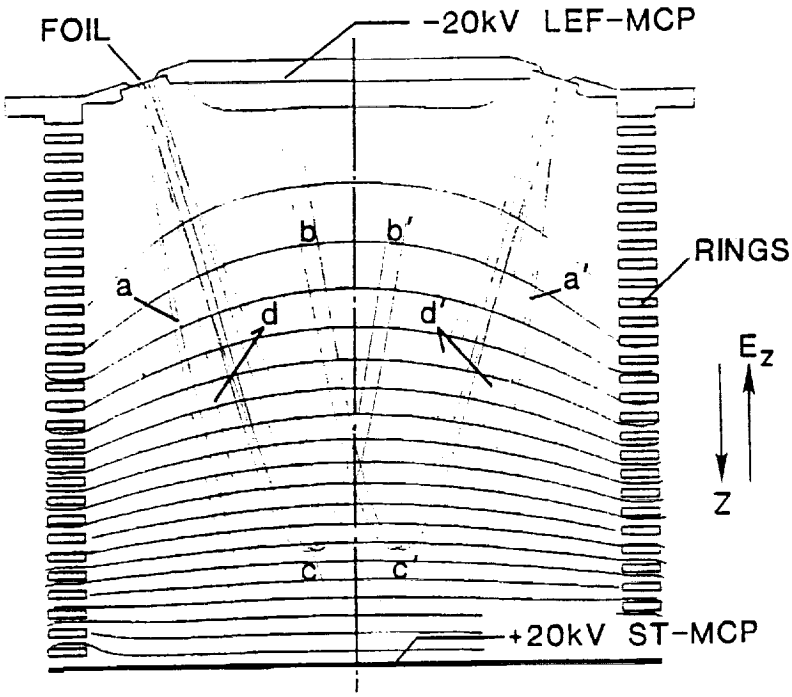

aa´ - Electrons emitted by ions exiting the foil.

bb´ - Ions incident on foil with 30 keV/e, transmitted through foil as ions.

cc´ - Ions incident on foil with 30 keV/e, transmitted through foil as neutrals.

dd´ - Ions with charge state 2incident on foil with 30 keV/e, transmitted through foil as ions with charge

Figure 5. Sample trajectories in the LEF portion of the IMS for ions with energy/charge of 10 keV/e external to the IMS and accelerated by 20 kV to a total of 30 keV/e before impacting the foil.

aluminum rings along which a potential gradient is established that varies with Z^2. An electron ejected from a foil by an incident ion is accelerated and focused by the LEF (trajectories aa´ in Fig. 5) onto the large area MCP (termed the "ST-MCP") at the bottom of the LEF region. The electron strikes the ST-MCP, giving rise to a sharply defined timing signal that initiates two identical timing circuits (one for the LEF-MCP, one for the ST-MCP) located in the DPU. An ion exiting the foil with a total energy below 44 keV/e (i.e. an external energy below 24 keV/e) is turned around by the +20 kV potential applied to the bottom end of the LEF (trajectories bb´ in Fig. 5). Most of these ions

reach the MCP located at the top of the LEF region (termed the LEF-MCP). The reflected ion strikes the LEF-MCP, producing a signal that stops the LEF timing measurement started by the electron and causes the event to be processed by the DPU.

The principle behind the excellent mass resolving capabilities of the LEF is the simple harmonic motion executed by positive ions that essentially bounce in the electric field. Ions in the LEF experience a retarding force which is proportional to their distance down the device. Because this restoring force is linear with distance, the equation of motion for these ions is that of a simple harmonic oscillator with a period proportional to $(M/Q)^{1/2}$. The LEF is designed so that the ion returns to the same value of Z from which it started in the field (bb′ in Fig. 5). This causes the motion to be harmonic and the flight time to be rigorously independent of incident angle and energy. A simulated TOF peak, obtained with our 3D ray-tracing code and a Monte Carlo routine for selecting particle energy and angle, is compared with actual data in Figure 6a. Simulated TOF spectra for critical Saturnian ion species are shown in Figure 6b for 20 keV/e incident energy. Figure 6c shows molecular "cracking patterns" that result from H_2^+, H_2O^+ and N_2^+. The spectrum in Figure 6d simulates the neutral spectrum from ions that enter the IMS at 50 keV/e.

The LEF design uses a +20 kV potential that bounces ions with external energies up to 24 keV/e. Neutral particles and any energetic positive ions above this turn-around threshold pass through the LEF region and strike the ST-MCP (trajectories cc′ and dd′ in Fig. 5). The resulting pulse stops the ST-timing circuit and initiates DPU processing of the event. Timing pulses of all particles (electrons, neutrals, etc.) reaching the ST-MCP are taken from the back electrode of the MCP. A divided anode behind the ST-MCP contains 12 wedge-shaped segments, that code elevation angle information carried by the electrons, and a single circular region in the center (Fig. 4a), that codes events whose particle trajectories have minimum time dispersion, hence maximum resolution. Thus the position encoding function of the ST-MCP is completely separated from its timing function by this technique. Timing pulses can be taken from the entire ST-MCP collecting area to produce very high collection efficiency and somewhat lower (by ~30%) mass resolution, or from the smaller central anode section to produce somewhat lower efficiency and higher mass resolution. This is an option that can be exercised in software depending on measurement objectives.

Molecular species impacting the foils are broken into characteristic fragmentation patterns that are used to advantage by the IMS. Of particular significance for Cassini science objectives is the IMS ability to distinguish molecular and atomic species with equal M/Q values, for example H_2^+ from He^{2+}, or CH_4^+ from O^+. Consider, for example, measurement of H_2^+ and He^{2+} with the ESA set to an energy of E_0/Q (the resulting LEF TOF spectrum is shown with lab data in Fig. 6a and simulated data in Fig. 6a,c′). Then H_2^+ arrives at the carbon foil with an external energy E_0 plus the acceleration potential of 20 keV for a total of (E_0 + 20 keV). Solar wind He^{2+}, on the other hand, arrives at the foil with total energy 2(E_0 + 20 keV). Upon passage through the foil the H_2^+ molecule splits into two hydrogen atoms (Fig. 6a,c′), each with energy (E_0 + 20 keV)/2. The LEF is not perfectly isochronous due to fringe field effects and other departures from field linearity, which cause slight focusing aberrations such that H^+ at

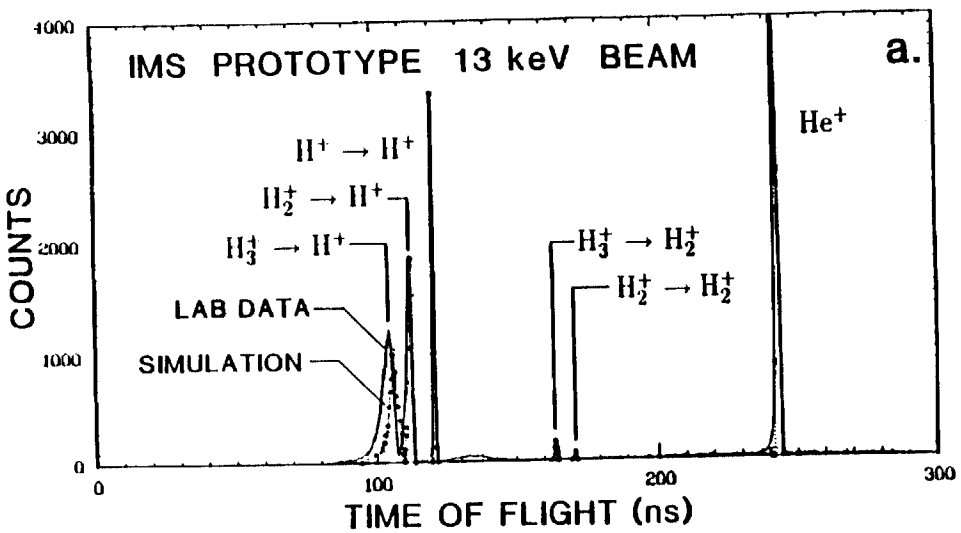

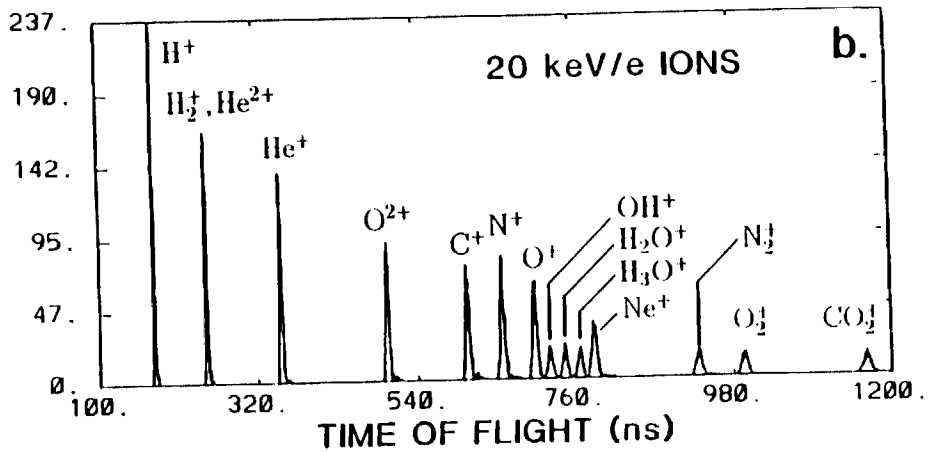

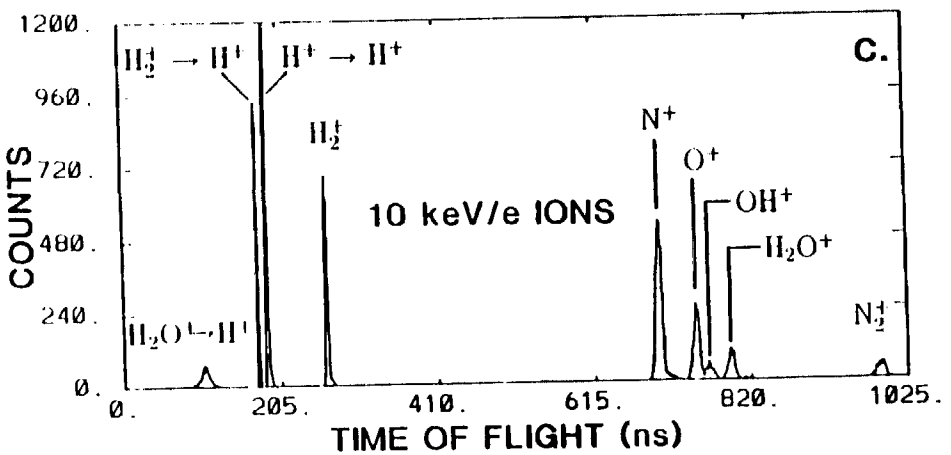

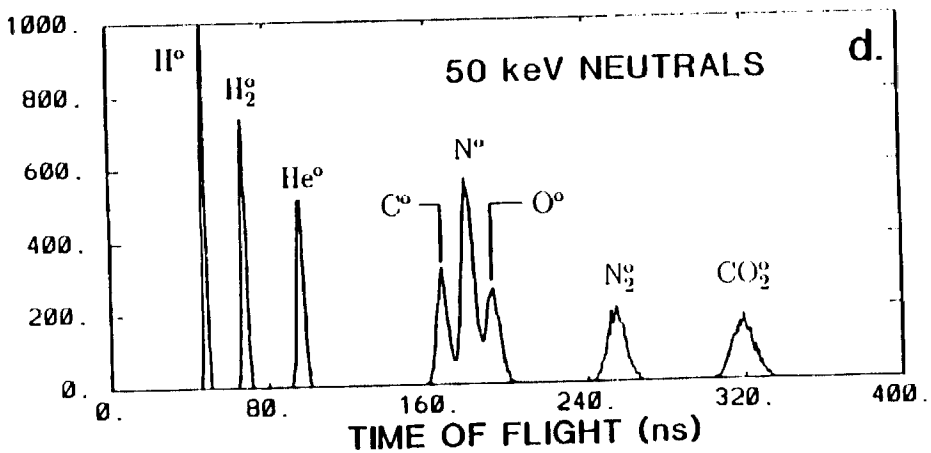

Figure 6.(a). Test data from IMS prototype (solid line) and Monte Carlo simulation (dots) for a 13.0 keV beam and +10 kV bias on LEF. TOF spectrum shows breakup of H_3^+ and H_2^+ in foil and the separated H^+ peaks that result. Note good agreement of lab and simulation data. **(b)** Simulation of IMS flight data for ions incident with 20 keV/e. Although it is recognized that few molecules will survive the foils intact as ions, they are shown in the spectrum to demonstrate LEFs excellent resolution. **(c)** Simulation of IMS flight data for breakup of 10 keV H_2^+, H_2O^+ and N_2^+ molecules. **(d)** Simulation of IMS flight spectrum at highest energy (50 keV) accepted by IMS. Note C, N, O resolution.

e

ORIGINAL PAGE IS
OF POOR QUALITY

(E_0 + 20 keV)/2 has a flight time slightly shorter than H^+ at E_0 + 20 keV. (Note that this small temporal separation (5 ns in Fig. 6c) corresponds to an energy difference of 50%, whereas the peak widths correspond to ±8% in energy.) On the other hand, He^{2+} charge exchanges in the foil to produce primarily He^+ at $2E_0$ + 40 keV. If this total energy is above 44 keV (i.e. if E_0 > 2 keV) then He^+ will be detected on the ST-MCP, where it is clearly distinguishable from any ion that entered the IMS originally as He^+ at E_0. Thus the observation of H^+ shifted by a known amount (5 ns in this case) implies that it entered the IMS as H_2^+. On the other hand, He^+ (or He^0) detected on the ST-MCP at a shifted time implies ion entry as He^{2+} rather than He^+. Since H_2^+ and He^{2+} fractionation and charge state patterns can be accurately and uniquely determined beforehand by calibration, the IMS gives a method whereby H_2 and He^{2+} can be separated reliably. In similar fashion, for example, water ions (H_2O^+) will break up into OH^+ or O^+ and one or two hydrogen atoms. As for H_2^+ breakup, the H^+ are distinguishable in the LEF at times shifted from normal H^+ for this energy (Fig. 6c), although because of their very low energies (e.g. 1/18 of the incident H_2O^+) the H^+ bounces in the part of the LEF that is not very linear and the peak is poorly focused, but still separable, as shown in Figure 6c.

Extensive testing of a small, low resolution version of the LEF sensor has been carried out. A sample of those data is shown in Figure 6a together with an overlay of simulated TOF data computed with our 3D Monte Carlo ray-tracing program. These tests demonstrate that 1) the principle of the LEF works well in practice, 2) there is little or no internal particle scattering which can cause ambiguous "ghost" peaks, and 3) the ray trace simulation agrees well with laboratory results.

In summary, the LEF allows determination of the original molecular species on a statistical basis using TOF spectra from both ST and LEF detector/TOF systems to show all molecular fragments. The only charge-state separation of importance at Saturn is H_2^+ from He^{2+} which can be accomplished by IMS without the need for solid state detectors. This results in a significant savings in instrument mass and power. Mass identifications will be made automatically in the DPU for the more common and easily separated species. Detailed identifications and confirmations will be made on the ground. It is clear that rigorous calibration and TOF spectral simulations, similar to those presented here, are required to develop data analysis algorithms. This will be carried out through an extensive program of ion and neutral measurements on foils in ion beams at the University of Virginia and at SwRI. These calibration data are also expected to contribute to our understanding of atomic collision processes within the magnetosphere and atmospheres of Saturn and Titan.

D.2.c. Time-of-Flight Measurement. Timing measurements are made digitally with a 100 MHz clock that incorporates a set of delay line verniers to give a timing resolution of ±0.25 ns. Two such circuits are operated in parallel to allow LEF-MCP and ST-MCP events, which give high- and low-resolution mass spectra respectively, to be recorded independently. In addition, the direction of ion arrival from the ST-MCP position anode is encoded and stored in an accumulator together with the TOF data, giving the angular identification for each TOF event. The digital TOF circuitry was developed as part of the PIDDP program and has been tested with a laboratory prototype. It provides a direct digital readout with 12-bit resolution over a range of 1200 ns without deadtime and non-linearity problems associated with analog

methods of TOF measurement. The TOF data serve as an address at which counts are accumulated during a single sampling period of 52.1 ms while the E/Q value is kept fixed. Data from a single E/Q step look like spectra shown in Figure 6. At the next sampling period the E/Q analyzer is advanced by one step, and the TOF data from the previous step are read into one of two large memory arrays together with E/Q and angular position information.

The two large (128 kbytes) matrix memories labeled "M/Q - E/Q" in Figure 7 build up arrays corresponding to M/Q vs. E/Q vs. angle spectra over a 30s period (1/2 spin of the turntable). Similar data arrays are built up for ST-TOF vs. E/Q spectra and LEF-TOF vs. E/Q spectra in the four matrix memories (64 kbytes each) provided for that purpose. Details of this process are discussed in the DPU section (D.6); however, the basic premise is that on-board processing can be used to identify ion M/Q values from raw TOF data. A similar method has been implemented successfully for both the LOMICS/CRRES and TIDE/Polar TOF spectrographs built by our team.

In summary, the IMS features simple, rugged construction and requires a minimum of high-voltage control. Only the voltage applied to the toroidal analyzer needs to be swept in order to obtain E/Q coverage; all others are fixed, except for MCP bias voltages in case a gain adjustment is needed in flight. The IMS design heritage draws heavily on TOF devices built for CRRES and Polar. The high voltage technology is straight-forward and sufficient resources are available to build highly reliable supplies. Similarly, the ion optics of the toroidal analyzer and LEF are well-studied extensions of earlier TOF designs, although this particular combination produces much higher mass resolution than either of our previous devices. Two IMS prototypes (including ESA and LEF sections) have been built and tested in the lab (cf. Fig. 2, Fig. 6a).

D.3. Ion Beam Spectrometer (IBS)

Complete resolution of narrow ion beams in both the Saturnian magnetosphere and solar wind is required to complement the broader resolution, higher sensitivity measurements of the IMS. The IBS consists of a single hemispherical electrostatic analyzer with three apertures (Fig. 4b) that produce a triple "crossed-fan" FOV pattern. The design is based closely on a similar system flown and operated successfully for 10 years on ISEE-1 (Fig. 2; Bame *et al.*, 1978). Its fan-shaped fields-of-view are oriented (Fig. 3) so that as the turntable spins, a 3D ion velocity distribution is scanned with three simultaneous cuts. The same technique was used on ISEE-1. Cross sections of the IBS are shown in Fig. 4b. The hemispherical analyzer plates are fitted with three entrance-aperture and channel-electron-multiplier (CEM) pairs to form three spectrometers with 1.4° x 160° fan-shaped FOVs. Three spectrometers have been used, rather than the two on ISEE in order to provide more complete coverage of the unit sphere. Plate spacings are very small in relation to plate radii to give very high energy ($\Delta E/E$ = 1.3%) and angular resolution (1.4°) needed for an instrument dedicated to ion beam studies. Of particular importance for magnetospheric beams, which may come from any direction, the central fan covers over 98% of the non-obscured portions of the unit sphere. Deconvolution of data from the two 30°-oriented fans allows calculation of all of the usual particle moments and other 3D features of the distribution such as heat flux. Examples of such calculations with ISEE-1 data are found in Bame *et al.* (1980).

CASSINI PLS BLOCK DIAGRAM

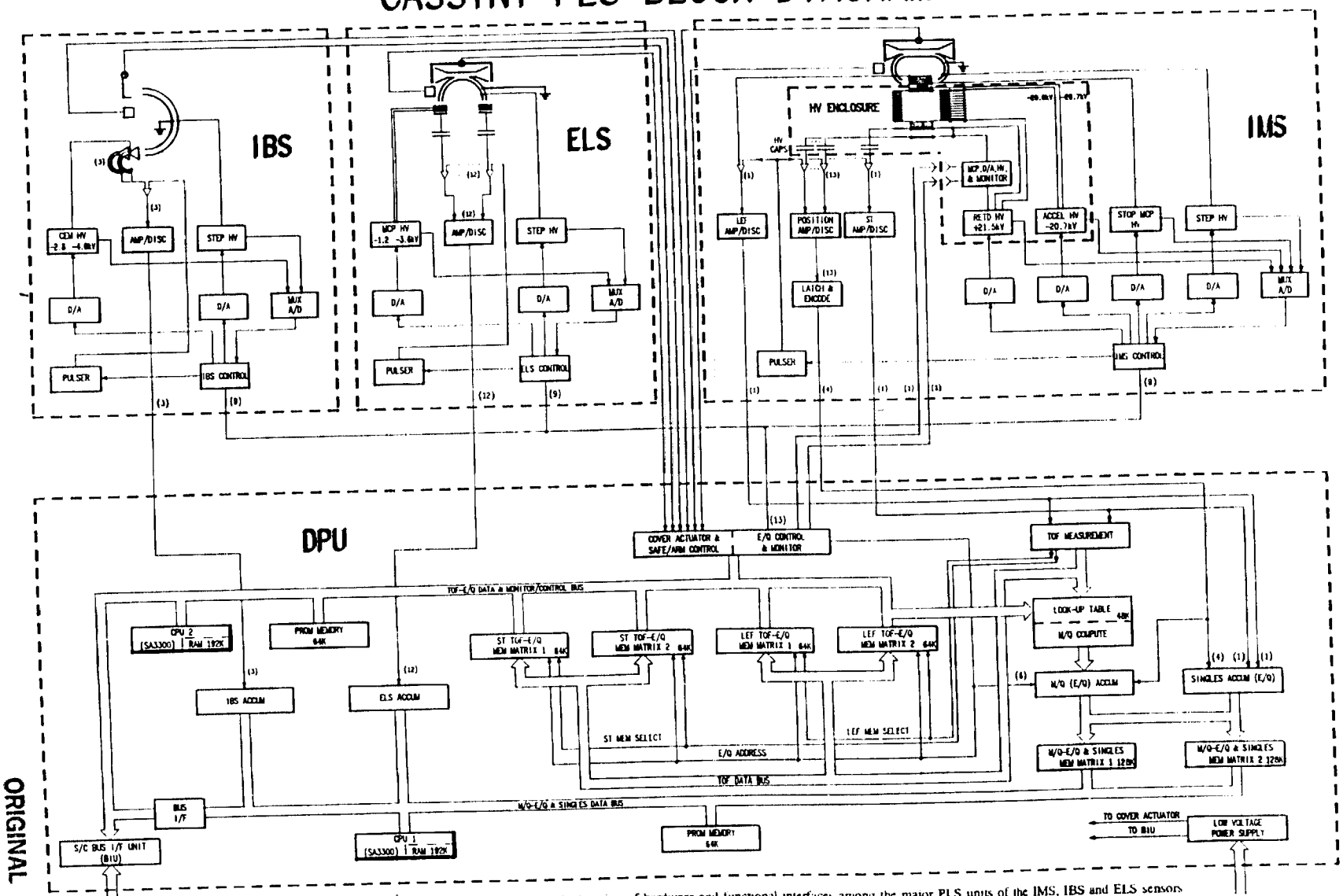

Figure 7. PLS system block diagram. Heavy dashed lines indicated the location of hardware and functional interfaces among the major PLS units of the IMS, IBS and ELS sensors and the DPU. Electrical interfaces among PLS units involve only logic-level signals since each sensor unit contains its own D/A, A/D and high voltage power supplies. The DPU contains two SA-3300-based microprocessor CPUs and 896 kbytes of RAM as well as 128 kbytes of PROM. The entire DPU and PLS system is rad-hardened to Cassini mission specifications.

When made together in one sensor, measurements of magnetospheric ion beams, and of the solar wind spanning 10 AU require an instrument with adjustable sensitivity. Because of this, the IBS is equipped with a movable baffle that is operated by command with the JPL-supplied hot wax actuator and an escapement driving mechanism. The baffle also provides protection from particulate contamination during launch as described in D.5.c. As Cassini moves outward, the baffle will be opened progressively in small increments to increase sensitivity. Should the escapement fail, a second wax actuator will fully open the IBS apertures.

D.4. Electron Spectrometer (ELS)

Electron measurements will be made using a spherical top-hat ESA based upon the PEACE design chosen for the European Space Agency's Cluster mission and a rocket experiment (Fig. 2). Cross-sectional views of ELS are shown in Figure 4c. The sensor covers the energy range from 0.8 eV to 20 keV with a field-of-view of 5° x 270° (Fig. 3). The 90° region of field-of-view obscuration is identical to that of the IMS top-hat. This dead region is used to pass signal cables from ELS to the DPU. Despite the field-of-view obscuration, the ELS is capable of obtaining a full electron pitch-angle distribution in 1/2 spin. Under certain magnetic field orientations the blind region due to the Orbiter body will interfere with this measurement objective, although this will be alleviated occasionally by opportunistic use of spacecraft roll maneuvers and assumption of gyrotropy. In order to reduce the PLS footprint on the turntable and ensure correct alignment of IMS and ELS fields-of-view, the ELS is mounted on top of the IMS collimator (Fig. 3). An analysis of the IMS collimator vibration modes indicates all resonances are > 100 Hz.

Electrons enter the ELS through a well-baffled collimator at spacecraft ground potential. They are deflected into the spherical section electric field plates by the field in the top-hat region (cf. Sharber *et al.*, 1988 and references therein). Electron energy is selected in the usual way by setting a positive voltage on the inner analyzer plate. An annular array of chevron-type MCPs based on AMPTE/Giotto design heritage is used to detect electrons that exit the analyzer. Anodes behind the MCPs are divided into twelve 22.5° sectors to give the required ELS angular resolution.

D.5. Common PLS Sensor Design Features

All three sensors share a number of basic features that contribute to sensor reliability, interface simplicity, and cost control. These are described in the following section rather than in the individual sensor discussions so that this commonality is apparent.

D.5.a. High Voltage Design. All three sensors rely on programmable high voltage power supplies to provide E/Q analysis of ions and electrons and detector bias voltages. These supplies are located entirely within the sensors and all have similar control and monitor circuits also located within the sensors as shown in the system block diagram (Fig. 7). All three sensors change E/Q steps in unison at intervals of 52.1 ms, although they may carry out widely different measurement programs by choosing E/Q values independently if desired. Particular care has been taken with the design of the

IMS ±20 kV supplies and of those sensor elements located at high voltage. Experience with CRRES and Polar high voltage designs renders the step up to 20 kV an incremental one that is attainable with only a modest development effort. During low-altitude (< 2000 km) flybys of Titan, high ram pressures will make it necessary to turn IMS and perhaps ELS off. We expect, however, that because of the very low gas conductance path to the CEM's, the IBS will safely return useful data when it sweeps through the Orbiter ram direction.

D.5.b. Detectors. Both IMS and ELS use standard-sized microchannel plates while IBS uses standard channel electron multipliers, all of which are available off-the-shelf from known commercial vendors. In the case of IBS and ELS the detectors and mountings are the same configuration as on previous flight designs. The MCPs for ELS will cover an annulus of 270° with 12 discrete anodes subtending 22.5° each. The IMS will use two standard round MCPs mounted in a manner identical to that of smaller round MCPs used on the TIDE/Polar instrument. Pre-flight burn-in of all detectors used in the PLS will be carried out in existing facilities at LANL and SwRI to select flight detectors and ensure high gain throughout the mission. If necessary, gain can be adjusted in-flight by ground command. Pulsers have been built into all three sensors in order to stimulate amplifier and detection circuits and provide in-flight TOF calibration. The pulsers will also stimulate the sensors during all phases of ground testing of PLS.

D.5.c. Sensor Cleanliness, Dust Protection, Covers. Several elements of PLS are sensitive to particulate and hydrocarbon contamination. These include detectors, carbon foils in the IMS, high voltage insulators, and blackened analyzer surfaces. During ground operations and up to launch, all three sensors will be protected with purge covers and high purity N_2 backfill. Covers will be opened following launch using JPL-provided wax pellet actuators. A cover similar to those of IMS and ELS is being built for TIDE/Polar. The IBS cover is fitted with a second actuator to fully open the aperturesin case the aperture-opening escapement mechanism fails *en route* to Saturn. Calculation of the expected dust fluence on the sensor apertures (using the JPL models) indicates that dust impact during ring plane crossings is not a hazard to PLS, hence there is no intention of closing the covers after launch.

D.5.d. UV Rejection. All three sensors are designed for excellent rejection of UV from the Sun and the environs of Saturn. In the worst case, photons must undergo at least three bounces to enter IMS and IBS and two bounces or more through the ELS collimator and analyzer plate system in order to reach a detector. In addition to multi-bounce paths, suppression techniques also include serration of analyzer plate surfaces and blackening with a conducting coating of chemically deposited copper oxide black with which the team has experience. Blackening also suppresses secondary electron emission in the ELS in order to reduce measurement background.

D.5.e. Radiation Tolerance and Shielding. Care has been taken in design of the sensors to reduce detector background due to penetrating radiation. In the IMS this is accomplished by use of triple coincidence (i.e. a valid event requires three pulses, namely "start", "stop", and "anode position" signals) timing circuitry inherent in the TOF measurement. The IBS uses CEM detectors of minimal aperture for the analyzer plate

exit size, which produces minimal detector background. In addition, a small amount of shielding is added around the CEM funnel-like detecting area. ELS relies primarily on detector shielding and large signal-to-noise ratio of the MCP detector to mitigate the effects of background. All electronic components have been selected to withstand a dose > 15 krad in accordance with MMII project requirements. Shielding mass, where required, has been included in PLS weight estimates.

D.6. Data Processing Unit (DPU)

D.6.a. Introduction. The DPU (Fig. 7) manages the acquisition and onboard compression of all PLS data as well as sensor command and control functions. It also forms the mechanical base for the three sensors (Figs. 2,3). The use of a single data acquisition and control system for all three sensors eliminates the duplication of these functions within each instrument. A single JPL-supplied spacecraft bus interface unit (BIU) within the DPU provides the path for the transfer of commands and data from the spacecraft through the DPU to the PLS sensors. Sensor interfaces with the DPU have been kept simple by placing all high voltage supplies and their control and monitoring functions within the sensors themselves. The three sensors communicate with the DPU via serial data interfaces and detector counts are transmitted as logic pulses so that no low-level signals are exchanged that might be susceptible to noise. The DPU incorporates two CPUs; both are flight-qualified SA3300-based microprocessors that share a total of 896 kbytes of data memory (RAM) and 128 kbytes of programmable memory (PROM). Our design draws heavily on experience with nearly identical SA3300-based DPUs used in the SPICE and CRIMS investigations on CRAF and TIDE on the GGS/Polar spacecraft. The PLS design also incorporates all interface aspects of the CRAF/SPICE experiment and is compatible with the use of a JPL Common Flight Computer (CFC) 7" x 7" microprocessor card if one becomes available during the Cassini accommodation phase.

D.6.b. Description. The DPU is designed around several rather simple concepts that arise from the way in which the three PLS sensors are operated. The primary CPU1 control functions are: (1) accumulatation of TOF spectra for ~2 to ~10 minutes at maximum mass resolution for transmission in parallel with other data at a rate that requires ~10% of the PLS telemetry rate, and (2) compression of all IMS data using standard root compression as well as more sophisticated encoding schemes such as noiseless encoding [Rice, 1979]. Primary CPU2 functions are: (1) command of all three sensor stepping programs including on-board analysis of IBS and IMS data in order to allow the IBS program to track peak-like features in the ion data, and (2) analysis of TOF spectra to determine the 8 most abundant ion species whose energy-angle spectra will be transmitted with highest temporal resolution. Commands are received via the BIU and routed to the appropriate CPU microprocessor, which then exercises control over the PLS subsystems. Standard sensor operating modes, together with the appropriate data processing modes, are time-tagged and are stored in PROMs and are initiated by single high level commands to the DPU.

In operation CPU2 will initiate a measurement sequence twice per TT spin period, nominally every 30s. Because the IMS and ELS fields-of-view subtend 270°, 1/2 spin of the TT allows nearly complete 4π coverage of particle arrival directions and

makes a natural unit by which to subdivide the taking and processing of data. This is done by sending a series of digital words to the three sensors to command a given E/Q step once every 52.1 ms. This sampling period results from consideration of the need to cover 32 E/Q steps 18 times per half spin in order to achieve required resolution. During the first 5 ms of the sampling period the sensor counting registers in CPU1 are read to the matrix memories and the high voltages on the analyzer plates are changed and allowed to settle. After the 5.0 ms dead time, accumulators in CPU1 are enabled for 47.1 ms. At the end of 52.1 ms the entire process is repeated until an entire 32 step E/Q program is scanned. A complete measurement sequence consists of 18 such E/Q programs (these are usually, but not necessarily, identical). All PLS stepping programs may be slowed by holding steps for multiples of 52.1 ms. Such a mode would apply, for example, in instances where time resolution is not critical.

Once the data collected from a full 30 s sequence is complete, computations begin while the subsequent data sequence is loaded into a second bank of identical memory. Thus by "ping-ponging" the memories the DPU can process data stored in one memory while accumulating in the second. These ping-pong memory matrices are shown as "mem matrix 1" and "mem matrix 2" for each type of data accumulation in Figure 7.

On-board data processing and compression is crucial to the success of IMS science objectives. Raw IMS data are produced at 4800 bytes/s or 24 times the 200 bytes/s rate allocated to the PLS instrument in the strawman data plan. This calls for sophisticated on-board reduction and compression routines in order to extract and return the maximum amount of data possible. This task is carried out by CPU1. The present telemetry allocation for PLS is 6000 (8 bit) words per half spin. If it is assumed that 5% of the telemetry allocation is used for housekeeping, header and engineering data, then a compression of approximately 25:1 is required to report the most important subset of the full data array in the remaining telemetry. We have tested lossless compression algorithms and find that they produce a compression factor of ~2-3 in the most detailed data sets. "Lossy" compression schemes are being tested and may lead to the compression factors needed for full 25:1 compression. Priority encoding of PLS data is the only means of guaranteeing a particular resolution and coverage. Basically, one selects a subset of data to be transmitted based on which measured parameter(s) are given priority: for example, energy resolution at the expense of angular resolution or vice versa (accomplished by averaging over energy or angle to reduce the number of samples). Alternatively one may select a restricted number of key M/Q species to be reported in great detail in E/Q-angle space and a larger number of species to be reported with little detail. During periods of high telemetry rate (16,000 bits/s) these priority schemes can be tested against completely transmitted data sets. To put this in perspective, the TIDE/Polar DPU performs on-board reduction and "lossy" compression of ~80:1 on a spectrum accumulated every 6 seconds using only a single SA3300 processor. Thus the actual DPU load for compression is significantly less on PLS than TIDE. The need for a dual SA3300 system arises from the large amount of processing required for the IMS time-of-flight on-board data analysis which is far greater than the needs of the TIDE TOF system.

D.6.c. Instrument Modes. Operating modes of the PLS sensors are designed to integrate the functions of the three sensors and the on-board data processing

into a single efficient program centered on a specific science objective. Full details of characteristic modes are contained in the attached Instrument Fact Sheets. As one example, the survey mode used for the 20-day "low activity" phase emphasizes full PLS spectral coverage by alternating sensor energy steps every 1/2 TT spin, by doubling the sampling period to 104.2 ms in order to reduce azimuthal angular resolution a factor of two, and by covering 2 M/Q species instead of 8 on every 1/2 spin. The data processing program would take into account all details of this mode in order to return the maximum amount of information. Although mode execution and data sampling are tied closely to TT phase, allowance is made for a slight (and variable) drift in the sampling period in order to avoid phase-lock and resultant sampling blind spots. There are, of course, a large variety of such modes that can be reprogrammed and tailored to actual conditions encountered on orbit. An initial set of modes will be based on our stated science objectives and on the Voyager and Pioneer 11 experience. The most important modes include solar wind (used in cruise and at encounter), Jupiter encounter, Saturn Orbital Insertion, Titan flybys, ring plane crossings, Saturn mapping, and icy satellite encounters. Details of the modes and their typical duration are given in the instrument fact sheets.

D.7. Electrical Ground Support Equipment (EGSE)

The DPU interfaces to both the spacecraft and the three PLS sensors will be simulated by a set of EGSE. The main EGSE will emulate all spacecraft functions and will accompany the PLS through all spacecraft level testing. It is also the sole interface between the DPU and the mainframe computer used for calibration data analysis at the PI institute. In order to assist and coordinate sensor subsystem level tests there will also be a set of sensor level EGSEs that emulate the DPU function and its interface to the sensors. Because all sensor-DPU interfaces are identical except for the number of detector signal power supply control lines (Fig. 7), the sensor EGSEs will be nearly identical PC/AT 286 or similar systems with a single custom interface card. This approach is low cost and easy to manage, and it ensures compatibility among the three sensors so that only a single interface definition and set of basic processing software will be required.

D.8. Calibration

Both pre-flight and in-flight calibrations play a critical role in the PLS investigation. They ensure the correct functioning of the three PLS sensors and determine the overall quality of data products and the scientific success of the investigation. High-quality reproducible calibrations are therefore of great importance and the PLS team is well-experienced in this area. Initial beam tests of the three PLS sensors will take place at each of the European institutes responsible for the sensors. Final pre-flight calibration of the sensors will be made in ion and electron beam facilities at LANL and SwRI. The University of Virginia will provide measurements of ion and electron production efficiencies and the fractionation patterns due to molecular breakup in foils. In-flight calibrations of the TOF system using the built-in pulsers to simulate TOF signals, will be carried out periodically (~1/month) throughout the Cassini mission. In addition, models of the sensors will be developed for comparison with calibration results.

The three PLS sensors share many aspects of calibration; however, the IMS poses the greatest challenge because of requirements for accurate mass identification and abundance determinations. These are discussed below. Common requirements of pre-flight calibration for all three sensors include the need to establish angular and energy response and absolute sensor efficiency. These requirements will be met by placing each sensor in an ultra high vacuum system (to ensure cleanliness) and then illuminating the sensor aperture with a highly collimated uniform beam of the appropriate energy and species (i.e., electrons or mass-selected ions). The sensor will be rotated in the beam, and the beam energy varied appropriately, so that energy-angular response is mapped out. This mapping process will be carried out for the various sensors at SwRI or LANL almost entirely under computer control. Beam current measurements made with a standard Faraday cup and CEM are compared to sensor count rates to obtain absolute detection efficiency. From these assembled data the sensor energy-geometric factors can be computed over the full range of response. An accuracy of ±10% or better is expected. Calibration data are then reduced to matrices that are subsequently used to convert count rates into particle distribution functions. From the latter it is then a straightforward calculation to obtain the usual plasma fluid parameters or any other desired data products.

Calibration of IMS is more complex than that of IBS or ELS because of the need to establish detection efficiencies and molecular fractionation patterns for all atomic and molecular ion species that are likely to be encountered at Saturn, Jupiter, and in the solar wind. An existing laboratory prototype of IMS will be used to obtain some of these fractionation patterns so that the entire program need not be carried out with the flight unit. Although calibration of IMS is complex, it is in principle no different than calibration of any other spaceflight mass spectrometer in terms of absolute efficiencies. The reason is that detector efficiencies, whether for MCPs, CEMs or solid state devices, are always dependent on ion energy as well as species. Thus mass spectrometer calibration must always rely on efficiency measurements made for all species and energies that are to be detected. Our team has extensive experience with mass spectrometer calibrations (both magnetic and TOF) in the ESA/GEOS, Giotto, CRRES, Polar, and CRAF programs, and both LANL and SwRI facilities are capable of the highest quality calibrations possible.

The complete PLS calibration results will be developed into appropriate formats and codes for the flight DPU and for data reduction and analysis on the ground. Sufficient flight data will be returned from all sensors, but particularly the IMS, to compare in-flight calibration and performance with ground calibrations. Each PLS sensor includes a pulser for in-flight test of all amplifier circuits, discriminators, and accumulation logic. Shifts in calibration during flight due to changes in detector gain are expected to be minor based on previous flight experience, and will be compensated with adjustments to detector bias voltages. Unlike the detectors, which have activated surfaces and are voltage-biased, the carbon foils that determine ion, neutral and electron emission efficiencies and molecular fractionation patterns are passive and highly stable components of the IMS. Total ion flux through the foils affects only a minuscule fraction of the carbon surface (less than 1 carbon atom in 10^6) and has no effect on efficiency.

D.9. Mission Operations

Primary responsibility for generating mission operations requirements for the PLS investigation will reside with the PI institute (SwRI). The project- supplied SPOC and associated communication links will be used for this purpose. The requirements will be determined by use of planning aids such as computer modeling and simulations developed by the investigation team, as well as by means of team meetings. Guest investigators will also play an important role in this process. An additional workstation dedicated to PLS mission planning and data analysis will be located at GSFC, communicating with the project by means of NASA's existing high-speed communication system. Since the PI for the CRAF/CREWE investigation (J. Scudder) is at GSFC, much of the development and expertise for these activities can be shared between the two investigations. All PLS-related activities will, of course, be coordinated with the PI at Southwest Research Institute. The PI institute also serves this function for the SPICE/CRAF investigation (PLS team member J. L. Burch is SPICE PI) and will share development efforts, expertise, and costs, particularly in view of the similarities of the CRAF and Cassini efforts.

Mission planning efforts will involve developing physical models of the various regions (e.g., Titan, Saturn's magnetosphere, rings, icy satellites, etc.) in terms of mission-event timelines and then combining these with the software tools describing spacecraft trajectory and attitude provided by the project. Members of this team have already participated in the development of such modeling efforts for the Saturn system, e.g., Hartle *et al.* (1982), Richardson and Sittler (1990), and Johnson *et al.* (1989). Phenomenological and mission models will be combined with a model of the instrument performance to select operating modes that optimize the science return under the appropriate mission constraints. In addition, the team will support joint planning activities of the Cassini PSG, such as tour design and instrument operating scenarios. We will begin to develop and test our planning techniques early enough in the mission to be able to influence these activities in a timely fashion.

D.10 Data Analysis

D.10.a. General Approach. The PLS quick-look, instrument health, and key scientific data will be monitored at the PI institution, but routine data reduction and distribution will be done at GSFC. Data summaries containing complete time histories of PLS and ancillary data will be distributed to team members on a periodic basis for preliminary analysis. It is anticipated that on average about 10% of the full data set will be sent to each Co-I institute for detailed analysis of special interest or "event" data. Eraseable optical disk technology will be used as the archiving medium. Final reduced data products will be sent to the NASA archiving center, anticipated to be the NSSDC at GSFC, by the PI on a schedule as specified by NASA or the Project.

The data reduction software will be written primarily at GSFC using a modular architecture so that modifications can be incorporated without difficulty. Portions of code that already exist at LANL and SwRI from other missions will also be used, and analysis codes will be exchanged among the Co-I institutes. Three separate branches in the program will be used to process data from the IMS, ELS and IBS sensors

and separate data records will be written for each sensor. The data reduction software will routinely produce summary data in the form of moments of the particle distribution functions (density, flow velocity, temperature, temperature anisotropy, and heat flux), which will then be put in the form of data plots at various levels of time resolution (daily averages, hourly averages, down to the highest resolution of 30s for moment calculations) depending on the particular PLS investigation requirements. For example, during the cruise phase of the mission daily and hourly averages are most useful for surveying the solar wind, while for events such as a Titan flyby, data would be provided at the highest time resolution. Other data products include phase-space plots of particle distribution functions and detailed mass-spectra plots. Other anticipated products include energy-time spectrograms of electron and ion energy and number flux, which have proved invaluable for overviews of large data sets. This is a very powerful technique for detecting unexpected patterns in the data that might otherwise go undetected. We plan to have the capability of both displaying these on a color screen and producing hard copies. The files from which the plots are produced are then sent to other team members. Synoptic studies will be carried out through agreements among team members; actual computations will be carried out at GSFC or SwRI.

D.10.b Methods. The method for computing the particle distribution function f_i from the raw data is straightforward and is based on detailed pre-flight calibrations and on in-flight-calibration checks. Because the PLS instrument does not always have access to 4π steradian coverage (15% of the sky occulted by the spacecraft) one cannot simply perform weighted velocity sums of f_i to compute moments. The gap in phase space will first be filled in using interpolation and additional assumptions such as gyrotropy. For example, under conditions of optimum phase space coverage the data reduction programs will perform a peak search of f_i for the dominant ion species and then execute a bi-Maxwellian fit to the peak of the distribution function to obtain an estimate of the ion flow velocity V_i. It will then shift all the measurement points into the moving frame of the particular species and fill in the unsampled portion of f_i assuming gyrotropy. This is repeated for the remaining ions which, under most conditions, would have perpendicular flow velocities similar to the dominant ion. Once the particle distribution functions have been computed it is straightforward to compute their moments.

E. PRINCIPAL INVESTIGATOR AND CO-INVESTIGATOR RESPONSIBILITIES AND COMMITMENTS

E.1. As Principal Investigator **D. T. Young** will devote an average of 0.25 MY/Y throughout the 17-year program. His specific duties include:

a. Establish the scientific goals of the investigation and serve as a member of the Cassini science working group.
b. Ensure that the design and development of the PLS instrument is appropriate to the objectives of the investigation.
c. Ensure conformance with schedules, budgets, and MMII system specifications.
d. Participate in planning and execution of instrument operations.
e. Ensure that adequate documentation is developed and maintained.

APPENDIX C

THREE-DIMENSIONAL PLASMA MEASUREMENTS FROM THREE-AXIS STABILIZED SPACECRAFT

S. J. Bame, R. H. Martin, and D. J. McComas

Space Plasma Physics Group, Los Alamos National Laboratory, Los Alamos, NM 87545

J. L. Burch, J. A. Marshall, and D. T. Young

Southwest Research Institute, San Antonio, TX 78284

Abstract. Future planetary missions require that comprehensive three-dimensional measurements of electrons and mass-resolved ions be made from three-axis stabilized spacecraft. In order to make these measurements without requiring expensive and resource intensive platforms to scan space mechanically, we are developing various systems that are designed to scan space electrostatically. These systems also make it possible to circumvent the significant shadowing that would be present even with a scan platform, caused by necessary spacecraft appendages such as communications antennas and a power source (RTG or solar cell panels). The systems, which are axially symmetric, select particles arriving from 360° in azimuth along conical surfaces whose polar (or elevation) angles, referenced to the instrument symmetry axes, are determined by applying suitable deflection voltages to shaped deflectors. Particles thus selected in polar angle pass into spherically or toroidally-shaped electrostatic analyzers. After analysis, the 360° outputs of the analyzers are divided into discrete angular swaths to provide azimuthal angle resolution. In the case of electrons, the analyzed particles can be detected directly; in the case of ions, the particles in each swath can be counted directly, or further analyzed with time-of-flight or magnetic analyzers to obtain the velocity distributions of the separated major ion constituents. We present computer simulations of particle paths through the various analyzers of this type and show results from laboratory calibrations of prototypes.

Introduction

One of the fundamental realizations brought about by the planetary exploration program of the past two decades is the wide range of complex plasma physics phenomena that occurs in the vicinity of the terrestrial and Jovian planets, as well as comets. All of the solar system bodies which have been probed seem to exhibit strong and unique plasma and electrodynamic phenomena. However, in many cases the reconnaissance and exploratory missions which have been flown have left these phenomena only partially investigated and not completely understood. Two important limitations on the detailed understanding of plasma phenomena at other planets have been the incomplete coverage of plasma velocity distributions provided by previous missions and the absence of unambiguous composition measurements.

To obtain a quantitative understanding of the various plasma physical phenomena occurring in the vicinity of a planet or other body, it is important to have accurate measurements of the fluid moments, including the density, bulk velocity, temperature, and heat flux of each of the plasma components. These measurements must resolve the entire velocity distributions of electrons and ions with adequate temporal, angular, mass, and energy resolution. Full angular coverage is particularly important when the distributions are anisotropic in the spacecraft frame, either due to an actual pitch-angle anisotropy or to a significant flow velocity. Unfortunately, obtaining the requisite full velocity-space coverage is difficult because planetary missions typically use three-axis stabilized spacecraft in order to facilitate imaging experiments, and to maintain good telemetry links with Earth. Thus, one cannot take advantage of spacecraft spin to obtain full angular coverage of the plasma distribution. An additional problem exists even if a single scan platform is provided for plasma instrumentation. Necessary spacecraft appendages such as communications antennas and power sources (RTGs or solar cell panels), and the spacecraft itself block significant portions of velocity-space.

Accurate measurement of plasma moments requires knowledge of the ion composition, the importance of which has only recently begun to be appreciated. This appreciation has been fueled by spacecraft observations of significant populations of heavy ions, with clear terrestrial origins, within the Earth's magnetosphere (see Young, 1983, for a review), and even more so by the dis-

covery of major heavy-ion components in the plasmas of the Jovian and Saturnian magnetospheres (cf. Lazarus and McNutt, 1983). Voyager observations at Jupiter and Saturn suggest that the various satellites and rings within those magnetospheres may be the dominant sources of magnetospheric plasma. As a consequence, it is now clear that a knowledge of plasma composition is a first-order requirement for a proper understanding of the physics of various planetary magnetospheres.

The importance of understanding planetary plasma phenomena is now well recognized, and missions such as Galileo and Comet Rendezvous and Asteroid Flyby (CRAF) include comprehensive plasma and field instrumentation in their payloads. Two new missions now in the planning stages are the Mars Aeronomy Observer and Cassini, which is comprised of a Saturn Orbiter and Titan Probe. Fairly complete plasma instrumentation has also been recommended for these missions. However, the study reports for both missions assume that the needed instruments have already been developed for previous planetary or solar-terrestrial missions. Unfortunately, this is not the case. Previous plasma instruments on planetary missions have provided neither unambiguous mass analysis nor full velocity-space coverage. Furthermore, since for communication and imaging reasons planetary spacecraft are usually three-axis stabilized, plasma instrument of the present generation that make two-dimensional measurements, provide three-dimensional coverage of accessible portions of space only if mechanical scanning is available with scan platforms or separate spinning spacecraft sections. Even with such platforms, as mentioned above significant portions of velocity-space are blocked by spacecraft appendages.

Provision of a rotating platform introduces reliability problems, increases the cost of the spacecraft, uses limited spacecraft resources such as attitude control gas, and in any event does not solve the full accessibility to space problem caused by obstructions. Additionally, because of the need to conserve spacecraft resources, the measurement time resolution using a scan platform is necessarily constrained by the speed and number of operating cycles that can be allotted it.

The CRAF spacecraft presents a good example of the problems that arise when mechanical scanning is necessary to convert two-dimensional measurements into three-dimensional plasma distributions. CRAF, like Cassini, will use the Mariner Mark II spacecraft, which is three-axis stabilized with scan platforms. The proposed instrument for providing composition-resolved three-dimensional plasma measurements has a two-dimensional acceptance fan ($5° \times 160°$) and will need to rely on single-axis mechanical scanning projected to be provided by the CRAF low precision scan platform in order to obtain three-dimensional coverage. However, because of fuel limitations, scanning will be limited to a small fraction of the spacecraft operational time (less than 25%), a serious degradation of the measurement capability. Additionally, other experiments on the platform have pointing requirements that are incompatible with those of the plasma experiment, further reducing measurement capability.

Taking the lessons learned from CRAF and generalizing to future missions such as Cassini and Mars Aeronomy Observer as well as potential missions such as Lunar Polar Orbiter, Mercury Magnetospheric Orbiter, etc., it is important to examine how fully three-dimensional plasma velocity distributions might be obtained using fixed-attitude spacecraft. An optimum solution must avoid substantial blockage of velocity-space by the spacecraft and its appendages and should not require a scan platform. Search for an answer to this problem has been a major impetus for the work reported here that was carried out at the Los Alamos National Laboratory and the Southwest Research Institute (SwRI). As discussed in the following sections, mechanical scanning can be eliminated by the use of electrostatic scanning. Several candidate systems are presented. The problem of solid angle obscuration by the spacecraft and appendages can be overcome by appropriately locating two sensor heads on opposite sides of the spacecraft.

Measurement Objectives and Approach

As noted previously, the plasmas found within all of the planetary magnetospheres sampled to date are highly complex in makeup and in velocity distribution. Moreover, they are highly variable both spatially and temporally. For example, within the magnetosphere of Saturn plasma densities range from less than 10^{-2} up to $\sim$10 cm^{-3}, flow speeds range from $\sim$10 to $\sim$200 km s^{-1}, and both ion and electron temperatures range from several electron volts to $\sim$1 keV (e.g., Sittler et al., 1983; Richardson, 1986). Comparable or greater variations are found within other magnetospheres.

In addition, in many situations of great interest more than one particle population is present. For example, both very cold (several electron volts) and very hot (several hundred electron volts) electron and/or ion components commonly coexist in the same region, and several different elemental or molecular species may be present (for example, H, N, O, H_2O, CO, etc.). Each elemental species may also occupy more than one charge state (for example, O^+, O^{++}). Further, velocity distributions may be highly non-Maxwellian, and strong anisotropies may be present. Often strong streaming along the local magnetic field is observed. The plasma flow may be supersonic and therefore appear as a beam (typically transverse to the field within the magnetospheres of the outer planets), or subsonic and therefore more nearly isotropic in the spacecraft frame.

Measurement objectives during upcoming planetary missions should therefore be directed toward resolving and distinguishing these complexities with a sensitive instrument placed on a three-axis stabilized spacecraft, and if possible these observations should be made without requiring a scan platform and in such a way as to avoid obscuration of significant portions of space by such mission-essential elements as the spacecraft anten-

nas and the spacecraft itself. The plasma measurements should be fully three-dimensional or cover the pertinent portions of velocity space required for the specific scientific problems of interest with adequate angular resolution to resolve moderately narrow beams independent of their flow direction or the spacecraft orientation. The instrument should be sensitive enough to measure densities of major ion species as low as 10^{-2} cm^{-3} on a temporal scale of several tens of seconds or less, and should have an energy range extending from near 1 eV to ~30 keV where energetic particle solid state detectors can take over. Energy resolution should be adequate for both cold supersonic and hot subsonic flows. Major ion species should be separated under all conditions; their separation should not be dependent on fortuitous combinations of ion flow speed and direction. To implement these objectives, the SwRI/Los Alamos joint program has two major goals: (1) to explore and develop instrument concepts aimed at providing fully three-dimensional ion and electron distribution measurements on three-axis stabilized spacecraft that might have large, blocking appendages, without requiring mechanical scan platforms or spinning sections, and (2) to develop an appropriate mass analysis system to be used in conjunction with the three-dimensional ion instrument to resolve all important ion species. Principal emphasis in this paper is given to goal (1). A parallel development of time-of-flight (TOF) mass analysis is being carried out; some results of this development have been reported by Young et al. (1989).

Our approach to the field-of-view (FOV) problem associated with fixed-attitude spacecraft has been to develop the candidate electrostatic deflection systems described in the following sections. These systems scan a large fraction of the unit sphere with programmed deflection and analyzer voltages. The voltages required, that are no higher than those that have been successfully used in some previous space flight plasma experiments, are shielded from the external environment by grounded enclosures. Combining a FOV scanning system with a high throughput, lightweight, high-resolution TOF system will provide high time resolution and M/q composition-resolved measurements of the three-dimensional distributions of the plasmas which surround planetary objects of interest.

Elevation Analyzers Under Development

In this section we describe five "elevation analyzer" concepts that achieve desired fully steerable FOVs. These elevation analyzers are in various stages of development at SwRI and Los Alamos. Each concept has been demonstrated to be viable, but some require further characterization with computer ray tracing studies and verification measurements on laboratory prototypes. Names given to the five candidate systems described below, in the order of presentation, are Beacon-C, Beacon-D, fast ion mass spectrometer (FIMS), gridded truncated hemisphere (GTH), and CRAF non-scanning platform (NSP).

Beacon-C Elevation Analyzer for Ion Composition Measurements

The Beacon-C elevation analyzer is one of two versions of a system called "Beacon" under development at Los Alamos. With a single Beacon sensor on a fixed-attitude spacecraft, particles can be resolved in energy, azimuth, and polar angle over all or most of a 2π str hemisphere. Fully three-dimensional measurements over the entire 4π str unit sphere can be implemented by placing diametrically opposed Beacon sensor heads on opposite sides of a spacecraft. A single set of power supplies and data processing and control logics can be used to operate both sensor heads. The Beacon-C is an ion composition version of Beacon designed to measure separately, but concurrently, the velocity distributions of the major ion species to be found in a planetary or cometary magnetosphere. Another version, Beacon-D, which is described in the next section, is configured to measure the velocity distributions of magnetospheric and solar wind electrons. It can also be employed to measure both electrons and ions (without composition) with a single detector system on missions with severely constrained spacecraft resources. Both the -C and -D versions make use of a Beacon system of rotationally symmetric electrodes shown in Figure 1, to deflect parti-

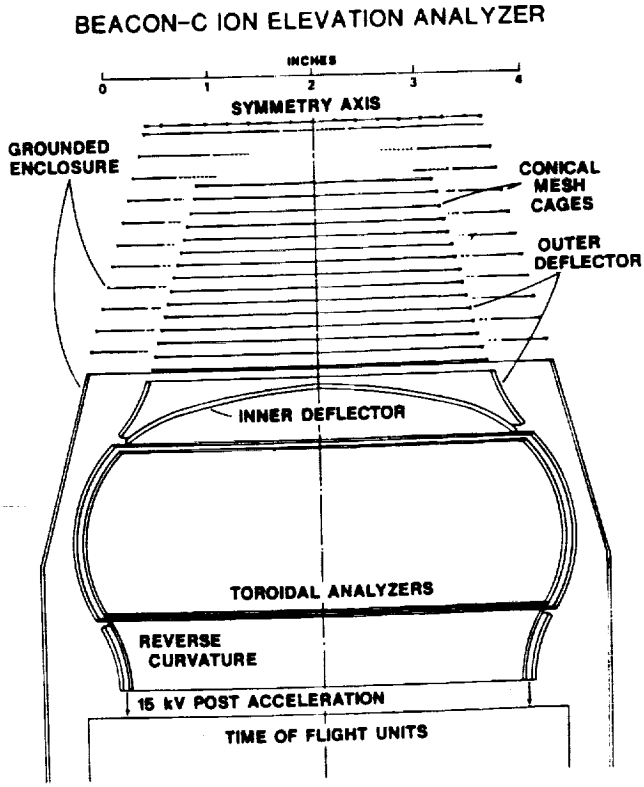

Fig. 1. The Los Alamos Beacon-C ion composition elevation analyzer, shown in a schematic cross-sectional view.

cles arriving along a conical surface into a toroidal electrostatic analyzer for E/q analysis. The acceptance cone angle, equivalent to the polar or elevation angle as referenced to the symmetry axis, is selected by applying appropriate voltages to the deflector electrodes. Particles arriving from 360° in azimuth around the conical surface are accepted and can be resolved in azimuth by physically dividing the 360° range. This division is implemented in different ways for Beacon-C and Beacon-D as described below.

Figure 1 shows a schematic, cross-sectional view of Beacon-C. This instrument employs the specially shaped inner and outer deflector electrodes of Beacon to deflect incoming ions into a two-stage toroidal analyzer. The deflector shapes were empirically determined using a 2 1/2-dimensional ray tracing computer program. This program, which traces only those rays that pass through the symmetry axes of rotationally symmetric systems, was utilized to maximize the deflection sensitivity vs. voltage of Beacon-C while permitting the desired range of polar angle acceptance to be achieved. The inner deflector, as shown, can be entirely solid, while the outer deflector is made up of a solid section, where bending is strongest, followed by a conical section of wire or mesh that is largely transparent to incoming ions.

The purpose of the second reverse curvature stage of the compound toroidal analyzer is to extend the bending angle of the analyzer to provide adequate energy resolution and UV rejection and at the same time to bring the analyzed ions out along a cylindrically shaped surface centered on and parallel to the instrument symmetry axis. For mass per charge separation the ions are then post-accelerated by −15 kV and injected into a circular array of TOF analyzers such as the array with 22.5° azimuthal resolution described by Young et al. (1989). Mass resolution might also be provided by an appropriate magnetic analyzer system, or a combination of TOF and magnetic analyzers, as used for the CRAF NSP instrument described in a later section.

Positive voltages are used on the deflectors and analyzer of the Beacon to avoid outward acceleration of the photo- and secondary electrons that will be produced on the instrument surfaces in space. The instrument is encased in a grounded outer container, as shown in Figure 1 to shield the instrument exterior from the interior voltages which may extend as high as 7 kV. (Such voltages have been successfully used in past space experiments and are not expected to cause any problems.)

Ray tracing with the 2 1/2-dimensional computer program has verified and characterized the capability of the Beacon deflection system. The program calculates the electrostatic configuration of an axially symmetric system and then incrementally traces particles launched with given initial conditions through the system along a plane which contains the symmetry axis. Further characterization of the Beacon response is in progress using a program which tracks particles through the three-dimensional representation of the instrument without constraining them to any particular plane.

Results using the 2 1/2-dimensional program are given in Figure 2. The program calculates rays one at time; a number of them have been superimposed in the figure. With an appropriate positive potential applied to the outside analyzer plate, ions launched from deep within the analyzer follow central paths out through the analyzer entrance and the deflectors. For electrostatic systems the rays are, of course, completely reversible. The rays shown were traced for a selection of voltages on the deflectors. They exhibit a pattern extending from ~1° to ~78° in polar or elevation angle. (This pattern prompted the name "Beacon" for this elevation analyzer.) Rays at polar angles extending from 46° down to 1°, near the sensor equator, were obtained with outer deflector voltages extending from 0 V to +7000 V in 700 V increments. Rays from 46° up to 78°, 12° from a polar angle of 90°, were obtained with the same voltages applied to the inner deflector. In either case the opposite deflector is held at 0 V. For these calculations, the ion launch energy was 34.0 keV/q corresponding to an incoming energy of 35.5 keV/q. (The energy difference is ~1/2 the analyzer voltage.)

Figure 3 is a plot of ion deflection angle vs. deflection voltage applied to the inner and outer deflectors. The slope of the curve is a measure of deflection sensitivity, which increases from high to low polar angle. This is understandable from inspection of Figure 2 which shows that larger portions of the trajectories of

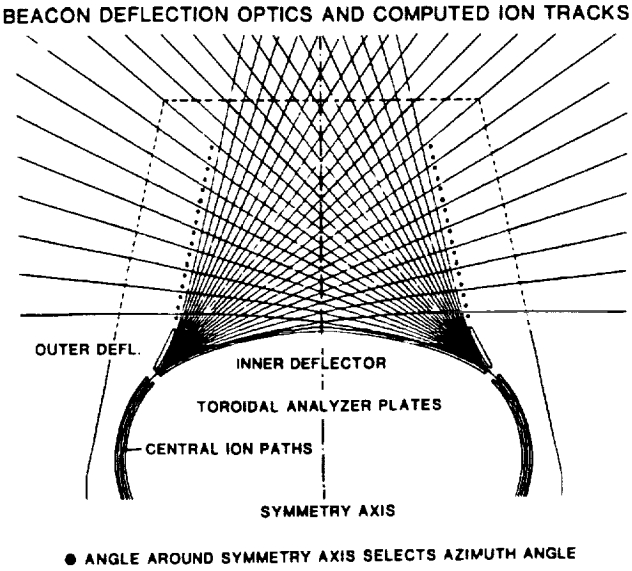

Fig. 2. Beacon coverage of the hemisphere. 35 keV ions with polar angles extending from ~0° to ~78° are deflected into the analyzer with voltages extending from 0 to 7000 V.

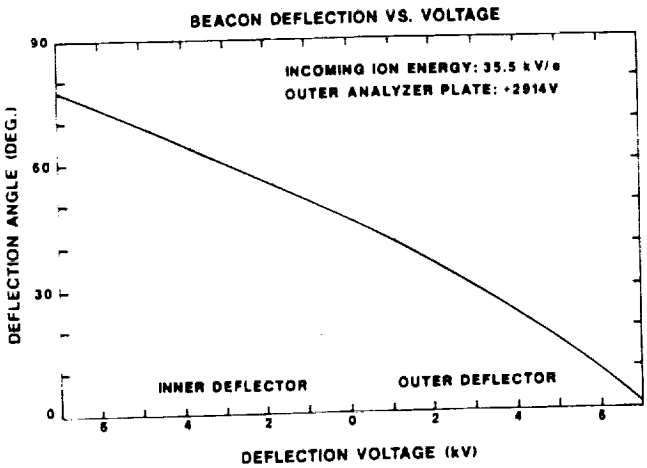

Fig. 3. Beacon deflection angle vs. voltage. Voltage is applied to one deflector at a time holding the other at 0 V.

ions deflected from low polar angles lie in regions in which the field strength is high and appropriately directed in comparison to the trajectories of ions deflected from high polar angles.

The ray tracing program has also been used to verify that the reverse curvature analyzer shown in Figure 1 performs as desired. A particle launched downward from near the entrance of the top toroidal section successfully passed into the lower section and exited with a trajectory parallel to the symmetry axis. Further simulations have shown that the Beacon can be configured to accept particles from an entire hemisphere. The version of Figure 1 accepts particles up to ~78° polar angle, which allows coverage of ~98% of the unit sphere with two sensor heads. Giving the outer deflector a more nearly cylindrical shape, coverage up to 100% has been calculated. The penalty for this small amount of additional spatial coverage is either a reduction of the maximum energy covered or a requirement for higher deflection voltages. For most applications the particle distributions to be encountered are broad enough that 98% coverage is quite adequate.

In order to verify that the Beacon operates as simulated and to further characterize its full three-dimensional behavior, a proof-of-principle test model was constructed at Los Alamos and taken to SwRI for preliminary tests in the SwRI calibration facility. A photograph of the test model is shown in Figure 4. It is constructed of aluminum alloy with Kel-F insulators in such a way that it can be assembled in both the Beacon-C and Beacon-D configurations. The figure shows it in the -C configuration without the external grounded container. The dome-shaped electrode in the center is the inner deflector; the outer deflector, visible above the inner, is extended by the wire cage continuation of the solid part of the deflector. The wire is 0.5 mm diameter BeCu which is relatively thick in comparison to the 1.5 mm analyzer plate spacing. Some of the Beacon response characteristics at low polar angle may have been affected by the thickness of the wire. We plan to do further tests with smaller wire or mesh.

At SwRI the calibration tests were conducted by placing the Beacon-C in the calibration system beam, mounted to permit rotation in both the azimuthal and polar angle directions. A broad parallel beam of 1120 eV N_2^+ ions was used for all the tests and the analyzed ions were detected in an imaging microchannel plate (MCP) system which had adjustable spacing behind the test model. Figure 5 shows 12 MCP images of the spatial distribution of the output ions from Beacon-C as displayed on a storage oscilloscope screen. For this series the deflectors were at 0 V, the instrument was set so that the beam polar angle was 44°, and the analyzer voltage was tuned to 84 V. As the figure shows, the analyzed beam at this polar angle is bifurcated at close and distant spacings but has a broad, well-defined crossover or focussed distribution at intermediate spacings extending from ~8 to ~21 mm. This bifurcation, which is under further study with fully three-dimensional simulations, is thought to result from transmission of those

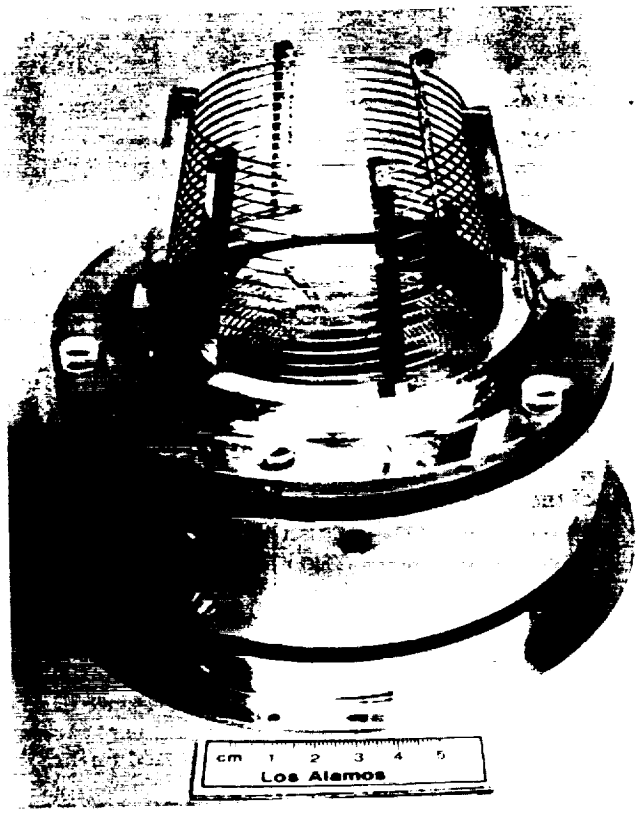

Fig. 4. Photograph of the Beacon proof-of-principle test model, with the outer grounded enclosure removed.

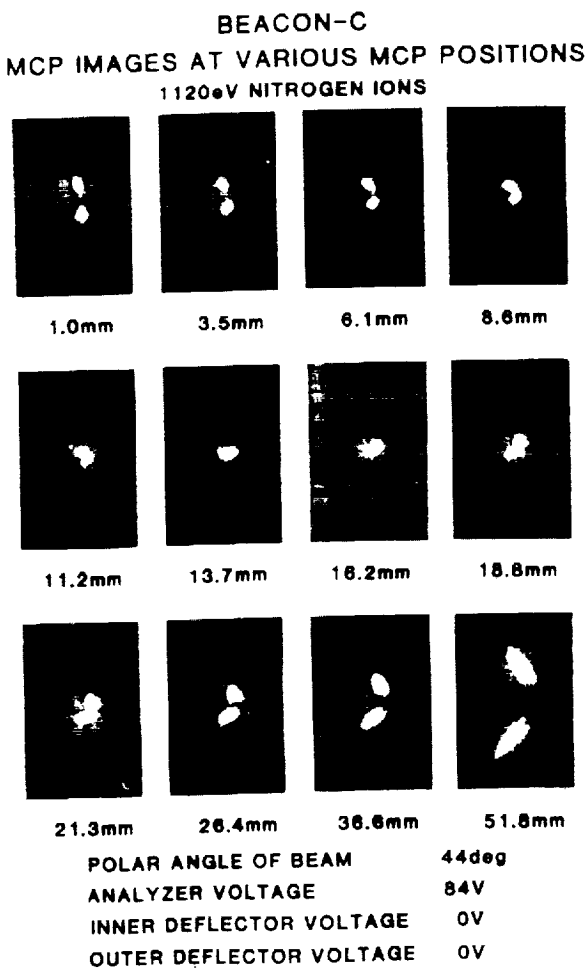

Fig. 5. Photographs of the spatial distributions of ions striking the imaging MCP taken at various MCP positions behind Beacon-C with the beam at a polar angle of 44° and deflectors at 0 V.

ions in the broad parallel beam which pass on either side of the region around the symmetry axis. Any of these intermediate focussed distributions would be suitable for 15 kV post acceleration into a TOF system such as that described by Young et al. (1989).

Figure 6 shows count rate contours taken over a field composed of the relevant ranges of analyzer voltage and polar angle. Both deflectors were held at 0 V for this set of measurements. The contours show evidence of structure in the response peak which is probably caused by grid wire shadows; this will be investigated further using finer grid wires.

Significant responses were found for Beacon-C over a range of polar angles extending from 0° to 79°. At angles above 79° the outer deflector wire cage interferes with the incoming ions. Figure 7 shows photographs

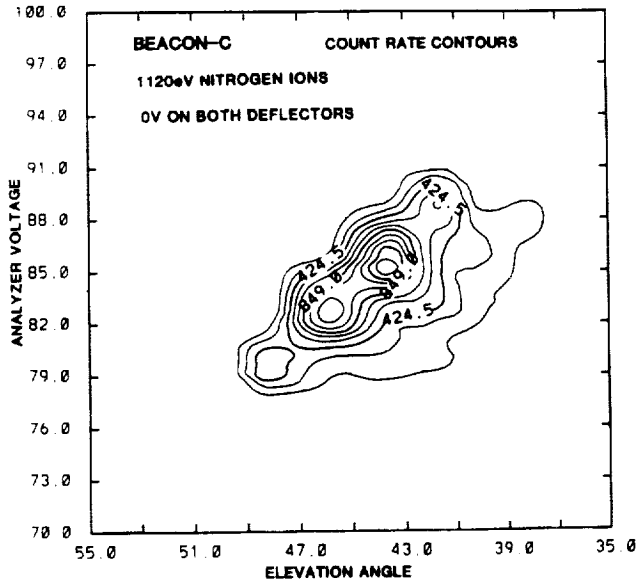

Fig. 6. Count rate contours taken over the relevant ranges of analyzer voltage and polar angle with both deflectors at 0 V.

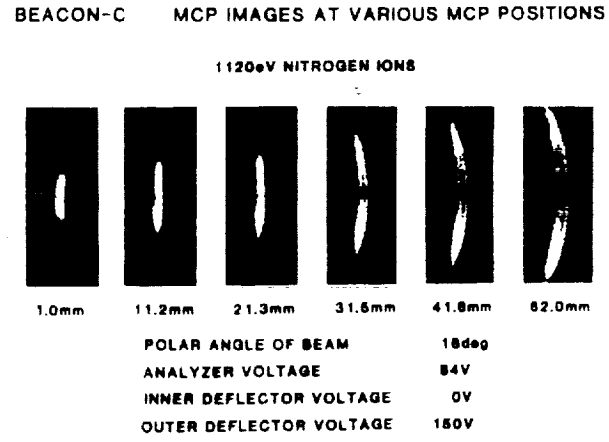

Fig. 7. Photographs of the spatial distributions of ions striking the imaging MCP at various spacings with the beam at a polar angle of 16°.

of MCP images for a beam at a polar angle of 16°, obtained with 84 V on the analyzer, 0 V on the inner deflector, and 150 V on the outer deflector. For this angle the beam is somewhat broader than for the previous case, but the image is still quite adequate between ~8 and ~20 mm to feed into a TOF system. Count rate contours over the relevant ranges of analyzer voltage and polar angle for 150 V on the outer deflector are shown in Figure 8. Multiple response peaks are not as

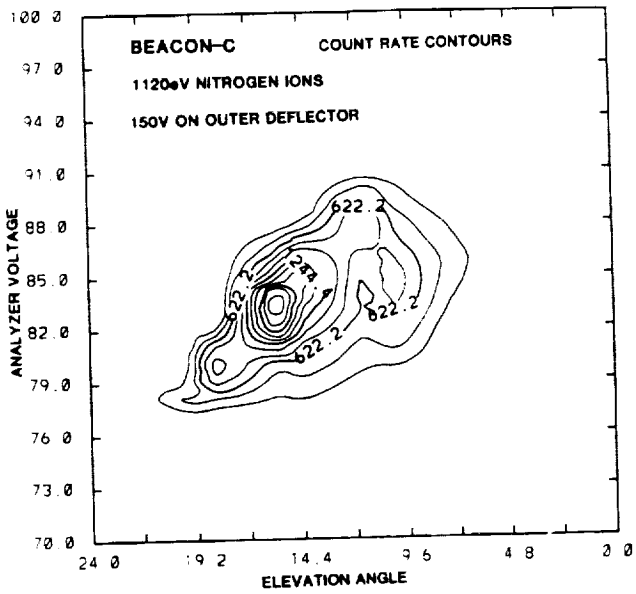

Fig. 8. Count rate contours taken over the relevant ranges of analyzer voltage and polar angle with the outer deflector at 150 V.

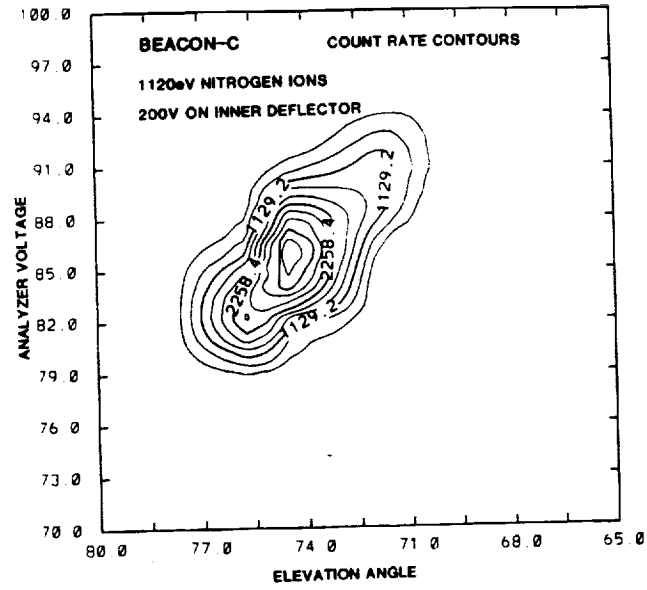

Fig. 9. Count rate contours taken with 200 V on the inner deflector, resulting in high polar angle response.

prominent here as for the previous case. Count rate contours for 200 V on the inner deflector are shown in Figure 9, and again there seems to be only one principal peak, positioned at ~74° polar angle and 85 V analyzer voltage. Here the beam does not go through the wire grid.

As a final test of the Beacon-C capabilities, the analyzer voltage was set at 84 V and polar angle sweeps were made for deflector voltages set at 0, 50, 100, 150, and 200 V, first on one deflector and then on the other. The results, given in Figure 10, show clean separation of the polar angle deflection ranges, particularly at high polar angles. At low polar angles, fine structure in the response peaks, as mentioned above, appears to be real and repeatable. Again, we believe this structure is probably due to the relatively large deflector wire size in comparison to the analyzer plate spacing. Future tests using finer deflector grid wire or mesh should help resolve this issue and reduce the amplitude of the fine structure, if indeed the wire size is the source of this response.

Beacon-D Elevation Analyzer for Electron Distribution Measurements

The Beacon-D analyzer shown in Figure 11 is intended for measurements of the velocity distributions of electrons in planetary magnetospheres and in the solar wind. It has deflection optics identical to those of Beacon-C, but instead of utilizing a compound toroidal analyzer, it uses a single toroid with a 133° bending angle. Analyzed electrons are post-accelerated, e.g., by +200 V, into an exit aperture housing where they strike a secondary emitter and create secondary electrons which are attracted into an MCP with its front face at +400 V. Since the azimuthal angle distributions of the

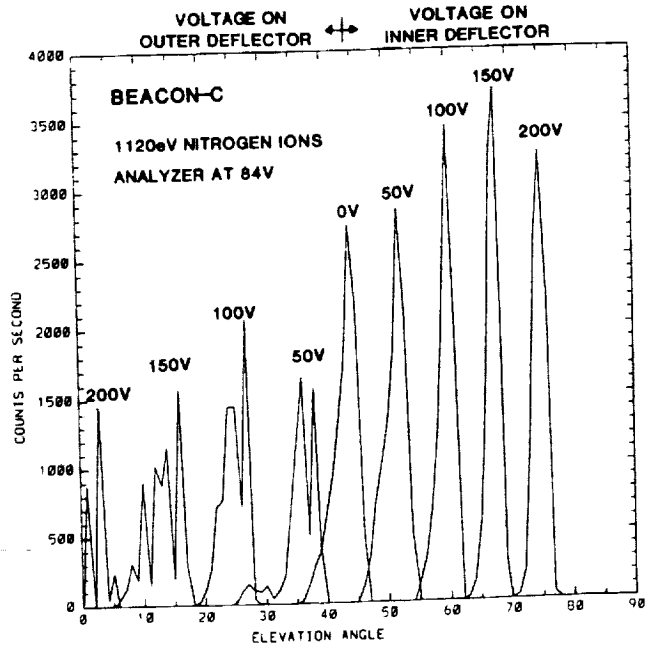

Fig. 10. Polar angle response of Beacon-C, measured at SwRI, for the various deflector voltages on the inner and outer deflectors shown above each peak.

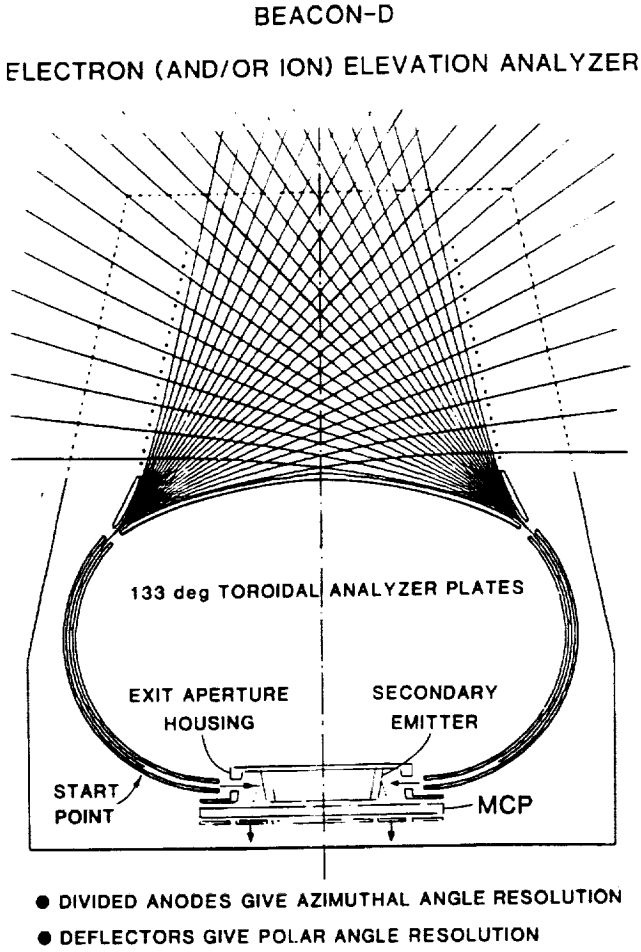

Fig. 11. Beacon-D configuration for detecting magnetospheric and solar wind electrons. The deflection optics are identical to those of Beacon-C.

electrons entering the sensor from outside are retained after deflection and electrostatic analysis, azimuthal angle resolution can be obtained by spatially resolving the electrons striking the MCP by employing a divided anode. For example, division of the anode into 16 parts would give 22.5° resolution.

As mentioned earlier, this configuration could be used to detect both electrons and ions for missions where both need to be measured, but spacecraft resources do not allow for flying independent electron and ion detectors. Referring again to Figure 11, ions as well as electrons can be analyzed if a second analyzer supply is provided. No additional deflector voltage supplies are required since the existing set serves to deflect both electrons and ions. To detect both electrons and ions after analysis, a programmable secondary emitter supply must be added to change the voltage configuration of the exit aperture housing/secondary emitter suitably. Computer simulations show this scheme to be viable; we plan to demonstrate it with a breadboard model as well. However, if resources permit, it is of course preferable to measure electrons and ions with separate instruments, to allow concurrent measurements.

At SwRI the Beacon-D configuration was tested in the same manner as Beacon-C with similar results. Polar angle sweeps for deflector voltages of 0, 50, 100, 150, and 200 V on the two deflectors, shown in Figure 12, demonstrate that the polar angle response of Beacon-D is similar to that of Beacon-C.

Fast Ion Mass Spectrometer (FIMS) Elevation Analyzer for Ion Composition Measurements

At SwRI, work has proceeded over the past several years on a class of gridded hemisphere elevation analyzers. This work was motivated by the need for three-dimensional, composition-resolved plasma measurements on CRAF, coupled with a lack of sufficient availability of mechanical scanning because of fuel limitations. Three instrument concepts that have been investigated are described here, beginning with FIMS. A schematic cross-sectional sketch of the FIMS is presented in Figure 13. This system, an outgrowth of an elevation analyzer system described by Wilhelm (1985), consists of three parts, which for convenience have been called an "elevation" analyzer, an "energy" analyzer, and an "azimuth" analyzer. The system is designed to cover a hemisphere, like Beacon, and would require two sensor heads with opposed viewing axes to cover the 4π str unit sphere. For ion mass measurements, the "azimuth" analyzer could directly feed into a cylindrical array of TOF analyzers as described by Young et al. (1989).

The elevation analyzer consists of a hemispherical system with the outer hemisphere made of grid or

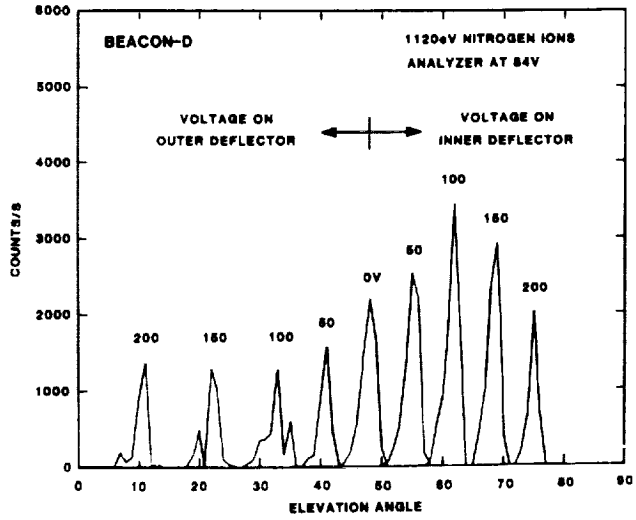

Fig. 12. Polar angle response of Beacon-D, measured for the deflector voltages shown above the response peaks.

mesh material. The inner elevation hemisphere consists of concentric conducting rings electrically isolated from each other. By programming the analyzer voltage onto first the bottom unshaded #1 ring, then the first two rings, the bottom three rings, etc., ions with polar angles beginning near 90° and extending down to near 0° can be accepted and further energy analyzed in the central truncated hemispherical analyzer. Particles then cross over from the energy analyzer into the azimuth analyzer which then brings them out in a cylindrical shell parallel to and centered on the instrument symmetry axis. By dividing the output of the azimuth analyzer into swaths, the azimuthal distribution of incoming ions, which is mirrored at the output, can be resolved, while polar angle resolution is achieved, as described, by programming the analyzer voltage on the rings of the elevation analyzer.

Figure 14 shows the results of a FIMS angular response measurement at SwRI. The instrument was placed in a 1 keV N_2^+ beam in the SwRI calibration chamber and the polar angle response was measured with 365 V on the various combinations of conducting rings. It is apparent that the FIMS can clearly resolve ion distributions in polar angle, as well as azimuth, thus facilitating three-dimensional determinations. By adding TOF units at the exit of the azimuth analyzer, the measurements of all major ion species can be made simultaneously.

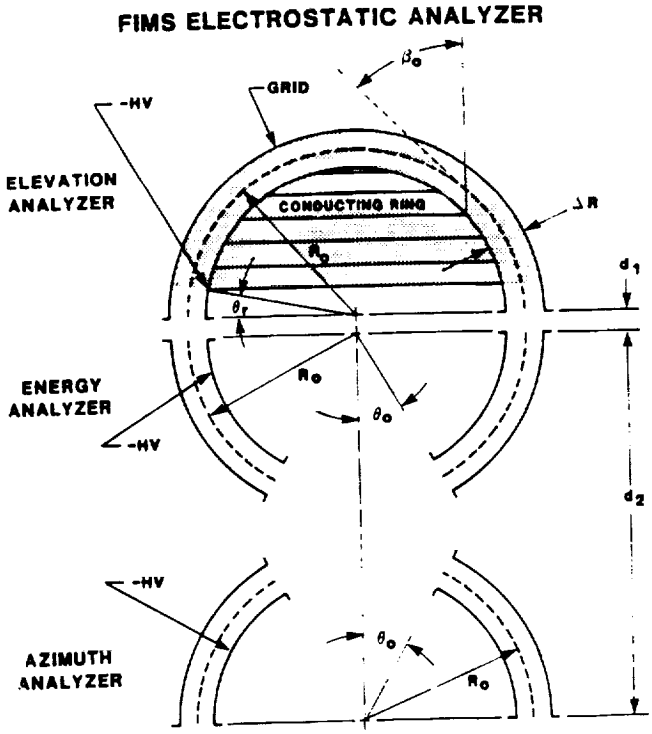

Fig. 13. Cross-sectional schematic of the FIMS electrostatic analyzer system.

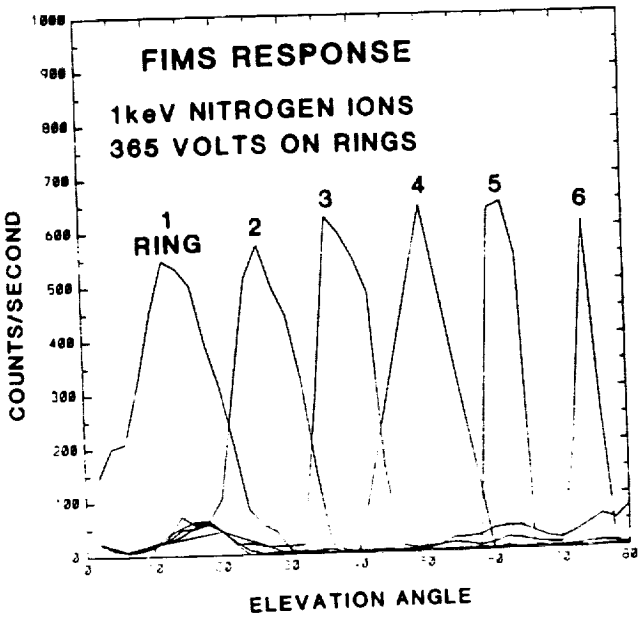

Fig. 14. FIMS polar angle response. The colatitude elevation or polar angle is used in this plot.

Gridded Truncated Hemisphere (GTH) Elevation Analyzer

Another member of the class of gridded hemisphere elevation analyzers under development at SwRI is the GTH, shown sketched in Figure 15. The inner deflection plate consists of a hemisphere that is truncated and closed with a flat surface at a latitude of 60°; i.e., it is a 360° by 60° hemispherical section, capped by a flat plate parallel to the equatorial plane of the section. The outer deflection plates are of similar geometry, but the flat plate is raised above the point of truncation. Both are made of 85% transmission conducting mesh or grid. In essence, the GTH consists of a parallel plate deflector followed by a spherical section deflector. For selecting particles from high polar (elevation) angle directions, as illustrated in Figure 15a, only the spherical section deflector is used, with no deflection occurring in the parallel plate deflector. To select particles from low polar angles, as in Figure 15b, the hemispherical analyzer is set at a constant deflection voltage, while the voltage of the parallel plate deflector is varied. The polar angle, α, is defined in Figure 16.

The reason two deflector systems are combined for the GTH, rather than using a full hemisphere, is that laboratory tests and ray tracing results have shown that if a full hemisphere is used the angular resolution (as measured by $dV/d\alpha$, where dV is the change in deflection voltage and $d\alpha$ is the resulting change in polar angle) becomes very coarse for polar angles less than about 30°. Figure 15a shows how the angle for 1 keV ions is controlled by varying the deflection voltage on the hemispherical section. In Figure 15b we show how

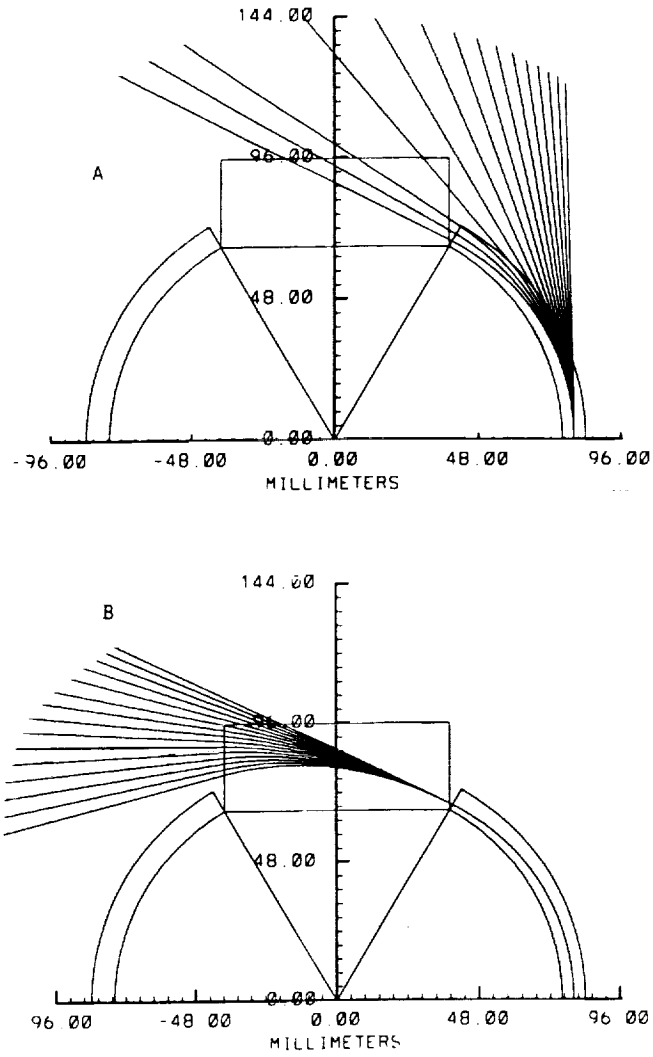

Fig. 15. (a) Cross-sectional view of the ion optics of the GTH elevation analyzer. Ions are shown entering from high polar angles through the outer walls of the parallel plate and curved plate deflectors which are made of screen or mesh. (b) Ions shown entering from low polar angles.

polar angles less than 30° are selected, with good angular resolution, by changing the voltage on the parallel plate deflector while holding the hemispherical section voltage constant. As shown in Figure 15b, good angular resolution is obtained even to polar angles beyond 0°, i.e., the instrument equatorial plane, with the circular parallel plate deflection system.

With the type of analyzer shown in Figure 15, it is necessary to have additional energy filtering because a large matrix of energies and elevation angles can enter the elevation analyzer at different locations along the entrance grid and pass through the analyzer exit. For this reason, the GTH deflector system is fitted onto a second hemispherical-section analyzer for energy analysis. Similarly to the FIMS, shown in Figure 13, these first two stages are referred to for simplicity as the elevation analyzer and the energy analyzer, respectively. Again like the FIMS, a third analyzer, which is referred to as the azimuth analyzer, is added to provide a relatively large annular output aperture which can be segmented to obtain good azimuthal angle resolution. The complete GTH stack is shown in Figure 16, which also shows the computed tracks of two ions passing through the entire system. The azimuth analyzer also provides a nearly parallel output beam, which can then be mass-analyzed with high resolution using either a magnetic or a TOF mass analyzer, not shown in Figure 16.

CRAF Non-Scanning Platform (NSP) Elevation Analyzer for Ion Composition Measurements

A recent addition to the SwRI candidate elevation analyzers for flight on the CRAF spacecraft, called CRAF NSP, would not require placement on the low resolution scan platform. Shown schematically in Fig-

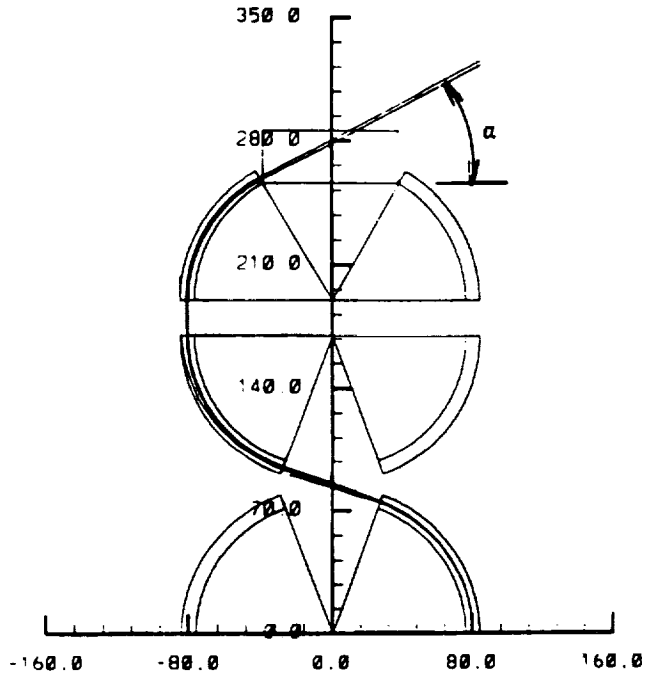

Fig. 16. View of the GTH stack, assembled with elevation, energy, and azimuth analyzers. Computed tracks of two ions are shown passing through the entire system.

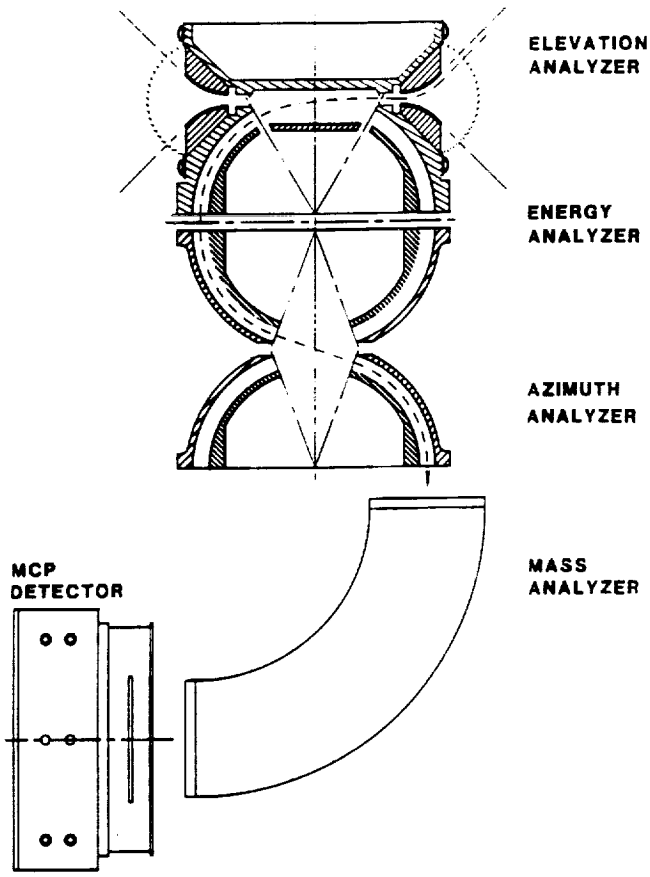

Fig. 17. Cross-sectional view of the CRAF NSP detector.

ure 17, it is composed of three truncated hemispherical analyzer sections in a stack with an additional deflection system on top. The top two truncated hemispheres comprise an energy analyzer which is followed by an azimuth analyzer. The upper elevation analyzer is no longer a hemisphere, but instead is composed of two curved deflector plates with rotational symmetry. The deflectors are enclosed in a grounded toroidal section of screen to isolate the deflection voltages from the spacecraft exterior. A distinct advantage of this geometry is that, like the Beacon geometry, particles entering into the deflector stage from outside pass through the screen almost normally, while with the FIMS and the GTH they pass through almost tangentially so that transmission is substantially reduced by the screen.

The energy analyzer for the CRAF NSP is composed of two near-hemispheres fed by the elevation analyzer. Referring again to Figure 17, ions from the energy analyzer cross over into the azimuth analyzer which separates them again to provide a nearly parallel output beam for mass analysis. In the present example, analyzed ions passed into a magnetic analyzer for mass analysis. Laboratory measurements with a prototype show that this system provides high-resolution separation of singly charged molecular ions of nitrogen and oxygen.

A TOF mass analyzer array like that described by Young et al. (1989) could also be used to mass analyze the ions passing out of the azimuth analyzer, or a combination of TOF analyzers and magnetic analyzers could be used.

Tests and ray tracing results show that the practical polar angle range that the CRAF NSP can cover is about $\pm 45°$ from the instrument equator. This range constitutes more than 70% of the full 4π str unit sphere and may provide sufficient spatial coverage for the CRAF mission.

Summary

The Los Alamos National Laboratory and the Southwest Research Institute are cooperating in a program to develop instruments capable of making three-dimensional measurements of space plasmas without requiring access to a spacecraft scan platform or spinning section. Such instruments could greatly reduce spacecraft requirements, simplify the acquisition of plasma data on planetary missions, and substantially increase the useful operating time of a plasma experiment. Importantly, the obscuration problem caused by spacecraft appendages such as antennas, RTGs, other instruments, and by the spacecraft itself can be circumvented by placing two 2π sensor heads on opposite sides of the spacecraft.

Five different instrument concepts have been explored. Instruments based on all five of these have the ability to select plasma particles from all pertinent directions in space by using electrostatic deflection techniques. In a continuing joint program these instruments will be investigated and tested further with the goal of developing one or more of them to a state of readiness for an appropriate planetary mission.

Acknowledgments. The authors wish to thank Bruce Barraclough, Jack Gosling, and Michelle Thomsen at Los Alamos who have generously contributed their time and enthusiasm in support of this joint SwRI/Los Alamos development program. We also wish to thank Tom Booker and David Strain at SwRI for their assistance with the calibrations of all the instruments described in this paper. Work at Los Alamos has been under the auspices of the U.S. Department of Energy. At SwRI this work has been supported by Internal Research Project 15-9455.

References

Lazarus, A. J., and R. L. McNutt, Jr., Low-energy plasma ion observations in Saturn's magnetosphere, J. Geophys. Res., 88, 8831, 1983.

Richardson, J. D., Thermal ions at Saturn: Plasma parameters and implications, J. Geophys. Res., 91, 1381, 1986.

Sittler, E. C., Jr., K. W. Ogilvie, and J. D. Scudder, Survey of low-energy plasma electrons in Saturn's magnetosphere: Voyagers 1 and 2, J. Geophys. Res., 88, 8847, 1983.

Wilhelm, K., W. Studemann, and W. Riedler, Observations of the electron spectrometer and magnetometer (Experiment 1 ES 019) onboard Spacelab 1 in response to electron accelerator operations, Earth-Orient. Applic. Space Technol., 5, 47, 1985.

Young, D. T., Near-equatorial magnetospheric particles from ~1 eV to ~1 MeV, Rev. Geophys. Space Phys., 21, 402, 1983.

Young, D. T., J. A. Marshall, J. L. Burch, S. J. Bame, and R. H. Martin, A 360° field-of-view toroidal ion composition analyzer using time-of-flight, these proceedings, 1989.

A High-Speed Low-Power Spectrum Accumulator Using Dual-Port RAM and State Machine Control

WALTER L. LOCKHART, JOSEPH H. GREENE, MEMBER, IEEE, AND DAVID T. YOUNG

Abstract—**A high-speed spectrum accumulator circuit intended for use with a time-of-flight mass spectrometer is described. Advantages of this design include high-speed data acquisition (> 400 kHz periodic, 2.5-μs pulse-pair resolution), high resolution (256 channels, expandable to 1024), low power (~2 W), and circuit simplicity. This performance is achieved with an optimum combination of an 8-bit flash analog-to-digital converter, dual-port RAM, and erasable programmable logic device (EPLD) state machine controller.**

INTRODUCTION

A. Time-of-Flight Mass Spectroscopy

SATELLITE-BORNE instrumentation is constrained in many ways in comparison to similar laboratory devices. Not only must these instruments survive the vibration, thermal, and radiation environments associated with space-flight, but they also must be highly reliable for mission durations of up to 10 years. Moreover, the instrumentation itself must be lightweight, be of low power, and perform at the state-of-the-art limits for the time at which the device is designed. One type of instrument that typifies these problems very well is the time-of-flight (TOF) ion mass spectrometer that our group has been developing over the last several years (Young *et al.* [1]). The heart of this device is a time-of-flight unit that functions by first collecting electrons that are emitted from a thin (50 Å) carbon foil by an ion that has been selected according to its incident energy per charge (E/Q) (Fig. 1). These electrons are focused onto a microchannel plate (MCP) that provides a "start" pulse for the time-of-flight circuitry. The ion will be scattered slightly and will lose a small amount of energy in the foil, but basically its velocity is unchanged as it travels from the foil through a field-free region where it impacts on a second MCP that generates a "stop" pulse. The time difference between the start and stop events is proportional to ion velocity, and since the TOF distance and ion E/Q are known, ion mass per charge may be determined.

The advantages of such an instrument are that it images all ion species simultaneously (i.e., at a rate comparable to the incident differential ion flux rate) and does this with relatively simple requirements on ion and electron optical systems. The disadvantage of TOF is the complexity of electronic circuitry and, if the circuit is run at very high rates (several 10^5 Hz), the power required to operate it.

Manuscript received January 24, 1989; revised March 1, 1989. This work was supported by Southwest Research Institute Internal Research Project 15-9522.

The authors are with Southwest Research Institute, P.O. Drawer 28510, San Antonio, TX 78284.

IEEE Log Number 8928096.

In the remainder of this paper we address the design of a high-speed spectrum accumulator, which is a partial answer to the resource constraints on TOF instrumentation.

B. Electronics Approach

In this proof-of-concept design an approach for a spectrum accumulator is presented that makes use of readily available off-the-shelf integrated circuits. A follow-up design will address the selection and qualification of flight circuits. The circuits included in this design were chosen as good candidates for radiation hardness and reliability level screening. Wherever possible, data on radiation hardness and quality level availability have been included.

Time-of-flight measurements are made using MCP's, which detect the impact of either electrons or ions (see Young *et al.* [1] for a description). The start and stop MCP's produce pulses that are processed within the instrument electronics to yield an analog voltage level. This level is proportional to time-of-flight and is stored in a sample-and-hold circuit. A strobe signal is provided by the instrument electronics to inform the spectrum accumulator of a valid event. The spectrum accumulator then digitizes this level, generates a bin address, and increments the bin contents by one. In this manner the spectrum accumulates until the end of a preset sample period.

Typical design approaches for spectrum accumulators involve either discrete counter chain arrays or a microprocessor/memory combination. The choice between the two depends on instrument specifications and requirements. For space applications the data throughput, resolution, radiation hardness, and instrument power consumption are the primary constraints.

Counter chain arrays, while having high count bandwidths, quickly become unwieldy when more than 16 channels are involved. Discrete arrangements of eight-channel 16-bit counters occupy approximately 25–30 in^2 of board area. A 16-channel 24-bit counter custom integrated circuit (gate array) [2] can be made to fit in approximately 1–1.5 in^2. Even with this integrated approach the requirements of only 100 channels would force an unreasonable package size.

Microprocessor/memory combinations are perhaps best suited to spectrum accumulator applications, but they have their drawbacks as well. The advantages of the microprocessor/memory combinations are the relatively low parts count and the resulting packaging efficiency of such a system, but the requirement for processing data at event rates of at least 400 kHz eliminates most microprocessors from consideration due to the overhead processing time required by the micropro-

0018-9499/89/0800-1396$01.00

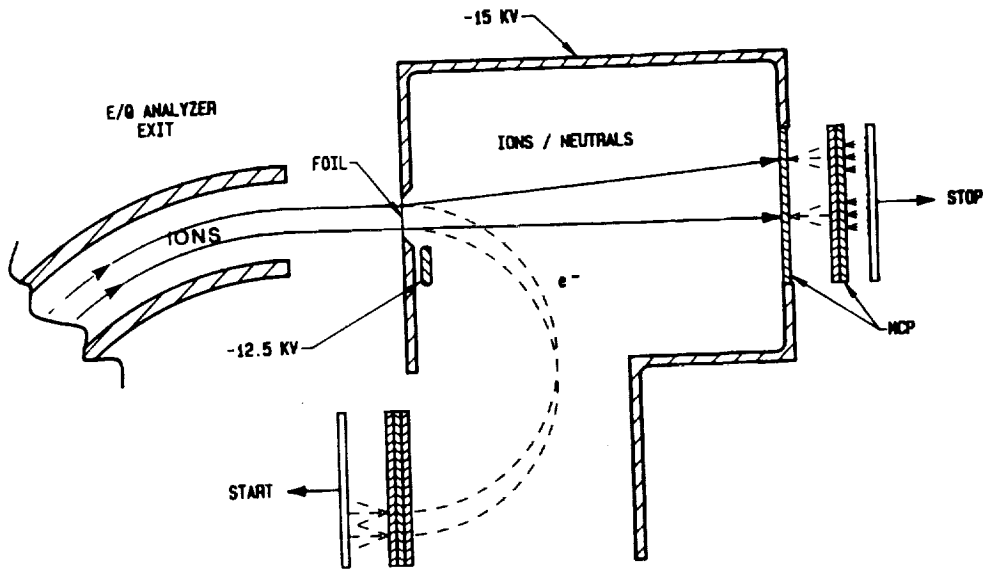

Fig. 1. Time-of-flight sensor schematic diagram.

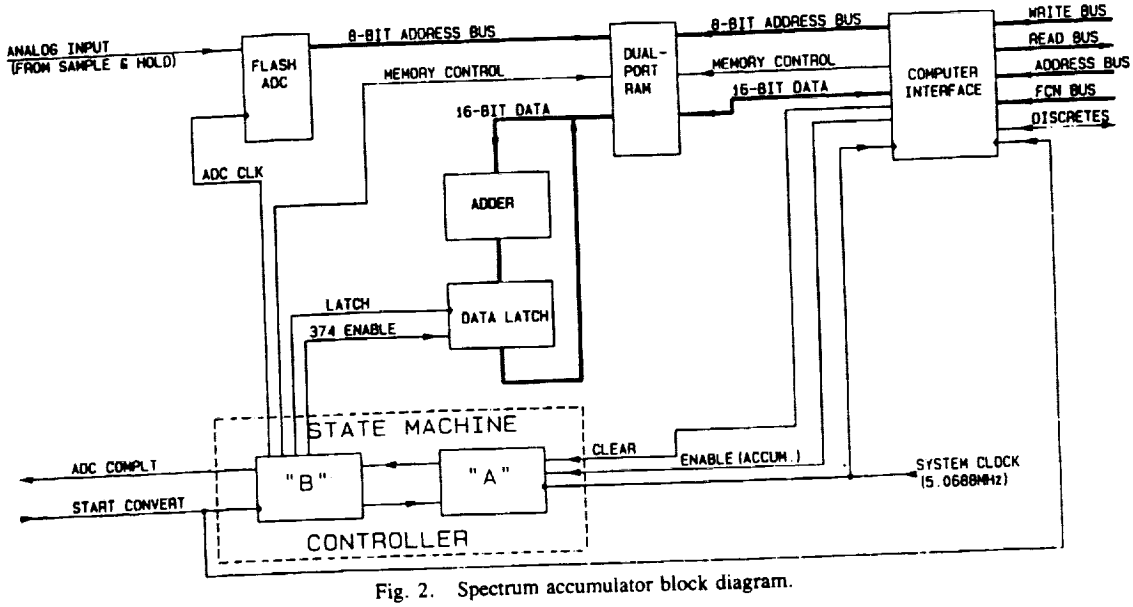

Fig. 2. Spectrum accumulator block diagram.

cessor to execute the read, modify, and write algorithm of a spectrum accumulation cycle. While chip sets (ALU's and ASIC's) [3], [4] exist that could execute these instructions at a higher throughput rate, the power consumption of these devices is prohibitive.

It was determined that the best approach for spectrum accumulation in this application would combine the advantages of the high throughput available from counter chains with the memory organization and packaging efficiency of a microprocessor-based system.

Circuit Description

A block diagram of the 256-channel spectrum accumulator is shown in Fig. 2. The system consists of five main parts:

1) flash analog-to-digital converter (ADC)
2) dual-port RAM
3) adder/latch
4) state machine controller
5) computer interface.

The flash ADC section is implemented using a MP7684 circuit from Micro Power Devices. The circuit is an 8-bit-resolution complementary metal-oxide-semiconductor (CMOS) 20-Msample/s converter with three-state parallel outputs. Devices meeting a radiation hardness of 1×10^5 rad(Si) are available for special orders; 5×10^3 rad(Si) is a typical hardness for off-the-shelf. The particular device chosen has a combined differential and integral nonlinearity of $+/-1$ bit over the operating temperature range. Supporting circuitry is provided to buffer the input analog signal from the time-of-flight electronics' sample-and-hold circuitry and to give a stable voltage reference for the ADC.

The spectrum accumulation is stored in the dual-port RAM circuit. An IDT7130S device, manufactured by Integrated Device Technologies, is used for this purpose. The device is a

1K × 8-bit dual-port CMOS static RAM with a 120-ns access time. Two devices are used, side by side, to accommodate the 16-bit word width required to accumulate a spectrum at the specified (400 kHz) count rates and typical accumulation intervals of 5–50 ms. The dual-port feature allows for easy access to accumulator memory from either the data acquisition side (ADC, adder, and state machine controller) or the computer interface. Radiation hardness of these devices is in the range of 1×10^4 to 1.5×10^4 rad(Si).

It should be noted that in this application only 256 of a possible 1024 locations (channels) are used in the dual-port RAM. Higher resolution ADC's (10-bit maximum) could be accommodated with little impact on the existing circuitry. Alternately, the memory could be divided into fourths, and separate accumulations could then occur in each of the four memory sections. This would simplify the implementation of multichannel analyzer operations such as spectrum stripping; Spectrum A could be subtracted from Spectrum B and so on.

The spectrum accumulation stored in the dual-port RAM is the result of an interactive process of reading, modifying (adding one), and writing to a memory address pointed to by the ADC output word. The adding function is performed by HC283 4-bit adders and HC374 data latches configured to accept 16 bit word widths.

The process of accumulating a spectrum depends on the proper sequence of commands given to the ADC, dual-port RAM, and adder circuits. This is provided by the state machine controller circuit. The controller is implemented using a 5C060 erasable programmable logic device (EPLD) from INTEL. This device is capable of implementing over 600 equivalent gates of user-customized logic functions through programming. Individually programmable output registers greatly enhance this device for use in state machine applications.

Communication between the spectrum accumulator and computer is performed within the computer interface section of circuitry. System operation requires computer interaction to initialize the memory, set the sample size, and select the accumulation mode. Accumulation mode can either be total counts (ADC conversions) or elapsed time. Mode selection is done by the computer selectively setting or resetting a mode register within the interface electronics. Mode selection affects the clock source for the down counter chain: the ADC convert pulse is used for total counts, while a prescaled system clock is used for elapsed time.

Operation

A. Overview

Prior to a spectrum accumulation cycle the memory and down counter portions of circuitry must be initialized. The memory is reset by writing zeroes to all addresses used during an accumulation. Once the memory has been cleared, the down counter is loaded with the desired count and the accumulation mode (integral or elapsed time) is selected. These functions all occur through the computer interface circuits.

The spectrum accumulator is now armed and ready to accept analog data from the time-of-flight front-end electronics. An analog voltage proportional to time-of-flight is strobed into the spectrum accumulator by the START CONVERT pulse. START CONVERT is sensed by the state machine controller, which then initiates the following sequence of commands to perform an accumulation cycle:

1) clock the ADC
2) read the memory (ADC address)
3) latch the sum (memory data + one)
4) write to memory (ADC address)
5) return to standby state.

This sequence will continue until the down counter reaches zero. At this point the state machine controller is disabled and the computer is flagged that the accumulation is complete. The spectrum is then read out of the dual-port memory circuit, with the address being proportional to time-of-flight and the stored data yielding the actual count.

The time required for the spectrum accumulation cycle (the A/D conversion and binning of one time-of-flight data point) is 2.5 μs and could easily be halved with faster system clock speeds and parts. The time required for a spectrum accumulation is affected by the mode selection: elapsed time mode accumulates for a preset time (0–210 ms), while integral mode accumulates for a preset number of conversions (0–65 535). Since the measured events are not contiguous, the accumulation time will vary from sample to sample in the integral mode.

Spectrum clearing and readout both take the same amount of time to execute. The difference is that one function executes repetitive writes (zeroes) to sequential memory addresses (clearing), while the other performs repetitive reads (readout).

The spectrum clearing/readout time is controlled by the bus speed of the computer interface. In this instance the bus executes memory writes or reads in one microsecond. Clearing/readout of the 256 spectrum addresses then takes the sum of 256 memory writes/reads plus two instruction execution cycles for address counter initialization and memory selection (≈ 260 μs). Spectrum clearing, accumulation, and readout time is then determined by

$$T_t = T_c + T_a + T_r$$

where

- T_c spectrum clear time, which equals 260 μs
- T_{a1} elapsed time mode accumulation time, which equals 0–210 ms
- T_{a2} integral mode accumulation time, which equals present down counter (0–65 535)/event rate (Hz)
- T_r readout time, which equals 260 μs.

The next section discusses the operation of the spectrum accumulator in more detail.

B. EPLD State Machine Controller/ADC/Dual-Port RAM

The 5C060 EPLD used for the state machine controller is a UV-erasable device. The 5C060 uses sum-of-products logic, providing a programmable AND with a fixed OR structure. The package provides four dedicated data inputs and two synchro-

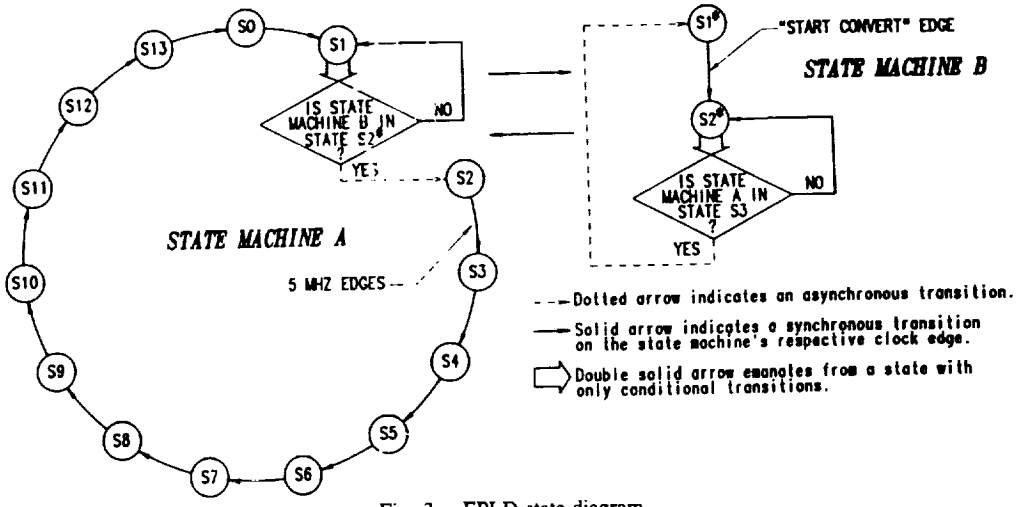

Fig. 3. EPLD state diagram.

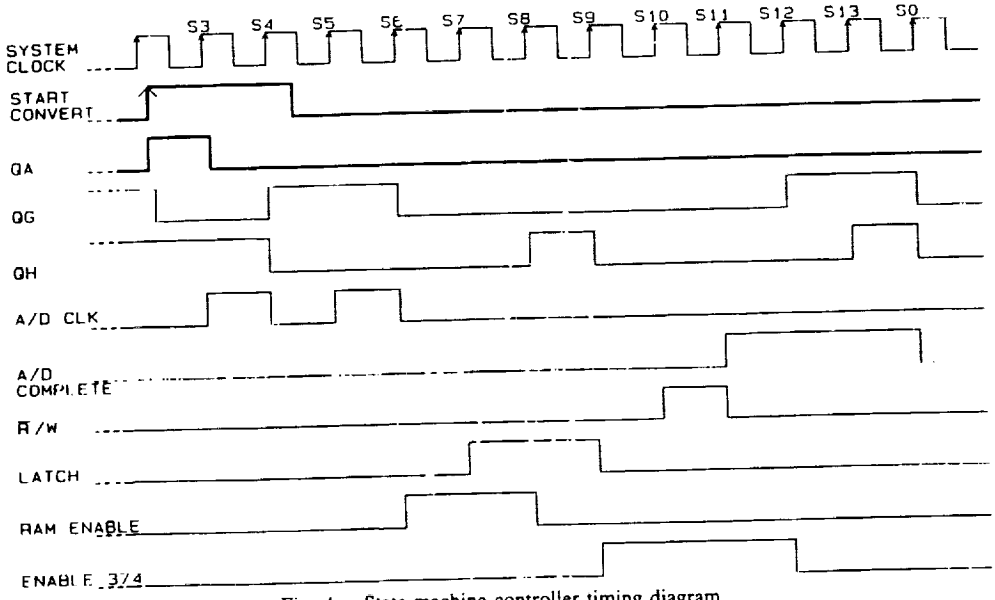

Fig. 4. State machine controller timing diagram.

nous clock inputs. Also supplied are 16 I/O pins (macrocells), which may be individually programmed for input, output, or bidirectional operation. All I/O pins are internally fed back to the AND array, and buried registers can be programmed to yield additional feedback. Each synchronous clock input is capable of controlling a bank of eight programmable registers, or the clocks can be tied together to create a single bank of 16 individually programmable output registers.

For this application the EPLD is programmed to accommodate two separate internal state machines, each controlled by a different clock signal. The 5.0688-MHz system clock controls the state machine referred to as state machine A, while the START CONVERT signal controls state machine B. Internal feedback is used to make these state machines interactive by allowing the current state of one to asynchronously advance the state of the other, and vice versa. Fig. 3 shows a state diagram for the EPLD.

On power-up the EPLD performs an asynchronous clear function on each output. However, a CLEAR signal has been provided so that the EPLD may be asynchronously reset through the computer interface to its initial state with all outputs inactive. Once the CLEAR signal returns to its unasserted logic level, the state machine is ready to control the spectrum accumulation sequence.

When the accumulation parameters are selected, the down counter enable signal is asserted, thereby causing state machine A to advance to the "armed" state on the next rising edge of the system clock. (The armed state is made different from the initial state to ease the design of the control algorithm.) Meanwhile, state machine B waits for a START CONVERT edge and advances to its only other state when one occurs. State machine A detects this change and asynchronously advances to its next state, where it then free-runs through the remaining control sequence.

Fig. 4 shows the timing diagram for the state machine controller. The first control signal that is generated is the pair of clock pulses for the analog-to-digital converter. The first pulse to occur generates a feedback signal internal to the EPLD, which is used to asynchronously reset state machine B. The result of the conversion appears at the ADC's output

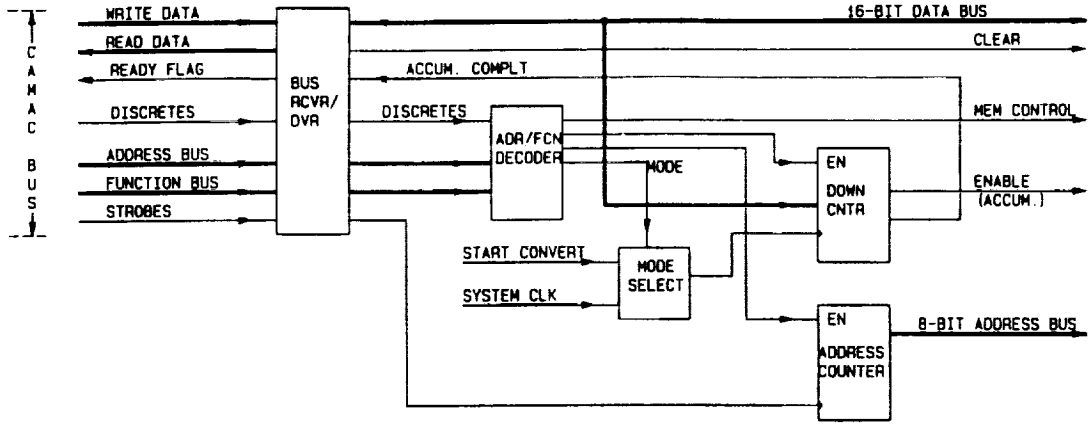

Fig. 5. Computer interface block diagram.

during the second pulse and correspond to a specific memory address. The next rising edge of the system clock generates a signal that turns on the outputs of the dual-port RAM devices, thereby placing the contents of the memory location pointed to by this address on the data bus. The data are presented to the string of 4-bit adders where they are incremented by one. On the following system clock edge the RAM output enable signal is preserved, and a new positive-going signal is asserted, which latches the incremented data. This new data appears back on the data bus two system clock cycles later and is written back to RAM on the subsequent cycle. A flag indicating conversion complete (ADC COMPLT) is generated on the next clock cycle and is maintained for three system clock cycles. This conversion complete signal is used in the time-of-flight front-end electronics to discharge the peak hold capacitor in preparation for the next acquisition. The next system clock returns the state machine to its initial state.

Provided that the preset accumulation time has not elapsed, the next START CONVERT pulse will begin another accumulation cycle. When the accumulation time (or count) has run out, both machines will immediately be reinitialized regardless of where they are in the control sequence. They are rearmed each time the accumulation parameters are selected and the down counter is enabled.

C. Computer Interface

The spectrum accumulator can easily interface with any bus or computer type. In this application it is designed to operate as a module in a CAMAC crate. Adaptations of this design to other computer bus configurations should be readily apparent to those schooled in the art. Regardless of the bus configuration, the commands needed to control the spectrum accumulator are identical. The required commands are

1) CLEAR MEMORY
2) LOAD DOWN COUNTER
3) SELECT ACCUMULATION MODE
4) ENABLE ACCUMULATION
5) SENSE "ACCUMULATION COMPLETE" FLAG
6) READ OUT MEMORY (SPECTRUM).

The CAMAC interface electronics must decode the function and address words from the CAMAC bus, and initiate the proper response. Additionally, the interface electronics must flag the bus that the module is ready to be read (ACCUMULATION COMPLETE). Fig. 5 shows the major blocks of the computer interface. The major blocks are

1) bus receiver/drivers
2) address/function decoder
3) mode selector
4) down counter/flag generator
5) address counter.

The bus receiver/driver section connects the dataway between the module and the CAMAC bus. All function, address, discrete, and status signals are communicated via this section. The CAMAC bus uses separate read and write buses to send data and receive data. In this application the spectrum word width is 16 bits and is easily accommodated by the 24-bit maximum data word width of the CAMAC bus.

The address/function decoder issues commands from the CAMAC bus to the addressed portion of the computer interface electronics. The address counter, down counter, and mode selector have unique addresses. These addresses are decoded and the proper functions are asserted during execution of computer commands. The address/function decoder is implemented using programmable logic and can be easily modified to respond differently by reprogramming.

Mode selection is used to switch between integral and elapsed time sample modes. The mode selector is a register-based clock selection circuit that either uses the START CONVERT or prescaled system clock to trigger the down counter.

The down counter is a presettable counter circuit that is loaded with the desired count prior to accumulation. Once enabled, the down counter counts down until it reaches zero. At this point the accumulation is terminated and a flag is generated to signal the computer that the accumulation is complete.

The address counter section works in the auto-increment mode and is clocked during each memory select assertion. This configuration forces the memory to no longer be true random access. Memory addressing is sequential with the address counter containing the next address at the end of a

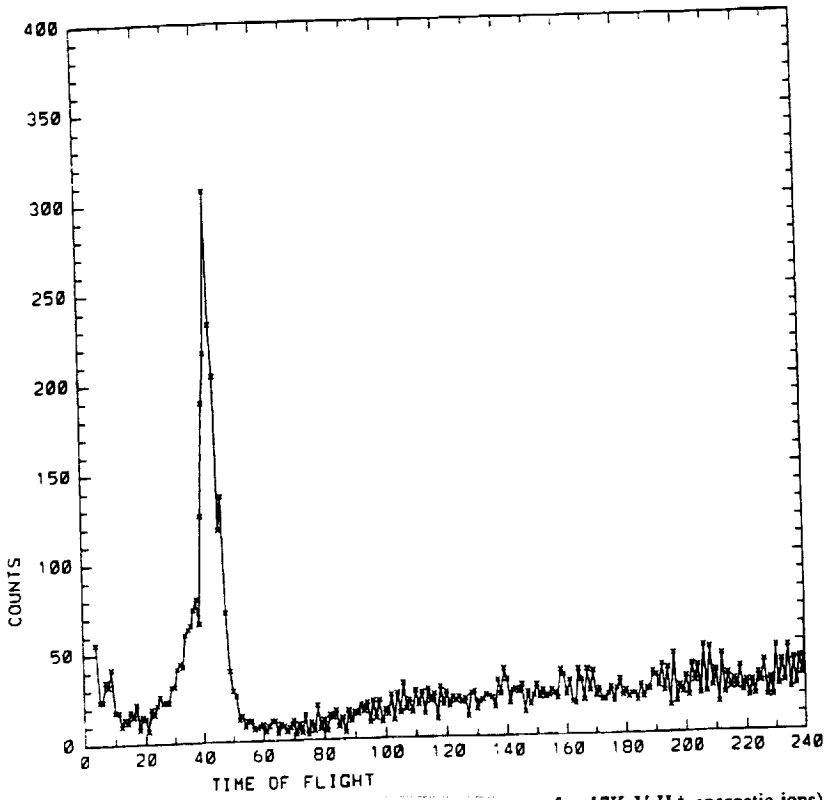

Fig. 6. Sample time-of-flight data, linear scale (spectrum of ≈ 17KeV H_2^+ energetic ions).

memory cycle. Therefore, for proper addressing of memory to occur, the address counter must be reset to zero prior to writing or reading a block of memory.

Results

A. Time-of-Flight Data

Mass spectra acquired using the spectrum accumulator are shown in Figs. 6 and 7. The spectra are acquired using the integral count mode. In Fig. 6 the data are displayed using linear count scaling. Fig. 7 shows the same data using log count scaling.

The ion beam is generated by an electron impact ion source floated to 10 kV above ground and collimated down a four-meter drift tube. Beam flux at the instrument aperture is on the order of 1 pA/cm^2.

B. Packaging/Power

The package for the accumulator electronics was completed using a CAMAC module board (size 11 × 7.5 in) (Fig. 8). The module occupies a double-width slot in the CAMAC crate. In addition to the accumulator electronics discussed here, there are additional circuits dedicated to the TOF instrument (specifically, a spectrum look-up table and binning section) that occupy approximately one third of the available board area.

The power for the accumulator electronics is derived from the +/−6-Vdc and +/−24-Vdc supply rails of the CAMAC crate. Three terminal regulators are mounted on the board to provide +/−15-Vdc supplies for the analog circuitry. Power consumption of the accumulator electronics was measured under quiescent and operating conditions. At quiescent the power required for operation is 1 W; Under operation at 400 kHz the power required is 2.1 W.

C. Accumulation Speed

Oscilloscope photographs showing the timing relationships of different key signals are shown in Figs. 9 and 10. The reference signal is START CONVERT followed by ADC CLK, etc. An accumulation cycle begins with the rising edge of START CONVERT and ends with the falling edge of ADC COMPLT. As shown in the photographs, an accumulation cycle takes ~2.5 μs (2.4 μs measured). These measurements are made with a periodic input test signal synchronized to the system clock; this allowed stable waveforms for observation. Under normal operation the inputs are asynchronous and noncontiguous and would appear blurred on a continuous time display.

Conclusion

A spectrum accumulator has been presented that exploits current technology in off-the-shelf circuits to achieve high-speed accumulation and low-power operation. The approach compares favorably with ASIC-based designs and allows the designer freedom to customize circuit function through the use of programmable logic elements.

Finally, a circuit concept for satellite-borne instrumentation has been proven. Implementation with radiation-hardened (through packaging, fabrication process, or both) and high-reliability circuits will conclude this design. Further refinements could improve the performance (accumulation speed) and features without greatly sacrificing power or packaging

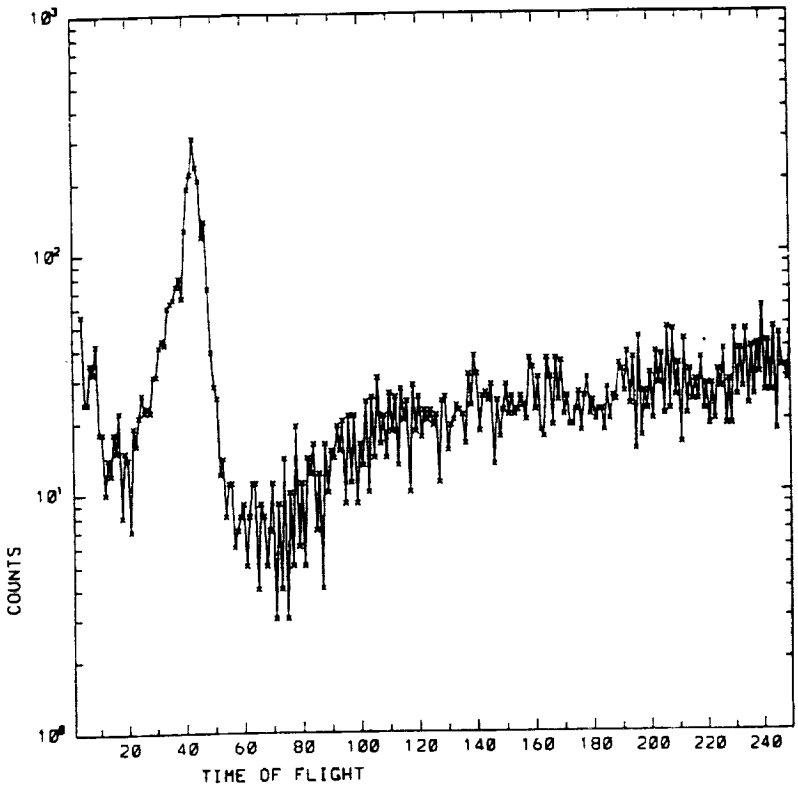

Fig. 7. Sample time-of-flight data, log scale (spectrum of ≈ 17KeV H_2^+ energetic ions).

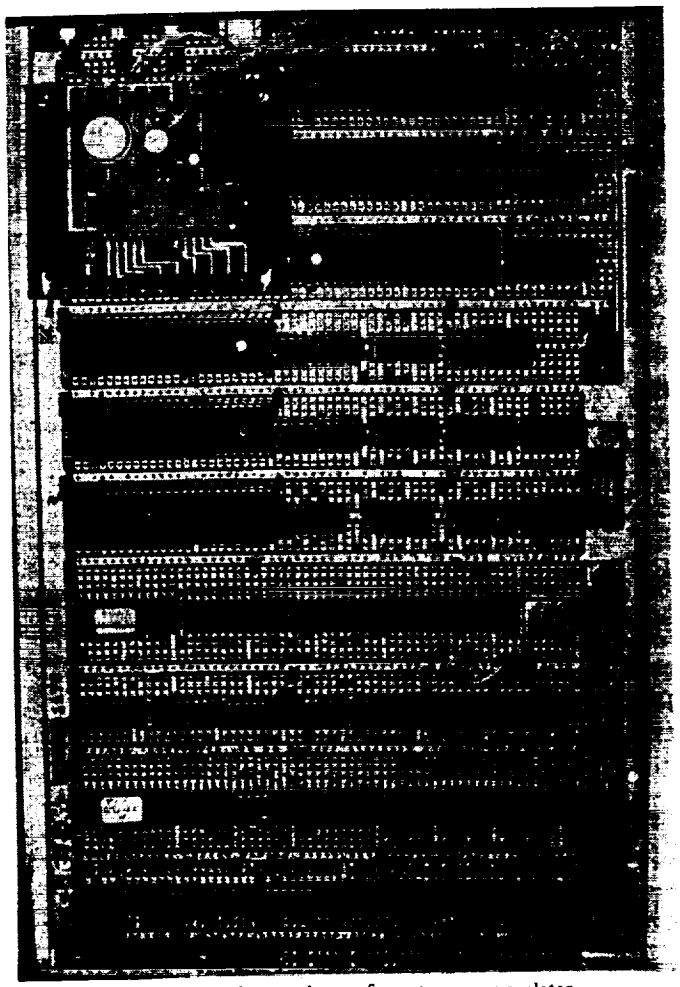

Fig. 8. Complete package of spectrum accumulator.

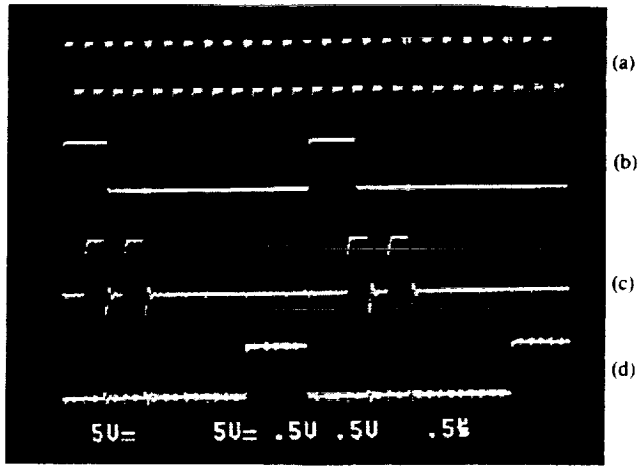

Fig. 9. Waveform photo of key control signals (all waveforms are 5 V/div, 500 ns/div). (a) 5.0688-MHz system clock. (b) START CONVERT pulse. (c) ADC CLK signal. (d) ADC COMPLT pulse.

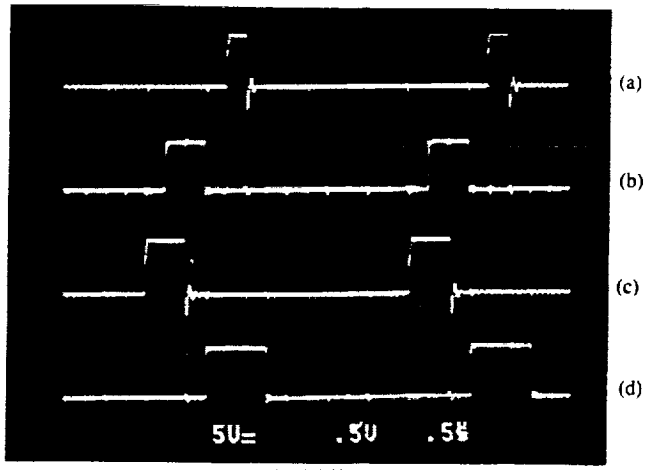

Fig. 10. Waveform photo of key control signals (all waveforms are 5 V/div, 500 ns/div). (a) R/W (dual-port RAM read/write control). (b) LATCH (data latch control signal). (c) RAM ENABLE (dual-port RAM enable signal). (d) ENABLE 374 (data latch enable signal).

resources. Successful implementation of this approach solves many of the problems associated with satellite-borne instrumentation of this type.

Acknowledgment

We would like to acknowledge the efforts of Mildred Lopez, Benjamin Piepgrass, and James Jackson for fabrication and testing of this design, and Thomas Booker for his assistance in the evaluation of time-of-flight instrumentation in the ion calibration facility.

References

[1] D. T. Young, J. A. Marshall, J. L. Burch, S. J. Bame, and R. H. Martin, "A 360 degree field of view toriodal ion composition analyzer using time-of-flight," *Proc. Yosemite 1988 Conf. Outstanding Problems in Solar System Plasma Physics: Theory of Experimentation,* Feb. 2-6, 1988, AGU Monograph no. 54, in press.

[2] R. C. Moore, Johns Hopkins University Applied Physics Laboratory, September, 1987, private communication.

[3] V. Goursky, P. Gallice, J. Kaiser, G. Hantelle, and R. Schmit, "ASIC's for spectrometry," *IEEE Trans. Nucl. Sci.*, vol. NS-35, no. 1, pt. 1, pp. 181-183, Feb. 1988.

[4] H. P. Spracklen, "7-MHz particle identifying PHA," *IEEE Trans. Nucl. Sci.*, vol. NS-29, no. 1, pp. 896-899, Feb. 1982.

New approach to 3-D, high sensitivity, high mass resolution space plasma composition measurements

David J. McComas and Jane E. Nordholt
Space Plasma Physics Group, Los Alamos National Laboratory, Los Alamos, New Mexico 87545

(Presented on 9 May 1990)

This paper describes a new type of 3-D space plasma composition analyzer. The design combines high sensitivity, high mass resolution measurements with somewhat lower mass resolution but even higher sensitivity measurements in a single compact and robust design. While the lower resolution plasma measurements are achieved using conventional straight-through time-of-flight mass spectrometry, the high mass resolution measurements are made by timing ions reflected in a linear electric field (LEF), where the restoring force that an ion experiences is proportional to the depth it travels into the LEF region. Consequently, the ion's equation of motion in that dimension is that of a simple harmonic oscillator and its travel time is simply proportional to the square root of the ion's mass/charge (m/q). While in an ideal LEF, the m/q resolution can be arbitrarily high, in a real device the resolution is limited by the field linearity which can be achieved. In this paper we describe how a nearly linear field can be produced and discuss how the design can be optimized for various different plasma regimes and spacecraft configurations.

I. INTRODUCTION

Space plasma ion distributions represent the combinations of a wide variety of plasma sources and sinks as well as modifications by various *in situ* plasma processes. Consequently, well-resolved measurements of the velocity space distributions of the constituent ion populations are crucial for understanding space plasma environments. In terms of measurement requirements this usually translates into the simultaneous need for (a) angular and energy resolved measurements over $\sim 4\pi$ sr, (b) extremely high sensitivity in order to provide good statistical accuracy and temporal resolution, and (c) high mass/charge (m/q) resolution over a large energy range. In addition, these measurements must be made by a compact and rugged instrument with low mass and power requirements (typically ~ 10 kg and ~ 10 W) and with the capability of making autonomous measurements over many years.[1]

Previously developed 3-D space plasma composition instrumentation has principally relied on two techniques: magnetic mass analysis and linear trajectory time-of-flight (TOF). While considerable progress has been made in both of these areas over the last several years[2] both techniques suffer from limitations which reduce their utility for making fast, highly mass-resolved measurements of the 3-D distributions of hot tenuous plasmas.[3] In this paper we describe a new type of space plasma composition sensor based on a different technique, which meets all of the measurement requirements given above in a compact and robust instrument design.

Our technique is based on the motion of ions in a cylindrically symmetric device with an axial, linear electric field (LEF).[3] This design is an extension of the LEF principle which is currently being developed into a 1-D instrument for measurement of the solar wind ion composition.[4,5] In a linearly increasing electric field region, $E_z \propto z$, where z is the axial direction, the force acting to retard an ion's motion, qE_z, is proportional to the depth the ion has traveled into the LEF region. Consequently, the ion's equation of motion in the z direction is that of a simple harmonic oscillator,

$$m\, d^2z/dt^2 = -qkz, \tag{1}$$

where m and q are the ion's mass and charge, and k is a constant determined solely by electromechanical properties of the device.

The solution to (1) has a frequency, $\omega = (qk/m)^{1/2}$ so that a particle entering the device at $z = 0$ returns to the $z = 0$ level when

$$t = \pi/\omega = \pi(m/qk)^{1/2}. \tag{2}$$

Since (2) is independent of both ion energy and launch direction, extremely high m/q resolution is possible by measuring particle bounce times in a LEF device. Ideally, mass resolution in such a device is limited only by timing uncertainties, however, in practice, resolution is limited by nonlinearities of the field.

II. IMPLEMENTING A 3-D LEF MASS COMPOSITION SENSOR

Figure 1 schematically displays our 3-D LEF-based mass composition sensor. This sensor is comprised of two coaxial, cylindrically symmetric parts: a front end electrostatic analyzer section (displayed generically in Fig. 1), and an LEF-based mass spectrometer back end. The electrostatic front end provides the energy and angular resolution needed to determine the velocity space distributions of the various ion populations. The cylindrically symmetric 3-D mass spectrometer described here and by McComas *et al.*[3] is flexible and can be mated to various types of electrostatic front ends to provide plasma composition measurements for different missions.

On a spinning spacecraft (or rotation platform) the mass spectrometer can be mated to electrostatic analyzers with divided wide angle fields-of-view (FOVs), such as the toroidal top-hat analyzer.[6] This combination has a very large acceptance aperture and high throughput to provide

 0034-6748/90/103095-03$02.00

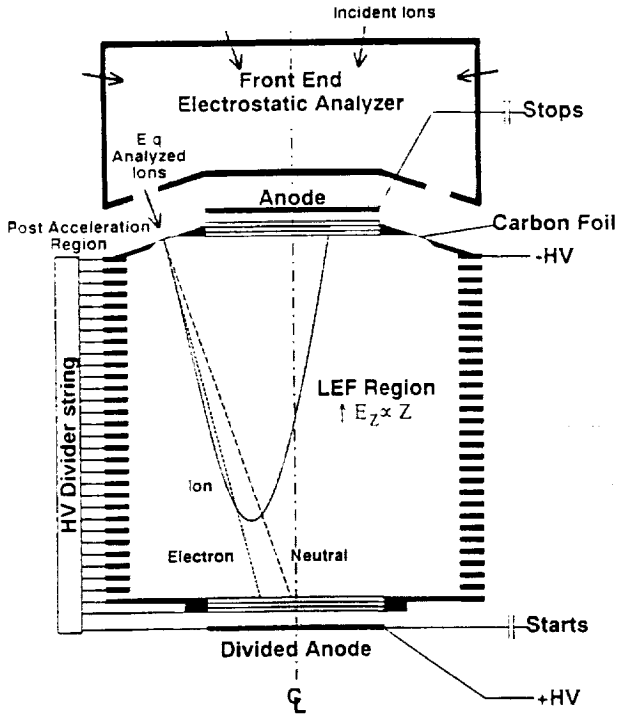

FIG. 1. Schematic diagram of our cylindrically symmetric, 3-D LEF-based mass spectrometer. The generic electrostatic analyzer front end could be any one of a number of designs, depending on the specific mission requirements (see text). After E/q analysis, incident ions are post-accelerated into the LEF region through thin carbon start foils. Particles which exit the foil ionized are reflected in the LEF, providing high mass resolution measurements, while the larger, neutralized fraction travels straight through the device providing simultaneous lower mass resolution, but higher sensitivity, composition measurements.

high sensitivity.[3] On 3-axis stabilized spacecraft without rotation platforms, 3-D measurements can still be made by combining our mass spectrometer with an electrostatic elevation analyzer.[7] In addition, many other sorts of cylindrically symmetric electrostatic front ends such as retarding potential analyzers, electrostatic mirrors, etc. could be used.

After being E/q analyzed in some sort of electrostatic front end, the ion is post accelerated and injected through one of a series of thin ($\sim 0.5\ \mu g/cm^2$) carbon foils[8] arrayed around the entrance to the LEF mass spectrometer section. Secondary electrons ejected from the backside of the foil by the passage of the incident particle are used to initiate timing in the LEF region. These electrons are focused by the LEF onto a microchannel plate (MCP) at the opposite end of the device. Flight times for the electrons are ~ 1 ns and a divided anode behind the start MCP provides information on the direction of incidence of the ion as well as starting the TOF circuitry.

Of the ions entering the foil, $\sim 10\%$ exit positively charged, depending on the ion's species, energy and angle, and the particulars of the thin carbon foil.[3,5] These ions are reflected in the LEF and detected on a central stop MCP which is at the same potential as the foils. This stops the timing and provides the ion's time-of-flight.

For most ion species the remainder of the particles leaving the foil are neutral and are unaffected by the LEF. These neutrals pass straight through the LEF region and hit the start MCP as shown in Fig. 1. These neutrals provide linear trajectory TOF measurements over a long transit path for the majority of the incident ions. Duty cycles are sufficiently low, and TOFs short enough, that there is essentially no confusion between electron starts and neutral stops on the same MCP.

III. CYLINDRICALLY SYMMETRIC LINEAR ELECTRIC FIELDS

In a gridless axial LEF (e.g., $E_z \propto z$), the potential can be calculated from the cylindrically symmetric form of Laplace's equation:

$$\frac{1}{r}\frac{\partial \Phi}{\partial r} + \frac{\partial^2 \Phi}{\partial r^2} + \frac{\partial^2 \Phi}{\partial z^2} = 0, \tag{3}$$

where Φ is the potential as a function of radial (r) and axial (z) location. To produce a linearly varying field, $\partial^2\Phi/\partial z^2 =$ constant, and this term must be balanced by the other terms in Eq. (3). Near the symmetry axis where r is small, this term can be easily balanced by a $1/r\ \partial\Phi/\partial r$ term of the opposite sign. However, away from the axis an increasingly radial electric field is necessary to balance the z-directed LEF. Because the signs must be opposite, a restoring z field is balanced by a defocusing radial field. This unavoidable effect causes ions to be pushed away from the central axis of the device, so that some of the ions miss the stop MCP which, thereby, reduces the overall detection efficiency.

One method of producing a cylindrically symmetric, axial, LEF is to use equipotential surfaces of rotation to fit a quadratic solution of Laplace's equation (3). Our solution to the problem of producing the desired LEF is more straightforward. Instead of using large equipotential surfaces, our linear eletric field is achieved directly by imposing electrostatic potentials along the boundaries of the region where it is desired. As it is difficult to achieve a continuous voltage variation, we have approximated this variation by applying voltages to a series of guard rings.

Figure 2 shows equipotentials for a fairly high resolution LEF mass spectrometer which are spaced so that $\Phi \propto z^2$; even spacing between the lines indicates good field linearity. There is a good approximation to a linear electric field near the center of the device with some distortions near the ends. At the low field entrance end of the LEF (top of the figure) these distortions have a very small effect on the resolution because the field is weak there. In fact, carefully tuned departures from linearity near the entrance have a beneficial effect in allowing molecular ions to be separated unambiguously from atomic ions with nearly identical m/q ratios (e.g., He^{++} vs H_2^+)[3].

The best mass resolution is achieved for those ions with the appropriate energies to be reflected in the central, most highly linear region. Because ions are post-accelerated before entering the LEF region, they all have at least that E/q. Thus, ions which remain intact must penetrate to a minimum depth, indicated in Fig. 2 by the dashed line, before turning around. For a given E/q range

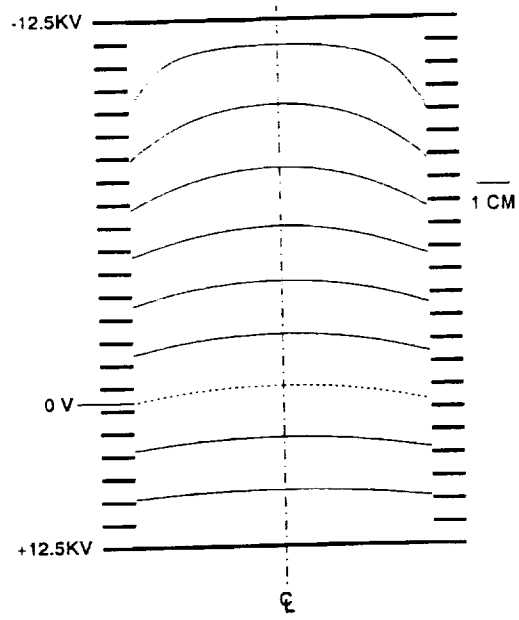

FIG. 2. Calculated equipotentials spaced such that $\Phi \propto z^2$. The evenness of the spacing and flatness of the contours over much of the region, especially away from the ends of the device, demonstrate that a good field linearity has been achieved. Ions are injected into the LEF at the top; the dotted ground potential line indicates how deep an ion with only the post-acceleration energy will travel into the device.

selected by the front end analyzer (and modified by energy straggling in the foil) all ions penetrate approximately the same distance into the LEF. Consequently, far better mass resolution can be achieved for real space observations, where ion E/q determination is important, than would be achieved for non-E/q resolved measurements.

Since end effects are less important in LEF devices which have greater length-to-width ratios, such devices provide better mass resolution. Unfortunately, the radially outward force on ions also causes long, thin devices to have lower throughputs. One of the main elements in designing a 3-D LEF-based mass spectrometer for a specific mission is to optimize the various tradeoffs such as that between mass resolution and instrument sensitivity.

IV. RESULTS AND DISCUSSION

A set of 3-D computer simulation programs has been developed at Los Alamos to characterize various electrostatic devices including electrostatic front ends and mass resolving sections. The validity of these codes has been demonstrated by comparison of the Monte Carlo simulations with prototype test results of an actual LEF device[3].

Figure 3 displays the results of a Monte Carlo simulation of various low energy ions in the LEF mass spectrometer configuration shown in Fig. 2. We have added a 10% FWHM Gaussian energy distribution about a 12.5 keV post-acceleration energy. Note that the neon isotopes are very well resolved as are ^{39}K and ^{40}Ar. The simulated mass resolution of this device for the conditions shown in Fig. 3 is ~ 100 $(m/\Delta m)$, fully resolved.

In this paper and in our previous work[3] we have described a new instrument development which offers 3-D

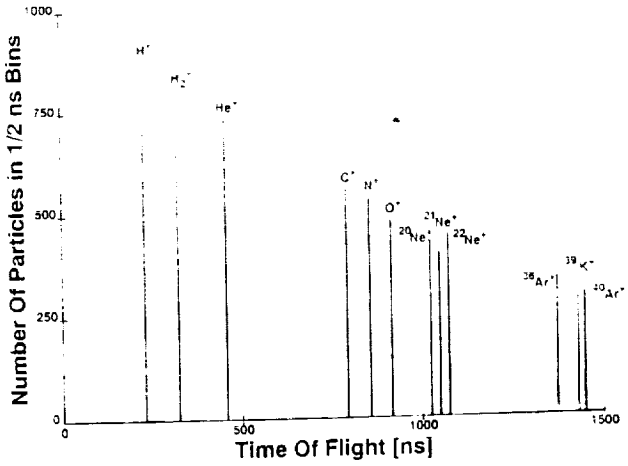

FIG. 3. Monte Carlo simulation of the mass resolution of a mass spectrometer based on the field configuration shown in Fig. 2. Each of the peaks contains ~ 2000 ion timings taken for an incident cold ion beam (~ 0 eV) with a 10% FWHM gaussian energy distribution about the 12.5 keV post-acceleration energy and varied over sufficient angular range so as to cover the stop detector. This is a relatively high mass resolution design providing $m/\Delta m \sim 100$ for fully resolved mass peaks.

high mass resolution, high sensitivity, plasma composition measurements in a compact and robust design. High mass resolution is achieved by reflecting ions in a linearly increasing electric field. High sensitivity is simultaneously achieved by combining this very large aperture mass spectrometer with any of a number of high throughput front-end electrostatic analyzers. In addition, this design simultaneously provides even higher sensitivity but lower mass resolution measurements of particles which exit the foil as neutrals using the linear trajectory TOF. In a reasonable sized toroidal top-hat-based sensor (a few kg), total instrument geometric factors of $\sim 10^{-2}$ cm^2 sr (eV/eV) for the straight through neutrals and $\sim 10^{-3}$ cm^2 sr (eV/eV) for the high resolution LEF analyzed ions, can be readily achieved providing excellent fast plasma composition measurements. These combined data significantly increase the flexibility of the instrument for measuring mass resolved plasma ion distributions in diverse space environments.

ACKNOWLEDGMENTS

We gratefully acknowledge input from S. Bame, B. Barraclough, K. McCabe, M. Thomsen, D. Young, and particularly J. Gosling who also provided a critical reading of this manuscript. We thank G. Gloeckler for pointing out the concept of 1-D linear electric field mass analysis to us. This work was carried out under the auspices of the United States Department of Energy.

[1] S. J. Bame, D. J. McComas, D. T. Young, and R. D. Belian, Rev. Sci. Instrum. **57**, 1711 (1986).
[2] D. T. Young, Geophys. Mono. Ser. **54**, 143 (1989).
[3] D. J. McComas, J. E. Nordholt, S. J. Bame, B. L. Barraclough, and J. T. Gosling, Proc. Natl. Acad. Sci. in press (1990).
[4] D. Hovestadt *et al.*, ESA SP-1104, 1988.
[5] M. Oetliker, Thesis, University of Bern (Bern, Switzerland, 1989).
[6] D. T. Young *et al.*, Rev. Sci. Instrum. **59**, 743 (1988).
[7] S. J. Bame *et al.*, Geophys. Mono. Ser. **54**, 441 (1989).
[8] Arizona Carbon Foils (Tucson, AZ) stock foil floated onto 333 lpi, 70% transmissive Ni mesh. Manuscript on foil preparation in progress.

Nuclear Instruments and Methods in Physics Research A298 (1990) 227–233
North-Holland

An isochronous poloidal geometry time-of-flight ion mass spectrometer for energetic space plasmas

D.T. Young and J.A. Marshall

Space Sciences Department, Southwest Research Institute, San Antonio, TX 78228-0510, USA

Space missions to the outer planets of the solar system require advanced mass-spectroscopic measurements that cover an unprecedented range of particle phase space. We present here a discussion of satellite-borne mass-spectrometer design considerations and put forward a design for an isochronous time-of-flight mass spectrometer based on poloidal ion trajectories in a set of three tandem toroidal electrostatic analyzers. The proposed instrument focuses a wide range of ion energies ($\Delta E/E = 0.10$) and entrance angles ($\pm 5°$) over a field of view subtending 360° with a mass resolution $M/\Delta M > 20$. In order to create such a large field of view, the device accepts a broad range of entrance angles in the nondispersive (azimuthal) direction of the toroids. Isochronous focusing takes place in the polar plane of the toroid, thus the optics of this device are poloidal rather than toroidal. Because of the lack of an analytical theory up to now, development has relied primarily on 3D ray tracing to find triple-focusing (angle–energy–displacement) solutions that are isochronous. The proposed device has the useful feature that it discriminates molecular species from atomic species of the same mass (e.g. CH_4^+ from O^+ or CH_3^+ from N^+).

1. Introduction

Space plasmas, whether encountered near Earth or in the outer solar system, are characterized by their low density (~ 1 ion cm^{-3}), high characteristic energies (few electron volts to several tens of kilo-electron-volts) directional anisotropy, and compositional heterogeneity. An effective study of plasma properties therefore requires very-high-sensitivity mass-spectrometric measurements on time scales of a few seconds in order to be commensurate with plasma phenomena. The plasma properties in which space scientists are interested can be adequately described by measurements of the particle distribution function $f_i = f_i(v_x, v_y, v_z, x, y, z, t)$ which gives the density in phase space for the ith major ion species found in the plasma. Using f_i one may calculate the usual bulk plasma parameters such as density, flow velocity and temperature. The presence of as little as a few percent by number of a minor ion species is known to have a significant impact on the behavior of the bulk plasma, e.g. on the dispersion relation for low-frequency wave propagation. Thus one is required to measure f_i for these minor species and, indeed, it is desirable to measure minor constituents to at least $\sim 10^{-3}$ of the major species. Instrument design considerations are guided by the need to make a limited sample of f_i over 4π sr and over energies from a few electron volts to ~ 50 keV and then to deduce f_i using only telemetered data containing detector counting rates and the voltage settings on electrostatic analyzer plates. To understand the measurement process it is helpful to consider the relationship [1] between f_i and the telemetered quantities of detector count rate C_i, ion energy E and mass M_i,

$$f_i(E) = kC_iM_i^2/(G_iE^2) \quad \text{s}^3\,\text{cm}^{-6}, \tag{1}$$

where $k = 5.45 \times 10^{-31}$ for energies measured in electron volt and mass measured in amu. The factor G_i is the energy-geometric factor, which is approximately constant with energy for a given instrument and ion species. The value of G_i is found by laboratory calibration. It expresses the instrument response in terms of its sensitive area A, its angular acceptance Ω, energy acceptance $\Delta E/E$ as well as detector efficiency ϵ_i and the grid transmission T. In general, G_i may be written [2]:

$$G_i = A\Omega T\epsilon_i(\Delta E/E) \quad \text{cm}^2\,\text{sr}, \tag{2}$$

where Ω represents the averaged angular response and $\Delta E/E$ the averaged energy response normalized to the energy of the central ion trajectory. (The estimated value for the isochronous time of flight (ITOF) presented here is $G_i = 1.8 \times 10^{-3}$ cm^{2}sr based on a 270° field of view.)

The quality of the measurement of f_i is thus seen to be determined by the minimum detectable counting rate and by the instrumental constant G_i. Because the limiting detectable count rate is set by detector noise and by the background due to high-energy radiation in the space environment, the only avenue open to the experimenter that will make an instrument more sensitive to f_i is to increase the size of the constant G_i. This is accomplished by increasing area, acceptance angle, detector efficiency, or transmission. As G_i is increased, however,

0168-9002/90/$03.50

there is a direct tradeoff against energy, angle and mass resolution, as can be seen from eq. [2]. To the space-plasma experimentalist, resolution of f_i in velocity space (i.e. in energy and angle) is as important as resolution of the plasma mass spectrum into its components. For example, precise measurements of the composition of space plasmas, which can be obtained by sacrificing all details of f_i except its zeroeth moment, may be useful for cosmochemical studies (such as determination of the $^2D/^1H$ or $^{13}C/^{12}C$ ratios) but will yield virtually no information on plasma processes that usually depend on the shape of $f_i(E)$ and on its higher moments. The scientific objective of the class of instruments represented here is therefore to separate the ion species necessary for cosmochemical study while at the same time preserving all essential details of f_i on a time scale that is meaningful for plasma physics.

The problem of data reporting of f_i is also a serious one for space physics, but cannot be gone into here in detail except as it affects choice of resolution. Suffice it to say that it is pointless to measure f_i at a resolution so fine as to preclude reporting it back to Earth due to telemetry bandwidth limitations. For example, the full reporting of f_i for *one* ion species at an energy resolution of 10% and angular resolution of $\sim 10° \times 10°$ would require a telemetry bandwidth of ~ 12 kbytes per full sampling of energy and angle phase space (usually one such sample is made per satellite spin period of ~ 6 s), or about 16 times the typical satellite bandwidth assigned to present-day experiments. Since the satellite can transmit only a small fraction of the available data, designed-in oversampling of f_i (e.g. by choosing very high resolution in angle and energy) is counterproductive. We justify our choice of $\Delta E/E \approx 0.1$ for ITOF by the need to adequately sample a typical Maxwellian distribution with 10% resolution near the peak in ion flux which occurs at $E = T$ where T is the plasma temperature in eV. The choice of 10° angular resolution is governed by typical ion flow Mach numbers and allows flows up to $M \sim 3$ to be resolved. In addition, 10° gives reasonable angular sampling of particle arrival directions when that sampling is obtained through typical spacecraft rotation rates of $< 60°/s$ (< 10 rpm). The amount of data acquired by ITOF will still be much larger than available bandwidth and on-board processing must be applied to select and compress data and transmit only the most essential information.

The principles of isochronous time-of-flight (ITOF) mass spectrometry are well known in their application to laboratory instruments [3–7]. In general, the ITOF designs described in the literature rely on the symmetry of ion trajectories in multisector electric and magnetic fields, but whereas a large number of optical elements are acceptable in laboratory practice, they are too cumbersome in the miniaturized world of satellite instrumentation. Nonetheless, the ITOF design presented here offers a long ion flight path (26 cm) by folding ion trajectories back on themselves. The design is reasonably compact but still allows adequate ion flight times for resolution and measurement.

In distinction to isochronous TOF systems, non-focusing TOF techniques based on timing signals derived from foil penetration have been used previously in space instruments [9–11] as well as in the laboratory [8]. Initially, foil-based devices found favor in space applications because they made possible mass analysis of ions at high energies ($\gtrsim 30$ keV) where magnetic mass spectrometers could no longer disperse ion trajectories [12]. The inherent anticoincidence nature of the TOF measurement also greatly reduces random background events due to penetrating radiation in space.

One other impetus for using the carbon-foil TOF technique in space research is the potential that it holds for resolving molecular species from atomic species of the same mass, e.g. H_2^+ from $^4He^{2+}$ or CH_4^+ from O^+. A number of simple molecules are of vital interest for understanding the chemical and physical processes in the outer ionospheric regions of comets, and of planets, their satellites, and rings. Unfortunately, these molecules often have masses that coincide with those of common atomic species. The ITOF is able to separate molecular species using the fact that a molecular fragment of mass M^* carries away a fraction M^*/M_0 of the incident molecule's original energy E_0. By tuning the ITOF postfoil electrostatic analyzers to an energy $E^* = (M^*/M_0)E_0$, the molecular fragment can be detected.

2. Instrument description

Fig. 1 shows a schematic view in the polar-angle (poloidal) plane of the ITOF analyzer. The analyzer is made up of three tandem electrostatic analyzer sections each of which is a toroid of revolution about the central axis of fig. 1. It should be clear from fig. 1 that the sense in which ions orbit in the ITOF toroid is fundamentally different from the way they orbit in toroids that are discussed in the literature [6,7]. Moreover note that ion paths lack symmetry in the poloidal plane due to the lack of symmetry of the poloidal components of the electric field, in contrast to laboratory isochronous designs in which ions travel in the equatorial plane of the toroid [6,7] and in which ion orbits are symmetric when viewed in that plane. (These remarks about symmetry apply equally to cylindrical geometries [5] for isochronous TOF.) By employing symmetry, usually involving more than one analyzer element, laboratory devices can be made isochronous to a very high order, but this is impractical for space applications requiring 360° field of view, compact design, etc. The ITOF

described here uses an asymmetric geometry dictated by the focusing properties of poloidal trajectories. This allows a greatly compacted and simplified mechanical design with only two TOF deflection elements and three drift spaces. Unfortunately, poloidal geometry has not been solved analytically, indeed the present device and that described at this conference by Ghielmetti and Shelley [15] seem to be unique in use of poloidal geometry. The lack of a transfer matrix solution makes it difficult to describe formally the optical properties of this device.

Ions enter the ITOF through a collimator section located in front of the sector-field electrostatic analyzer ESA 1. The collimator limits the angular range of ions reaching ESA 1 while at the same time rejecting UV photons from solar and planetary sources. Ion energy is selected by the choice of the negative potential on the inner toroidal plate of ESA 1. The surfaces of the collimator and the outer plate of ESA 1 are held at ground potential. The bandwidth of allowable energy and angle are chosen by science considerations to be $\Delta E/E = 0.10$ and $\Delta\alpha = \pm 5°$; respectively.

Upon exiting ESA 1, ions are accelerated by a potential $-V_{acc}$ that is chosen to be -15.0 kV. This is sufficient for all ion species to penetrate the carbon foils with tolerable scattering and energy straggling, yet low enough to be low risk technically. The potential $-V_{acc}$ is also the center reference potential for all optical elements beyond the foil. Ions of charge Q are accelerated to a final kinetic energy of $E_0 + Q|V_{acc}|$ and then impinge on a thin (~ 50 Å) carbon foil mounted on a 100 lines/inch grid of 85% transmission. Ions easily penetrate the foil, causing one or more secondary electrons to be emitted with high probability ($\sim 90\%$) as the ion exits. These electrons are emitted at low energy (~ 3 eV) and are captured by an electric field that penetrates into the region of the foil. They are focused in the plane of fig. 1 onto the "start" microchannel-plate (MCP) detectors. The ions themselves lose a small but variable fraction of their energy in the foil depending on species and energy, and undergo energy straggling and angle scattering due to collisions with carbon atoms. Obviously ion straggling in the foil is reduced with larger $|V_{acc}|$ thus increasing the efficiency and resolution of the device. Some fraction of ions exits the foil as neutral atoms or negatively charged ions (as in the case of oxygen). These are of course lost to the ITOF analysis. Charge exchange in the foil lowers the detection efficiency of the ITOF to a few tens of percent (for N^+) or a few percent (in the case of He^+). Fragmentation of molecular species in the foils and the detection of those fragments are discussed below.

Electrons are focused isochronously on to the start MCP where they give rise to a charge pulse that is further amplified and processed and then used to start the TOF timing circuitry. Variation in the flight time of the electrons from the foil to the MCP is typically < 0.3 ns, which is negligible in comparison to total ion flight times of ~ 100 to 1000 ns.

Ions that exit the foil continue to travel successively through the first drift space, DS 1, toroidal analyzer ESA 2, then DS 2, ESA 3, and DS 3, finally impacting

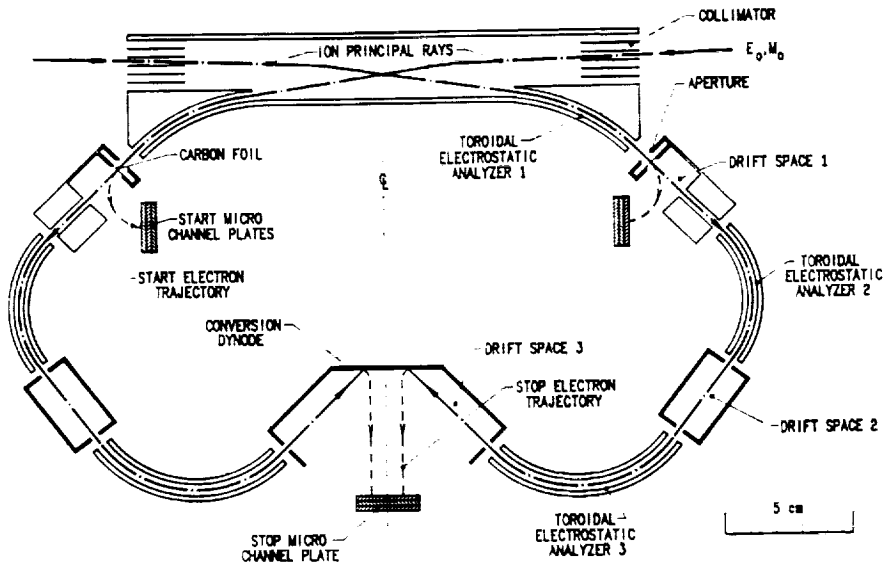

Fig. 1. Schematic diagram of the isochronous time-of-flight (ITOF) mass spectrograph developed for space-plasma measurement applications. The ITOF is made up of three toroidal electrostatic analyzers that are rotationally symmetric about the center line shown in the figure. The heavy broken line (dash/dot) indicates the central ion ray which travels along a poloidal trajectory. Heavy dashed lines indicate typical start and stop electron trajectories leading to the start and stop microchannel plates.

on the conversion dynode (fig. 1). Secondary electrons created at the conversion dynode then travel to the stop MCP. In the most general case, the analyzers ESA 2 and ESA 3 have negative voltages applied to their inner and outer plates. Toroidal analyzer-plate dimensions have been chosen such that the negative voltages on the two outer plates are equal, as are voltages on the two inner plates, and the combined voltages are always centered on $-V_{acc}$ regardless of ion energy. The stop MCP gives a pulse delayed by a time equal to the ion TOF plus a small fixed offset for the travel time of "start" and "stop" electrons. The measurement of TOF corrected for electron travel times, together with knowledge of the ion energy per charge measured by ESA 1, allows calculation of the ion mass per charge using the formula $\mathrm{TOF} = 22.85L(M/E_f)^{1/2}$ ns, where L is the ion path length in cm ($L = 25.86$ cm for the prototype in fig. 1), M is ion mass in amu, and $E_f = E_0 + Q|V_{acc}| - \Delta E_{foil}$ is the final ion energy entering the TOF section. Typical flight times vary from 80 ns for 50 keV H^+ to 1.0 μs for CO^+ entering the ESA 1 at near-zero energies. Electronic circuitry is able to make and process the TOF measurement in a time of ~ 2 μs so that in principle event rates up to $\sim 5 \times 10^5$ ions/s can be accommodated. The calculation and assignment of discrete M/Q values to different TOF signals will be carried out by the instrument's on-board 16-bit microprocessor.

The conversion-dynode feature solves the problem of decoupling the start and stop signals from the potential $-V_{acc}$ about which the ESA 2 and ESA 3 electrodes are biased. We thus use the stop electrons themselves to bridge the high-voltage drop rather than, for example, placing the MCPs at high voltage and then using high-voltage capacitors to decouple their signals. The same technique decouples the start electrons from the foil high voltage. Electron travel times introduce very little error into the TOF measurement because (1) they are quite short compared to ion travel times (typically < 1%) and (2) the dispersion in electron travel times Δt is also relatively small, being only about 25% of their overall flight time, i.e. $\Delta t < 0.3$ ns.

We now come to the problem of separating molecular and atomic species of the same mass. Small molecular ions very often fragment into two components in the foil, and one or both of these may exit in the +1 charge state. (This is true even of molecules having more than two atoms.) A charged molecular fragment of mass M^* will have an energy that is proportional to its mass, namely $E^* = (M^*/M_0)E_f$ where E_f is defined above. It is therefore possible to tune the voltages of ESA 2 and ESA 3 to select for the transmission of ion species with energies E^*, while leaving ESA 1 set on E_0. By scanning ESA 2 and ESA 3 through a set of voltage steps spaced in units of $\Delta E^* = E_f/M_0$ it is possible to search for the peaks due to other mass fragments. In this way, for example, it is possible to distinguish incident CH_3^+ (which should fragment primarily into CH_2^+ with lesser amounts of CH_3^+ and CH^+ roughly in the ratios 46 : 40 : 7 : 4), from $^{16}O^+$. One tunes ESA 2 and ESA 3 to $0.94E_f$ for CH_2^+ or $0.875E_f$ for CH_3^+ and then folds these fractions back into the incident $M = 16$ ion flux to determine the fraction due to CH_4^+. In order for this to work, the energy resolution of ESA 2 and ESA 3 must be better than $1/M_0$, or about 6% at the water-ion peak where resolution of molecular species is critical. This is in conflict with our earlier goal of high transmission with $\Delta E/E \sim 10\%$, and further tradeoff studies are required. Of course the calibration of such a system requires determination of the foil efficiency for producing all species concerned. We note, however, that even more precise efficiency calibrations are required for other TOF instruments presently under construction for spaceflight missions [13,14].

3. Ray-tracing results

The choice of major and minor radii for the toroidal analyzers ESA 2 and ESA 3, as well as their sector angles and the length of drift spaces between the analyzers determines ITOF focusing properties. These can be selected to focus the expected range of positions, angles and energies of ions exiting ESA 1 and the carbon foil. We found through ray tracing that energy–angle focusing alone did not, however, yield the necessary isochronous conditions and actually yielded greater temporal dispersion than field-free drift of ions. Ions with different angles but equal energies are easily compensated in flight times by the combination of the two separate analyzers (fig. 2) but energy-dispersed ions are not. In qualitative terms, the lack of symmetric trajectories and an intermediate energy focus between ESA 2 and ESA 3 causes lower-energy ions to remain on tighter, shorter trajectories that are close to the inner analyzer plates. Higher-energy ions do the opposite. The result is that despite spatial-energy focusing at the exit of ESA 3, an overcompensation occurs: slower ions actually travel on too short a path through ESA 2 and ESA 3 and get to the detector ahead of initially faster ions which are traveling on longer paths near the outer analyzer plates. We have found that one solution is to adjust the lengths of drift spaces DS 1, DS 2, and DS 3 such that ions of different energies are recompensated to some extent, and faster and slower ions end up taking approximately the same time.

Following on the work of Poschenrieder [3,4] and others, an attempt was then made to adjust the length of the three drift spaces in order to compensate for the lack of temporal focusing. Because it is not possible to treat poloidal trajectories in closed analytical form, many configurations had to be tried and several ray-

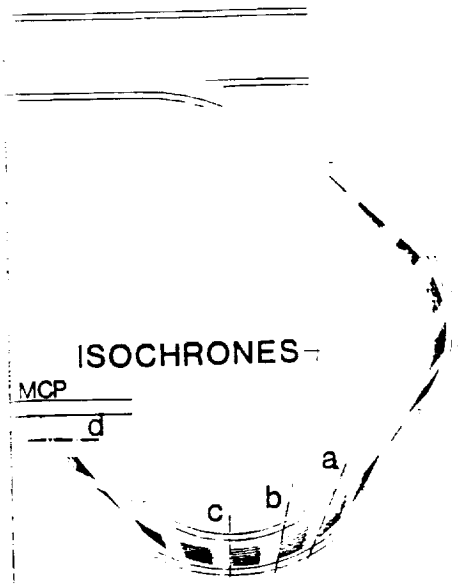

Fig. 2. Intermediate ITOF design. Interruptions in the ion trajectories establish points of equal time (isochrones) along them. Isochrones are indicated by the dashed lines labeled a, b, c, d. Isochrones a–b and b–c are 10 ns apart.

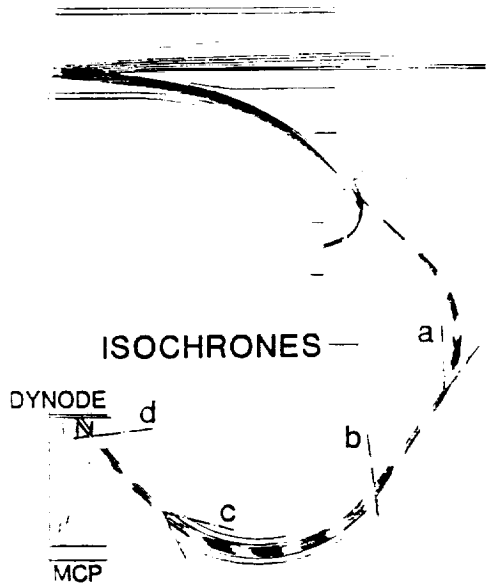

Fig. 3. Similar to fig. 2, but for a mixture of ion trajectories having dispersion in both energy (±3%) and angle (±3°). Note that some isochrones (a, c) are no longer straight lines. Electron trajectories are shown leaving the foil and stop dynode and reaching the start and stop detectors.

tracing methods were developed that allow graphical representation of the temporal divergence of ion rays as they travel through the ITOF. An example is given for a mono-energetic, angular-divergent ion beam in fig. 2. The bundles of rays are interrupted periodically at an arbitrary time of 10 ns so that the dashed lines a, b, c and d in fig. 2 represent isochrones, i.e., lines of equal ion travel time. (Ray tracing is originally done in color, with a color spectrum set to vary cyclically with time along the ion trajectory. This method allows isochrones separated by $\Delta T/T \sim 2\%$ to be observed.) Isochrone d in fig. 2 is seen to be nearly parallel to the MCP detector, indicating that ions are arriving at the detector nearly isochronously. In this particular case the time dispersion $\Delta T/T_0 = 5 \times 10^{-3}$. Many trial-and-error attempts with both energy- and angle-dispersed beams resulted in the configuration shown in fig. 3. This plot depicts a set of ion trajectories dispersed by $\pm 3°$ in angle and $\pm 3\%$ in $\Delta E/E$. Isochrones such as a and c in fig. 3 are no longer straight lines, primarily because of the energy dispersion of the beam. However, isochrone d (nearest the dynode) is nonetheless nearly straight and parallel to the dynode surface, indicating a nearly isochronous configuration. A more quantitative view of this result is presented in fig. 4 where we have plotted the relative time dispersion $\Delta T/T$ for ions arriving at the conversion dynode as a function of $\Delta E/E$ and $\Delta\theta$ for ions leaving the foil. The diagonal straight line represents time dispersion expected from (nonfocused) energy dispersion. The curve labeled "energy" has an average slope of about one half that of the relationship $\Delta T/T = \Delta E/2E$, demonstrating that temporal focusing does indeed occur in the ITOF with respect to an angle- and energy-dispersed beam.

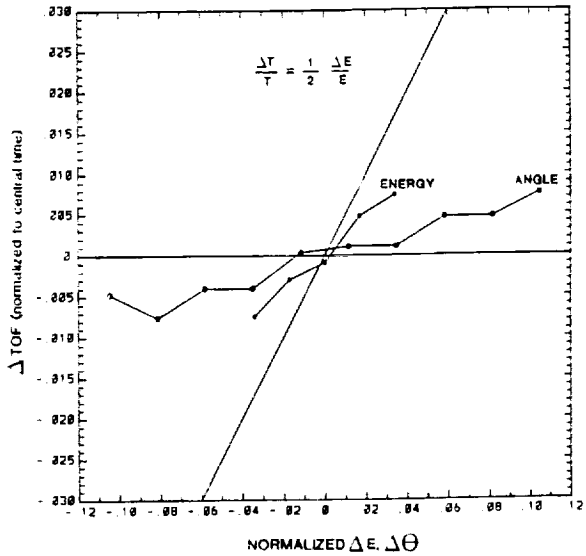

Fig. 4. Variation in time dispersion ($\Delta T/T$) of ion time of flight as a function of initial energy dispersion ($\Delta E/E$) and angle ($\Delta\alpha$). The straight diagonal line corresponds to the nonfocusing case in which $\Delta T/T = = \Delta E/2E$.

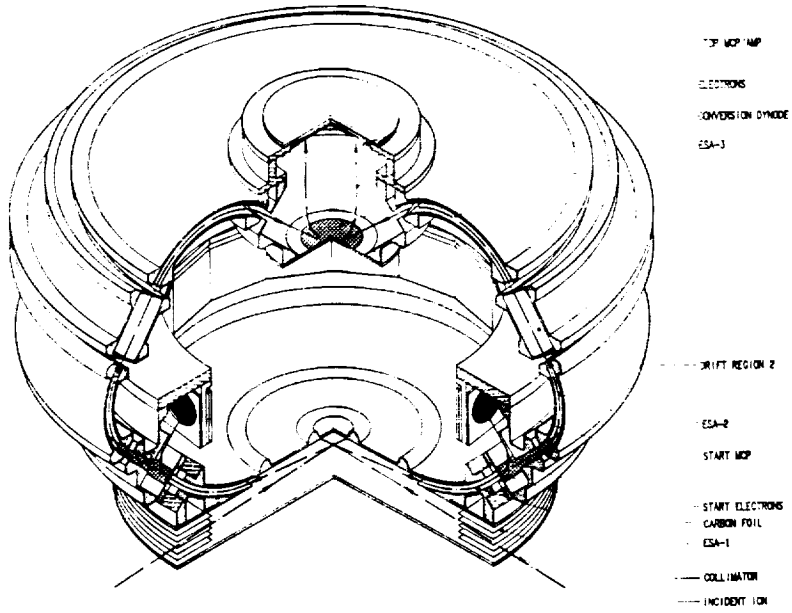

Fig. 5. Isometric drawing of the prototype ITOF. Diameter of the outermost plate of the prototype (i.e. ESA 2 outer toroidal plate) is 30 cm. In order to make the figure clearer in this perspective, the ITOF is shown inverted relative to the schematic in fig. 1.

Ray tracing was also carried out for the variation of rays across the width of the foil surface (4.0 mm) and in the direction perpendicular to the plane of figs. 1–3. Ray tracing in the "third" dimension was carried out using axisymmetric fields but three-dimensional trajectories. Both of these variations in position introduce time dispersion comparable to that for angular variations and about one half that of the energy dispersion. When all time variations are added as the square root of the sum of the squares of the individual terms we obtain $\Delta T/T = 0.02$, corresponding to a mass resolution $\Delta M/M = 0.04$, or in the more conventional notation $M/\Delta M = 25$.

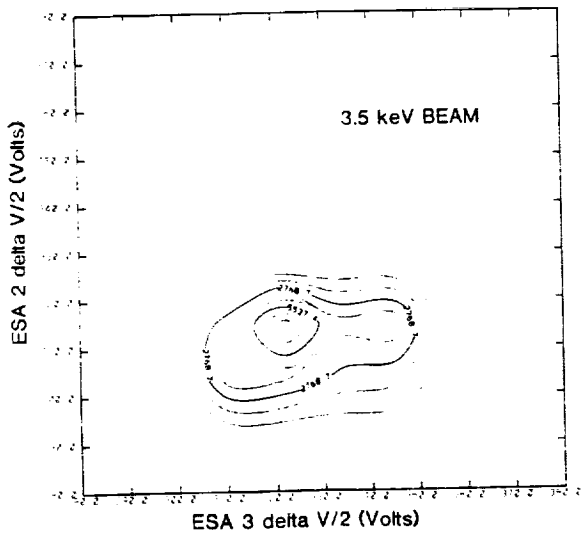

Fig. 6. Contours of constant stop MCP count rate for ESA 2 plate voltage as a function of ESA 3 plate voltage for a 3.5 keV incident beam. Ordinate and abscissa values correspond to one half of the applied voltages which were balanced about $V_{acc} = 0$. Thus 330 refers to applied voltages of ± 330 V.

4. Experimental results

A laboratory prototype of the ITOF was constructed as shown in the isometric drawing in fig. 5. Mechanical parts were first turned on a lathe and then sectioned at 270° as required to produce a prototype of an instrument being studied for possible inclusion in the NASA/ESA Cassini mission to Saturn. Although every attempt was made to fabricate the prototype accurately, some stress relaxation of the aluminum parts and mechanical inaccuracies resulted in toroid misalignments and consequent difficulties in obtaining ion beam transmission through the full ITOF. Fig. 6 is an example of initial data in which the dependence of ESA 2 and ESA 3 voltages and transmission are shown. In this case, an open grid is used in place of a carbon foil and $V_{acc} = 0$ so that ESA 2 and 3 are biased around ground potential. Based on ray tracing it was expected that the analyzer constants (i.e. the ratio of particle energy E_f to the ESA deflection voltage ΔV) of the two ESAs should be equal to 5.22. However, fig. 6 shows constants of $E_f/\Delta V = 5.32$ for ESA 3 and 5.56 for ESA 2, clearly indicative of analyzer plate misalignments of several

percent in $\Delta R/R$. Moreover, when the value of V_{ESA} is placed at -3.0 kV and ESA 2 and ESA 3 are biased above and below this potential the analyzer constants are about fifty percent closer to those predicted by ray tracing. This indicates some shifting of ion trajectories by stray fields, possibly in the region of the start MCP where electric fields penetrate to the surface of carbon foils in order to pull electrons over to the start MCP. At the present time we are still in the process of refining the voltage settings on ESA 2 and ESA 3 and are investigating mechanical misalignments and the interference caused to the ion and electron trajectories by stray fields that are not accounted for in the $2\frac{1}{2}$-dimensional electric field model of the ITOF.

5. Conclusions

We have found a nearly isochronous solution for poloidal optics which opens the way for a 360° field-of-view mass spectrograph for space-plasma measurements with mass resolution $M/\Delta M > 20$ and the possibility for separation of atomic and molecular species with the same M/Q value. Ray tracing of this design has shown that excellent isochronous performance is possible under requirements typically encountered in spaceflight instruments. A laboratory prototype has been constructed and preliminary results are encouraging. Final results on ITOF performance will be the subject of a later paper.

Acknowledgements

We wish to thank A. Ghielmetti for initial double-focusing solutions; D. Strain, T. Booker, R. Martin and W. Lockhart provided invaluable design and laboratory assistance. Portions of this work were supported by SwRI internal research funds, and by NASA grants NAGW-1286 and NAGW-1623.

References

[1] R.L. Kessell, A.D. Johnstone, A.J. Coates and R.A. Gowen, Rev. Sci. Instr. 60 (1989) 3750.
[2] G.C. Theodoridis and F.R. Paolini, Rev. Sci. Instr. 40 (1969) 621.
[3] W.P. Poschenrieder, Int. J. Mass Spectrom. Ion Phys. 6 (1971) 413.
[4] W.P. Poschenrieder, Int. J. Mass Spectrom. Ion Phys. 9 (1972) 357.
[5] H. Wollnik and T. Matsuo, Int. J. Mass Spectrom. Ion Phys. 37 (1981) 209.
[6] T. Sakurai, Y. Fujita, T. Matsuo, H. Matsuda and I. Katakuse, Int. J. Mass Spectrom. Ion Processes 66 (1985) 283.
[7] T. Sakurai, T. Matsuo and H. Matsuda, Int. J. Mass Spectrom. Ion Processes 63 (1985) 273.
[8] R.R. Betts, Nucl. Instr. and Meth. 162 (1979) 531.
[9] G. Gloeckler et al., IEEE Trans. Geosci. Remote Sensing GE-23 (1985) 234.
[10] B. Wilken, T.A. Fritz and W. Studemann, Nucl. Instr. Meth. 196 (1982) 161.
[11] D.T. Young, J.A. Marshall, J.L. Burch, S.J. Bame and R.H. Martin, Am. Geophys. Union, Geophys. Monogr. Ser. 54 (1989) 171.
[12] D.T. Young, Am. Geophys. Union, Geophys. Monogr. Ser. 54 (1989) 143.
[13] G. Gloeckler et al., in: European Space Agency Special Publication, SP-1104 (1989) 69.
[14] M. Oetliker, Thesis, University of Bern, Switzerland (1989).
[15] A.G. Ghielmetti and E.G. Shelley, these Proceedings (3rd Int. Conf. on Charged Particle Optics, Toulouse, France, 1990) Nucl. Instr. and Meth. A298 (1990) 181.